Magnetism at Large Scale Facilities

S. A Cavill

Physics, University of York, UK

ESM 2026, Uppsala

Magnetism at Large Scale Facilities

SPECTROSCOPY

- Synchrotron Radiation
- X-ray Absorption Spectroscopy
- Theoretical foundations
- XMCD
- XMLD

MAGNETIC IMAGING

- PEEM
- STXM
- Fourier Transform Imaging

TIME RESOLVED XMCD MEASUREMENTS

- Time resolved XMCD-PEEM
- XFMR

DIFFRACTION

- X-ray diffraction
- Resonant x-ray diffraction
- SXRD applied to non-collinear magnetism
- Time resolved SXRD

Note: The breadth and depth of all techniques cannot be covered in this lecture.
I will only focus on soft X-ray techniques.

Magnetic Measurements – wish list

1: A probe that is sensitive to magnetic moments

2: Provides information on which element is responsible, what chemical state the magnetic ion is in (valence) and its co-ordination.

3: Allows determination of both spin and orbital contributions

4: High sensitivity <<1ML

5: Differentiate between the surface and bulk

6: Provides a means to image magnetic structures down to nm length scales

7: .. and on ultrafast timescales

8: At temperatures between 1K and 600K

9: and in both E and B fields.

diamond

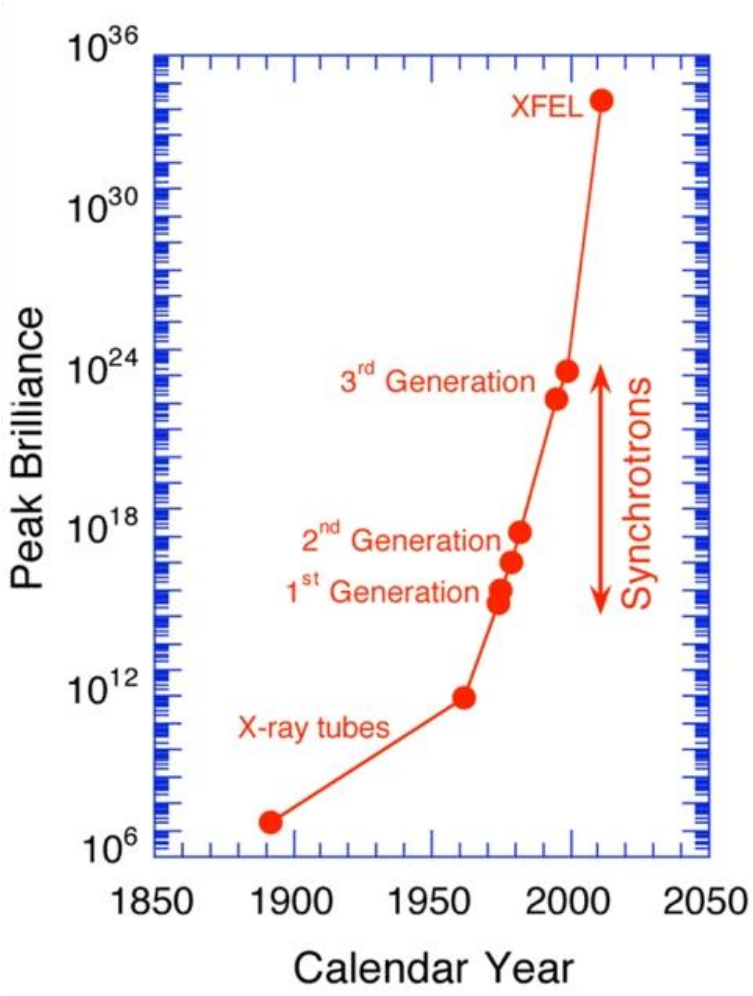

$$\text{Brilliance} = \frac{photons/s}{(mrad)^2(mm)^2(0.1\%\ bandwidth)}$$

Oscillating dipole radiation fields

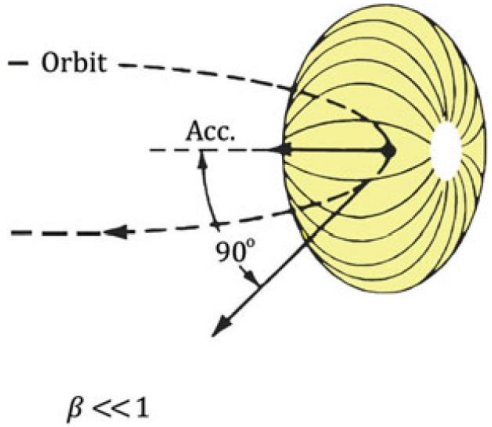

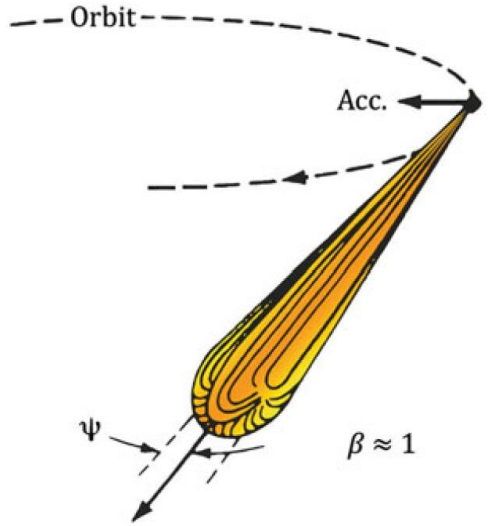

$$\gamma = \frac{1}{\sqrt{1-\beta^2}} \qquad \beta = \frac{v}{c}$$

Source: Synchrotron Radiation: Springer

Synchrotron Radiation – X-ray based techniques

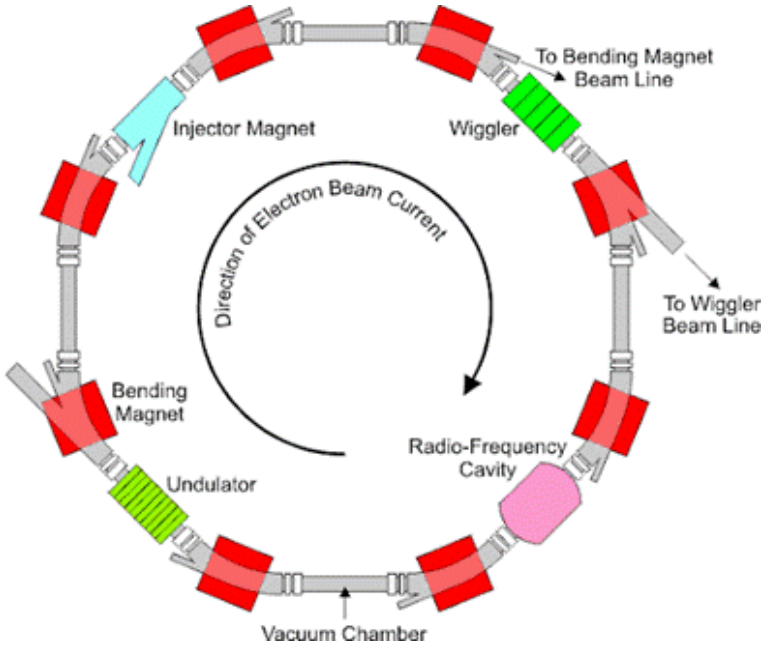

Source: ALS

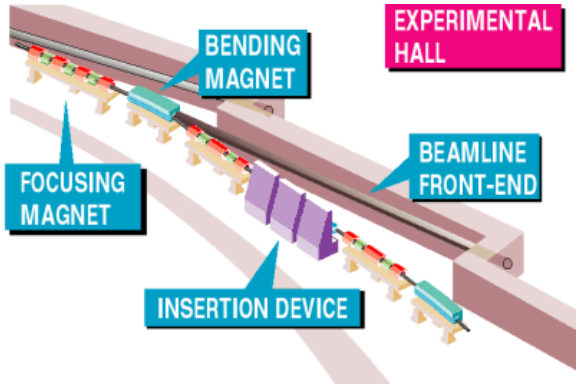

Source: ESRF

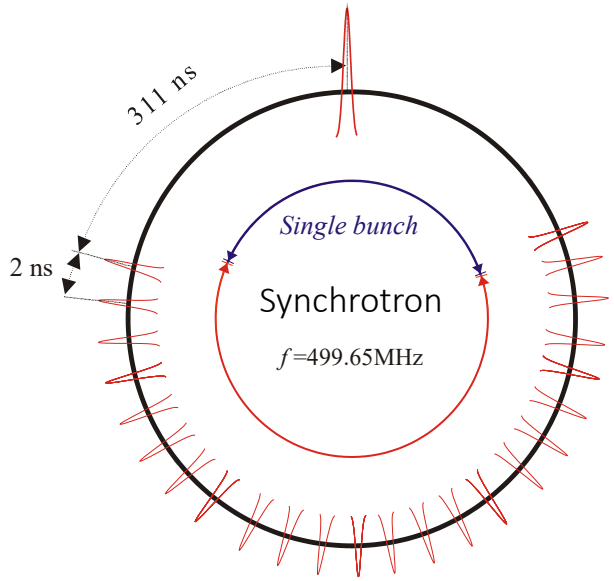

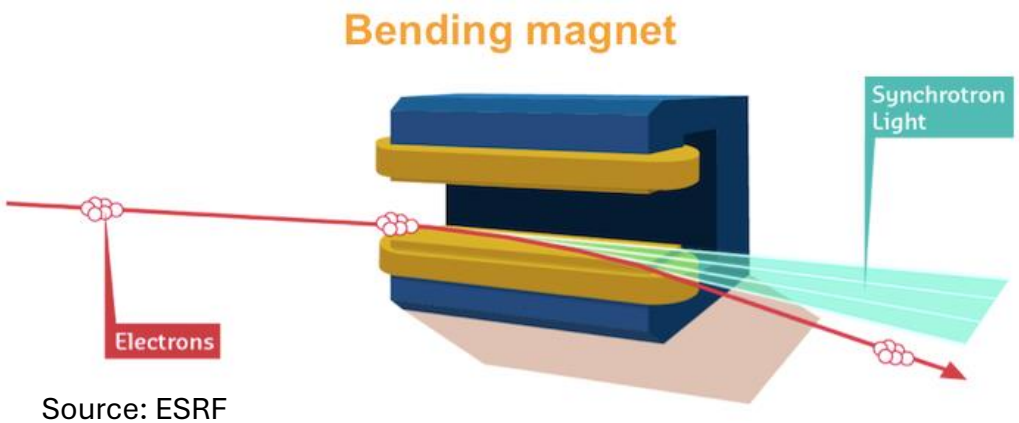

Source: ESRF

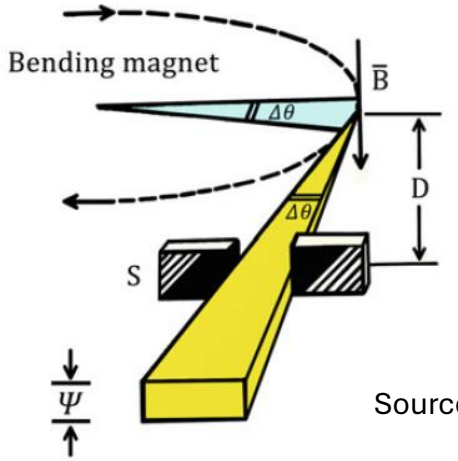

Source: Synchrotron Radiation: Springer

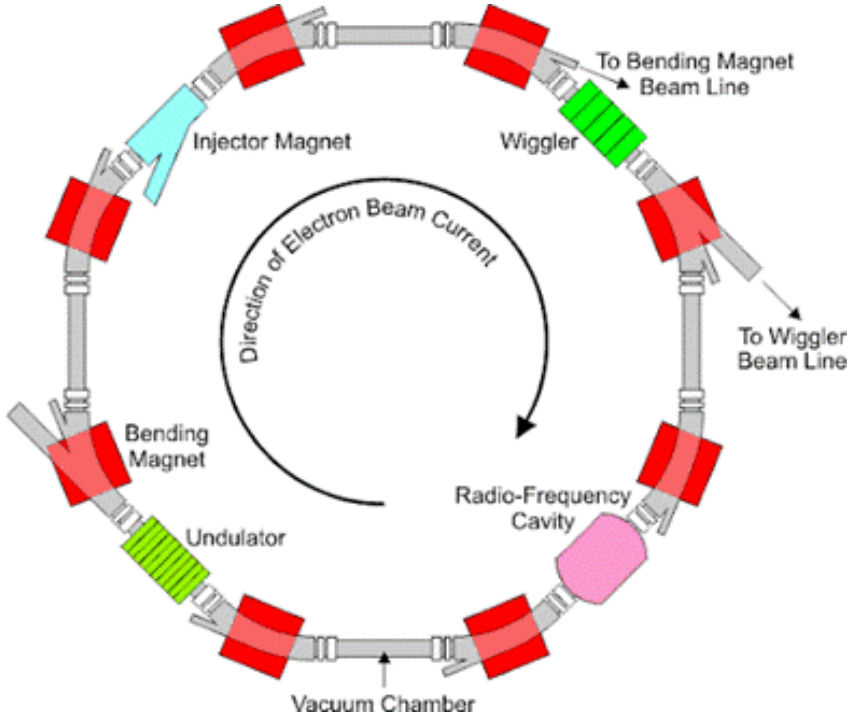

Source: ALS

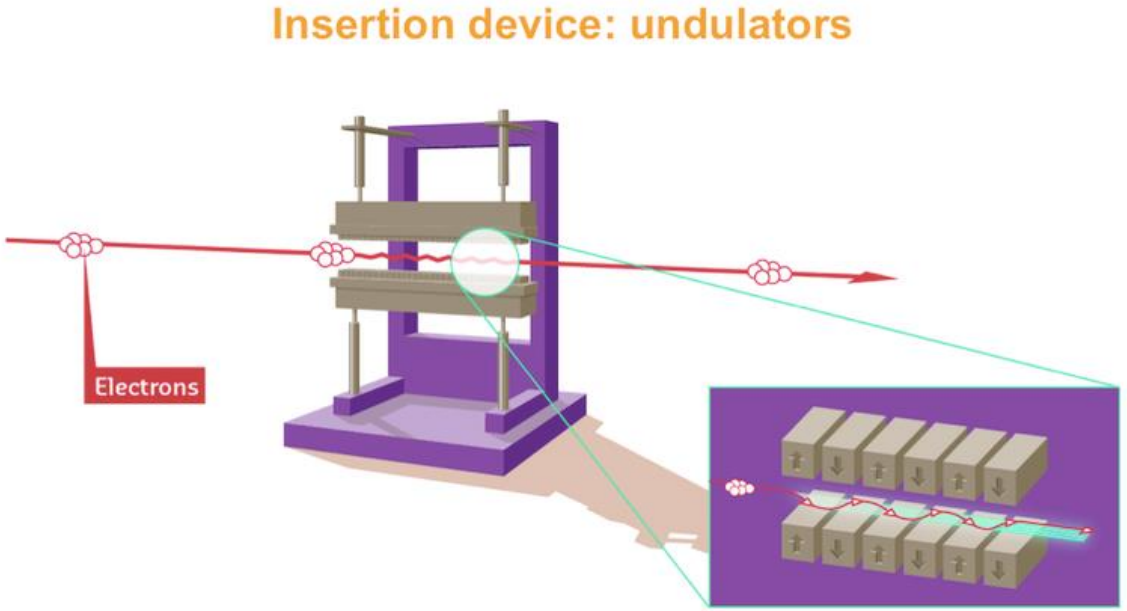

Source: ESRF

$$\sigma = \sqrt{\frac{3}{4\pi}\frac{1+(K^2/2)}{\gamma^2 nN}} \approx \frac{1}{\gamma}\frac{1}{\sqrt{nN}}$$

Bending Magnet

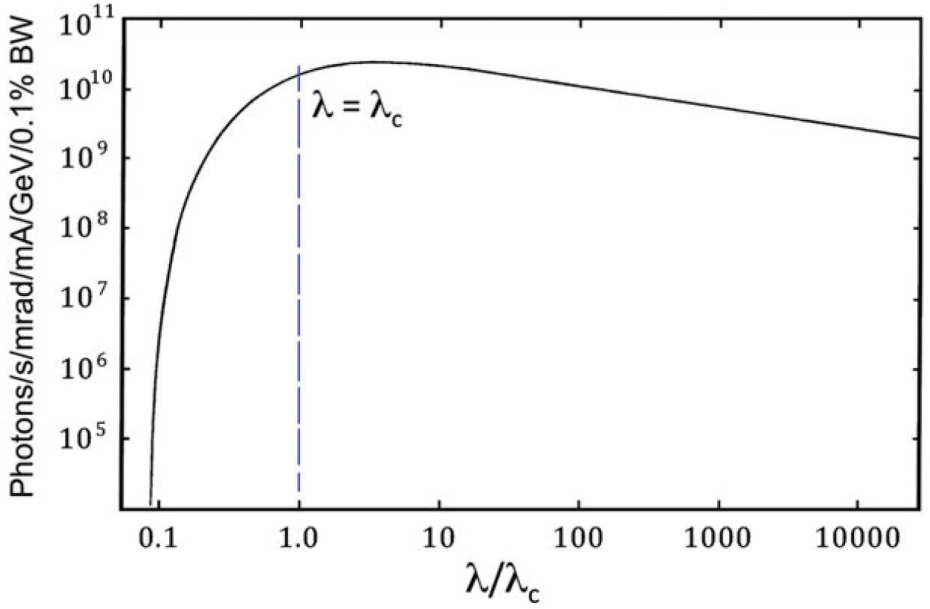

$$\lambda_c = \left(\frac{4}{3}\right)\pi R\gamma^{-3}$$

$$R = 3.34E(GeV)B^{-1}$$

Undulator

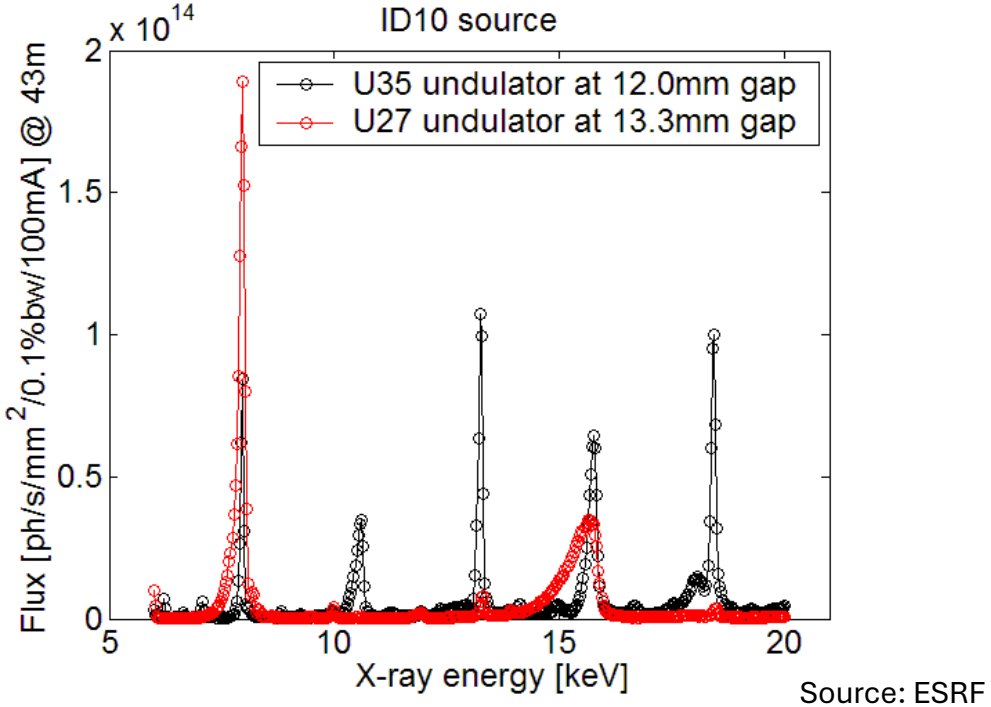

Source: ESRF

$$\lambda = \frac{\lambda_u}{2\gamma^2}\left(1 + \frac{K^2}{2} + \gamma^2\theta^2\right).$$

Standard ID – horizontal polarization

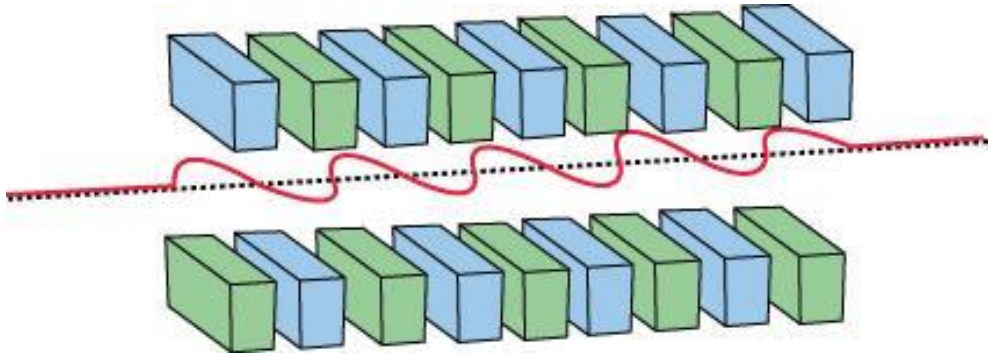

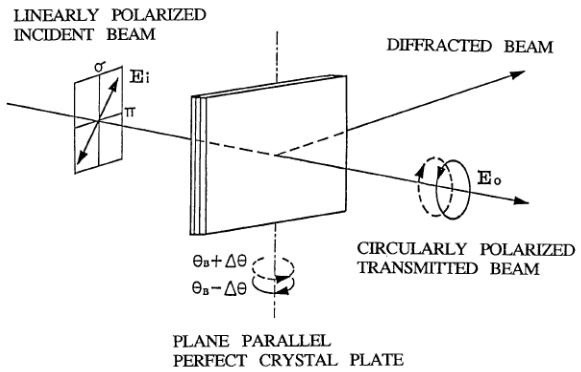

Apple II – variable polarization

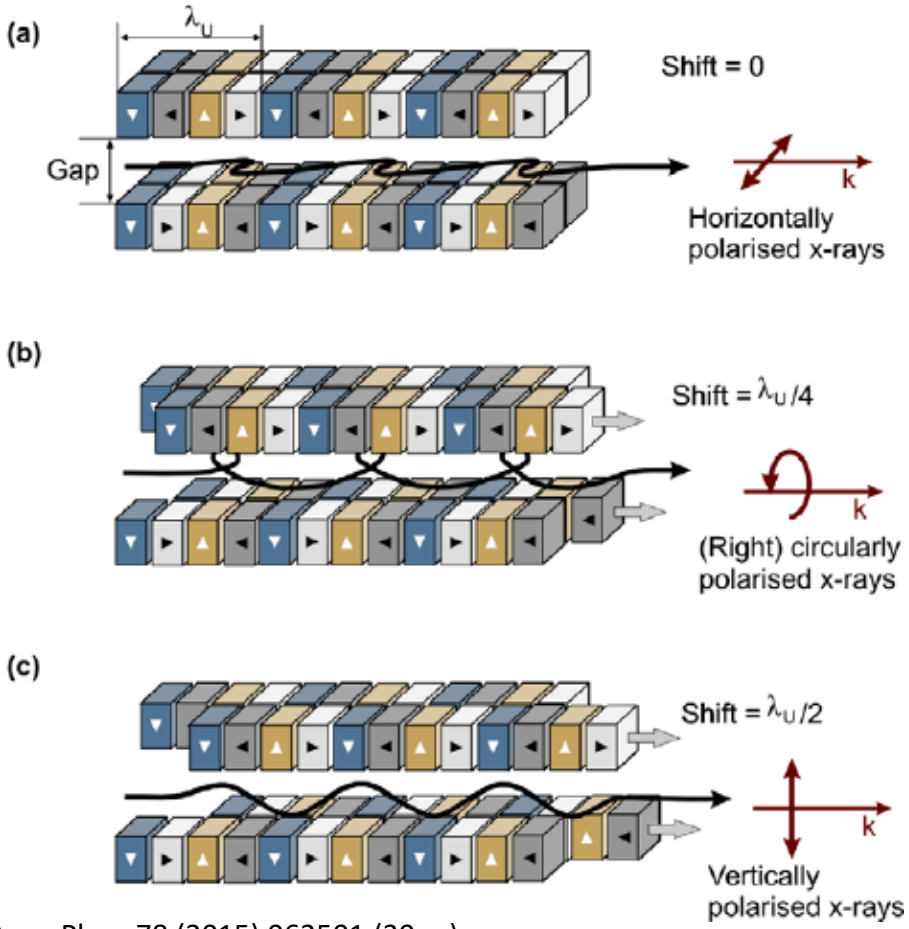

Rep. Prog. Phys. 78 (2015) 062501 (30pp)

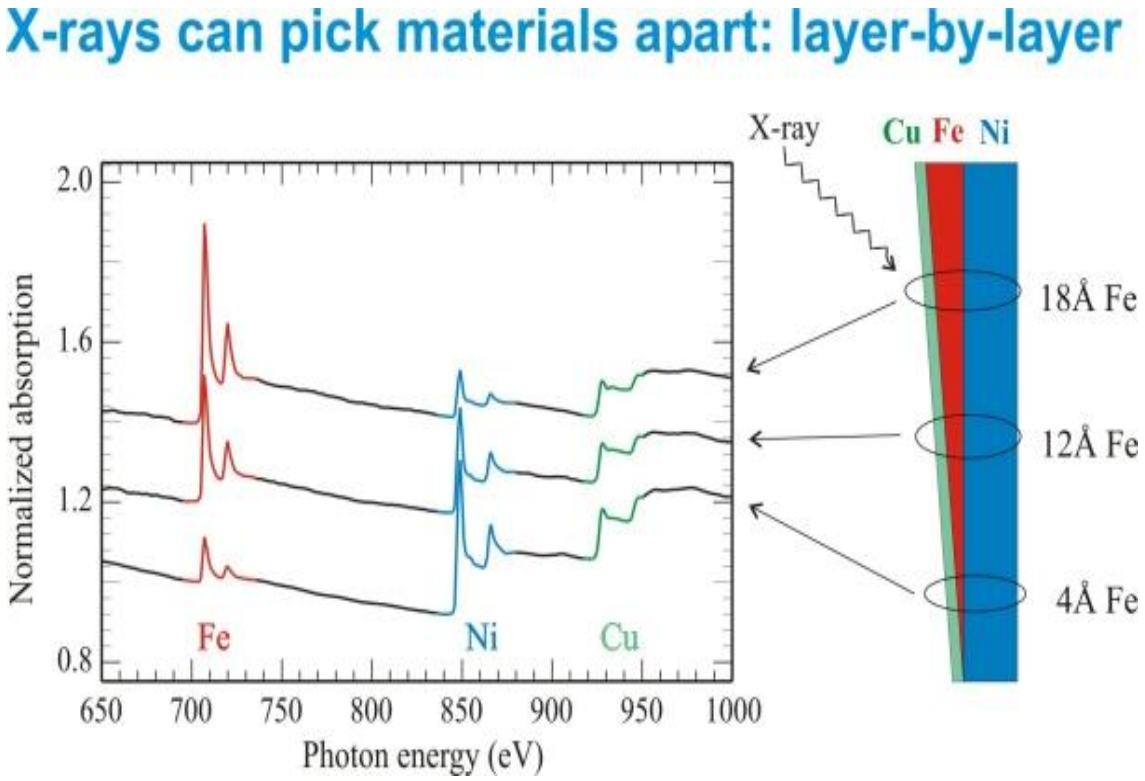

J. Stöhr and R. Nakajima, IBM J. Res. Develop. 42, 1998

X-ray Absorption Spectroscopy

- element specificity
- chemical state

Linearly Polarized X-rays

- orientation of molecules
- spin - orbit interaction
- magnetic anisotropy

Circularly Polarized X-rays

- orientation and size of the magnetic moments
- separate determination of orbital and spin moments

X-ray Absorption Spectroscopy

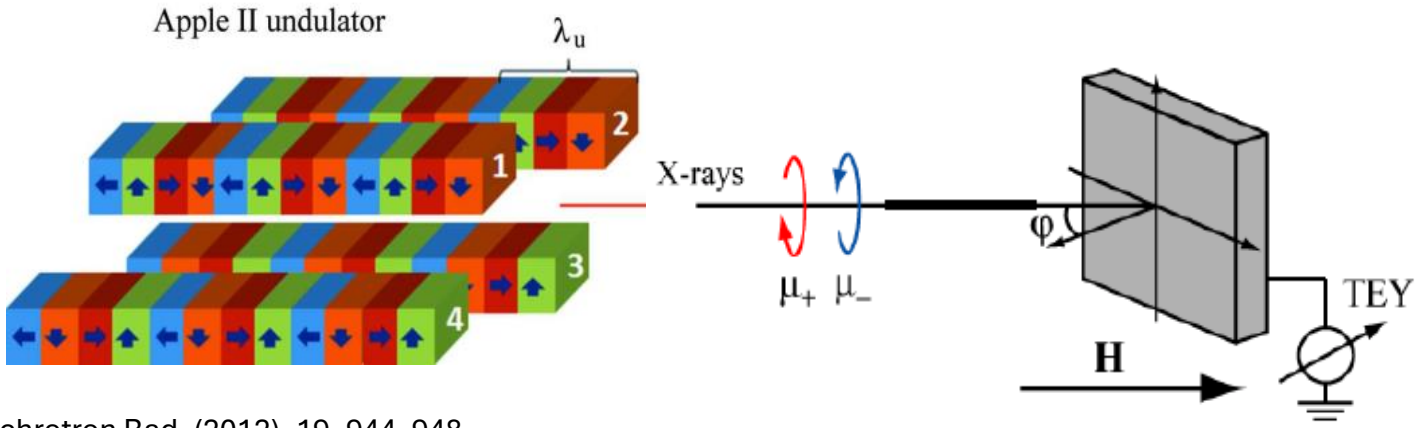

$I_s \alpha \mu$

x-ray absorption cross-section

J. Synchrotron Rad. (2012). 19, 944–948

https://www-ssrl.slac.stanford.edu/dichroism/xdsm/

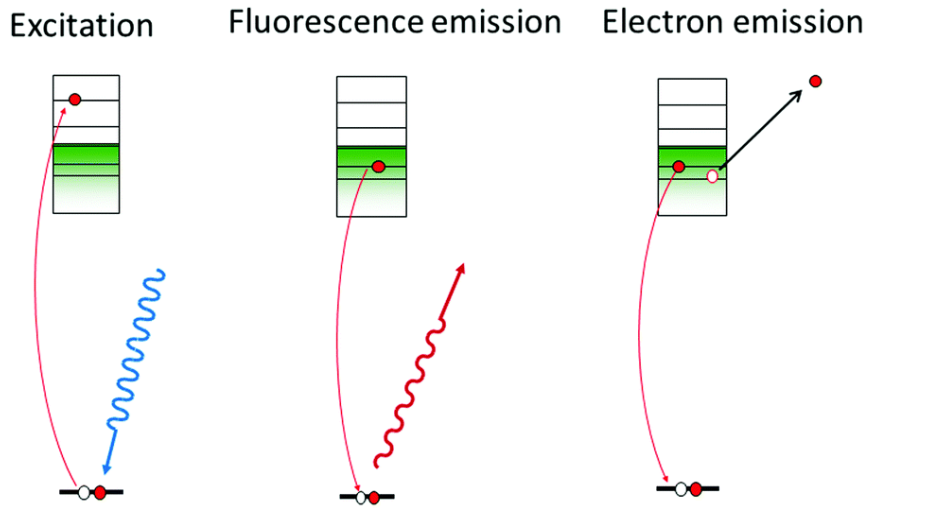

Chem. Soc. Rev. (2017) 46 (1): 102–125.

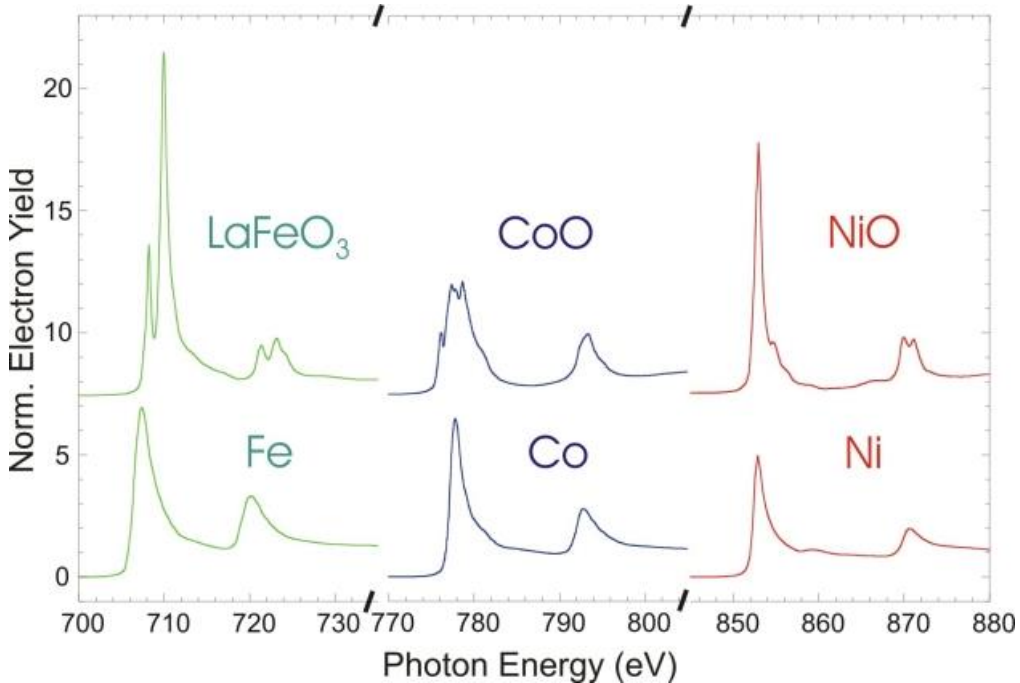

Matter - Photon interaction

$$W_{fi} = \frac{P_{fi}}{t} = \frac{2\pi}{\hbar}|\langle f|T|i\rangle|^2\delta(E_f - E_i - \hbar\omega)$$

Fermi's Golden Rule

$$|\psi\rangle = |\phi\rangle + \frac{1}{E - H_0 + i\epsilon}V|\psi\rangle$$

Lippmann-Schwinger equation

$$V|\psi\rangle = V|\phi\rangle + V\frac{1}{E - H_0 + i\epsilon}V|\psi\rangle$$

$$V|\psi\rangle = T|\phi\rangle$$

$$T|\phi\rangle = V|\phi\rangle + V\frac{1}{E - H_0 + i\epsilon}T|\phi\rangle$$

$$T = H_{int} + H_{int}\frac{1}{E_i - H + i\Gamma/2}T$$

$$T = H_{int} + H_{int}GH_{int} + H_{int}GH_{int}GH_{int} + \cdots$$

In the **First Born Approximation** the transition operator, T, is given by

$$T = H_{int}$$

so that the absorption coefficient, μ, is given by

$$\mu \propto \left|\langle\psi_f|H_{int}|\psi_i\rangle\right|^2$$

$$H_0 = \frac{\mathbf{p}^2}{2m} + V(\mathbf{r}) \qquad \mathbf{p} \longrightarrow \mathbf{p} + e\mathbf{A} \qquad H = \frac{1}{2m}(\mathbf{p} + e\mathbf{A}) \cdot (\mathbf{p} + e\mathbf{A}) + V(\mathbf{r})$$

$$H = \overbrace{\left[\frac{\mathbf{p}^2}{2m} + V(\mathbf{r})\right]}^{H_0} + \overbrace{\left[\frac{e}{m}\mathbf{A}\cdot\mathbf{p} + \frac{e^2}{2m}\mathbf{A}^2\right]}^{H_{int}}$$

The operator **A** is linear in the annihilation and creation operators so it can either destroy or create a photon. XAS corresponds to the former.

$$\boldsymbol{A}(r,t) = \sum_{k,q} \sqrt{\frac{\hbar}{2\varepsilon_0 V \omega_k}} \varepsilon_{k,q} \left(a_{k,q} e^{i(\boldsymbol{k}\cdot\boldsymbol{r} - \omega_k t)} + a_{k,q}^{\dagger} e^{-i(\boldsymbol{k}\cdot\boldsymbol{r} - \omega_k t)} \right)$$

k = wavevector, q = polarisation

$$H_{int} = \frac{e}{m}\left[A_0 \boldsymbol{\varepsilon_q} \cdot \boldsymbol{p} e^{i(k\cdot r - \omega t)}\right]$$

For a single wavevector and constants contained within A_0

In the electric dipole approximation $\exp(i\boldsymbol{k}\cdot\boldsymbol{r}) \approx 1$

$$e^{i\vec{k}\cdot\vec{r}} = 1 + i\vec{k}\cdot\vec{r} - \frac{1}{2}\left(\vec{k}\cdot\vec{r}\right)^2 + \cdots$$

$$[r, H] = \frac{1}{2m}[r, p^2]$$

$$[A, BC] = [A, B]C + B[A, C]$$

$$[r, H] = \frac{i\hbar p}{m}, \quad p = \frac{m}{i\hbar}[r, H]$$

$$\langle \boldsymbol{f}|\boldsymbol{H}|\boldsymbol{i}\rangle = \frac{\boldsymbol{e}}{\boldsymbol{m}}\boldsymbol{A}(\boldsymbol{t})\epsilon_q\langle \boldsymbol{f}|\boldsymbol{p}|\boldsymbol{i}\rangle$$

$$\langle f|\mathrm{p}|i\rangle = \frac{m}{i\hbar}\langle f|rH - Hr|i\rangle$$

$$\langle f|p|i\rangle = \frac{m}{i\hbar}\langle f|rH - Hr|i\rangle = \frac{m}{i\hbar}\left(E_i - E_f\right)\langle f|r|i\rangle$$

$$\langle f|p|i\rangle = im\omega_{fi}\langle f|r|i\rangle$$

$$H = A_0 r\cdot\epsilon_q[exp(-i\omega t)]$$

$$\langle \boldsymbol{f}|\boldsymbol{H}|\boldsymbol{i}\rangle = \mathrm{i}\boldsymbol{e}\boldsymbol{\omega}_{\boldsymbol{fi}}\boldsymbol{A}\langle \boldsymbol{f}|\boldsymbol{\epsilon}_{\boldsymbol{q}}\cdot\boldsymbol{r}|\boldsymbol{i}\rangle$$

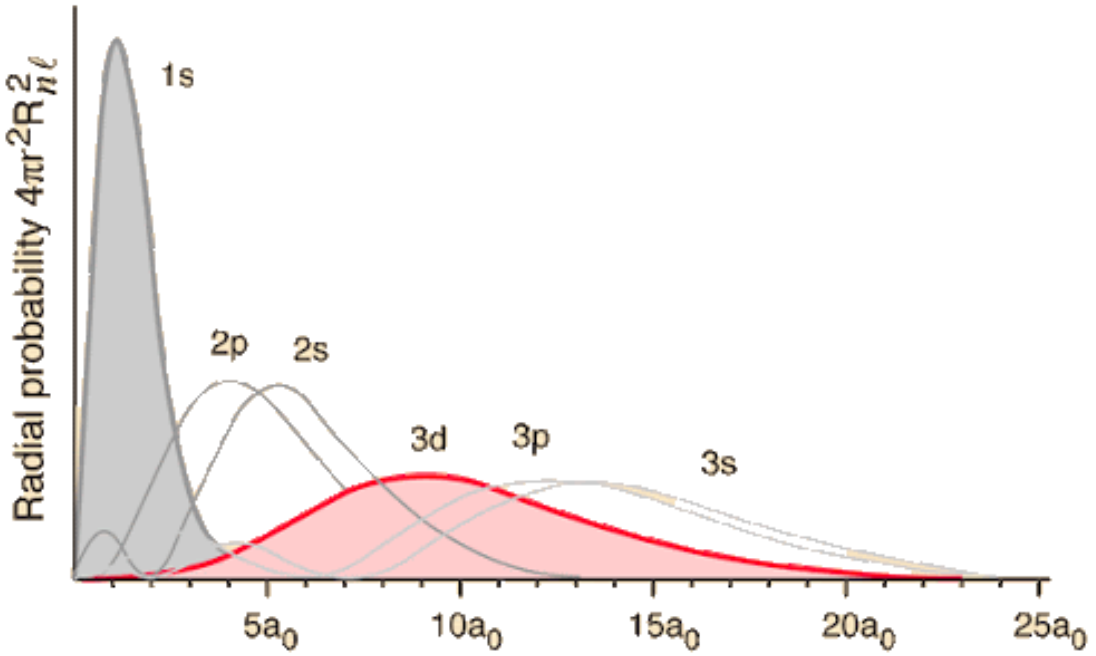

$$|\mathrm{i}\rangle = \mathrm{R_i(r)}\left|\mathrm{l_c}, \mathrm{m_c}; \mathrm{s} = \tfrac{1}{2}, \mathrm{m_s}\right\rangle \qquad |\mathrm{f}\rangle = \mathrm{R_f(r)}\left|\mathrm{l}, \mathrm{m_l}; \mathrm{s} = \tfrac{1}{2}, \mathrm{m_s}\right\rangle$$

Wigner – Eckart Theorem

Wigner 3j symbol

$$\left\langle j', m' \left| T_q^{(k)} \right| j, m \right\rangle = (-1)^{j'-m'} \begin{pmatrix} j' & k & j \\ -m' & q & m \end{pmatrix} \langle j' \| T^{(k)} \| j \rangle$$

RME

$T_q^{(k)}$ is a spherical tensor operator of rank *k* and component *q*.

In the electric dipole approximation *k* = 1 and *q* = 0, ± 1 for linear (0) and circular polarised light (±1).

Wigner 3j symbol calculation

$$\begin{pmatrix} j_1 & j_2 & j_3 \\ m_1 & m_2 & m_3 \end{pmatrix} = \Delta(j_1, j_2, j_3) \sqrt{(j_1+m_1)!\,(j_1-m_1)!\,(j_2+m_2)!\,(j_2-m_2)!\,(j_3+m_3)!\,(j_3-m_3)!}$$

$$\times \sum_t \frac{(-1)^{t+j_1-j_2-m_3}}{t!\,(j_3-j_2+t+m_1)!\,(j_3-j_1+t-m_2)!\,(j_1+j_2-j_3-t)!\,(j_1-t-m_1)!\,(j_2-t+m_2)!}$$

$$\Delta(j_1, j_2, j_3) = \sqrt{\frac{(j_1+j_2-j_3)!\,(j_1-j_2+j_3)!\,(-j_1+j_2+j_3)!}{(j_1+j_2+j_3+1)!}}$$

These can be calculated automatically within sympy.physics.wigner or Wolfram Alpha

Matter - Photon interaction

$$P_q^{(1)} = r \cdot \varepsilon_q$$

Electric dipole operator

$$C_q^{(k)} = \sqrt{\frac{4\pi}{2k+1}} Y_k^q(\theta, \phi)$$

Normalised Spherical Harmonic (Racah operator)

$$P_0^{(1)} = z = rC_0^{(1)} = r\sqrt{\frac{4\pi}{3}} Y_{1,0}$$

Electric dipole operator (linear polarization) written in terms of Racah operator

Wigner "parity" 3j symbol

$$\langle l' \| C^{(k)} \| l \rangle = (-1)^{l'} \sqrt{(2l'+1)(2l+1)} \begin{pmatrix} l' & k & l \\ 0 & 0 & 0 \end{pmatrix}$$

Reduced Matrix Element

Selection Rules

$$\left\langle l', m' \left| C_q^{(1)} \right| l, m \right\rangle = (-1)^{l'-m'} \begin{pmatrix} l' & 1 & l \\ -m' & q & m \end{pmatrix} \langle l' \| C^{(1)} \| l \rangle$$

Primary 3j symbol

$$\begin{pmatrix} l' & 1 & l \\ -m' & q & m \end{pmatrix}$$

Rule 1

$$-m' + q + m = 0;\ m' - m = q$$

$$\Delta m = m' - m = 0, \pm 1$$

Rule 2

$$[|l - 1| \leq l' \leq l + 1]$$

$$\Delta l = 0, -1, or + 1$$

$$\left\langle l', m' \left| C_q^{(1)} \right| l, m \right\rangle = (-1)^{l'-m'} \begin{pmatrix} l' & 1 & l \\ -m' & q & m \end{pmatrix} \langle l' \| C^{(1)} \| l \rangle$$

RME Parity 3j symbol

$$\langle l' \| C^{(1)} \| l \rangle \propto \begin{pmatrix} l' & 1 & l \\ 0 & 0 & 0 \end{pmatrix}$$

The parity rule for a 3-j symbol with all zeros on the bottom is that the top row must sum to an **even integer**

$l' + 1 + l = \text{even};\ l' + l = \text{odd}$

Two cases $\Delta l = 0;\quad \Delta l = \pm 1$

$\Delta l = 0$	$\Delta l = \pm 1$
$l' + l = 2l = \text{even}$	$l' + l = 2l \pm 1 = \text{odd}$
forbidden	*allowed*

Electric dipole selection rules

$$\Delta m = 0, \pm 1$$

$$\Delta l = \pm 1$$

The dipole operator can now be written in terms of Spherical Harmonics [Racah's tensor operators], where $Y_{l,m}$ are the spherical harmonics)

$$P_q^{(1)} = r \cdot \varepsilon_q$$

q = 0 ⇒ linear polarisation
q = ± 1 ⇒ circular polarisation

$$P_{\pm 1}^{(1)} = \mp \frac{1}{\sqrt{2}}(x + iy) = rC_{\pm 1}^{(1)} = r\sqrt{\frac{4\pi}{3}}Y_{1,\pm 1}$$

$$P_0^{(1)} = z = rC_0^{(1)} = r\sqrt{\frac{4\pi}{3}}Y_{1,0}$$

The photon absorption generates a transition from an initial core level to a final level close to the Fermi level: note the spin is not affected

$$|\mathrm{i}\rangle = \mathrm{R_i(r)}\left|\mathrm{l_c}, \mathrm{m_c}; \mathrm{s} = \tfrac{1}{2}, \mathrm{m_s}\right\rangle \longrightarrow |\mathrm{f}\rangle = \mathrm{R_f(r)}\left|\mathrm{l}, \mathrm{m_l}; \mathrm{s} = \tfrac{1}{2}, \mathrm{m_s}\right\rangle$$

$$\begin{aligned}
\langle l+1, m| C_0^{(1)} |l, m\rangle &= \sqrt{\frac{(l+1)^2 - m^2}{(2l+3)(2l+1)}} \\
\langle l-1, m| C_0^{(1)} |l, m\rangle &= \sqrt{\frac{l^2 - m^2}{(2l-1)(2l+1)}} \\
\langle l+1, m+1| C_1^{(1)} |l, m\rangle &= \sqrt{\frac{(l+m+2)(l+m+1)}{2(2l+3)(2l+1)}} \\
\langle l-1, m+1| C_1^{(1)} |l, m\rangle &= -\sqrt{\frac{(l-m)(l-m-1)}{2(2l-1)(2l+1)}} \\
\langle l+1, m-1| C_{-1}^{(1)} |l, m\rangle &= \sqrt{\frac{(l-m+2)(l-m+1)}{2(2l+3)(2l+1)}} \\
\langle l-1, m-1| C_{-1}^{(1)} |l, m\rangle &= -\sqrt{\frac{(l+m)(l+m-1)}{2(2l-1)(2l+1)}}
\end{aligned}$$

J. Stöhr and H. C. Siegmann, *Magnetism: From Fundamentals to Nanoscale Dynamics*

Matter - Photon interaction

$$\left\langle f \left| P_q^{(1)} \right| i \right\rangle = \delta(m_s', m_s) \langle R_{n',l}(r) | r | R_{n,c}(r) \rangle \sum_{m_c, m_l} e_\alpha^q \left\langle l, m_l \left| C_{\mathrm{q}}^{(1)} \right| c, m_c \right\rangle$$

$$\mathrm{R} = \langle R_{n',l}(r) | r | R_{n,c}(r) \rangle$$

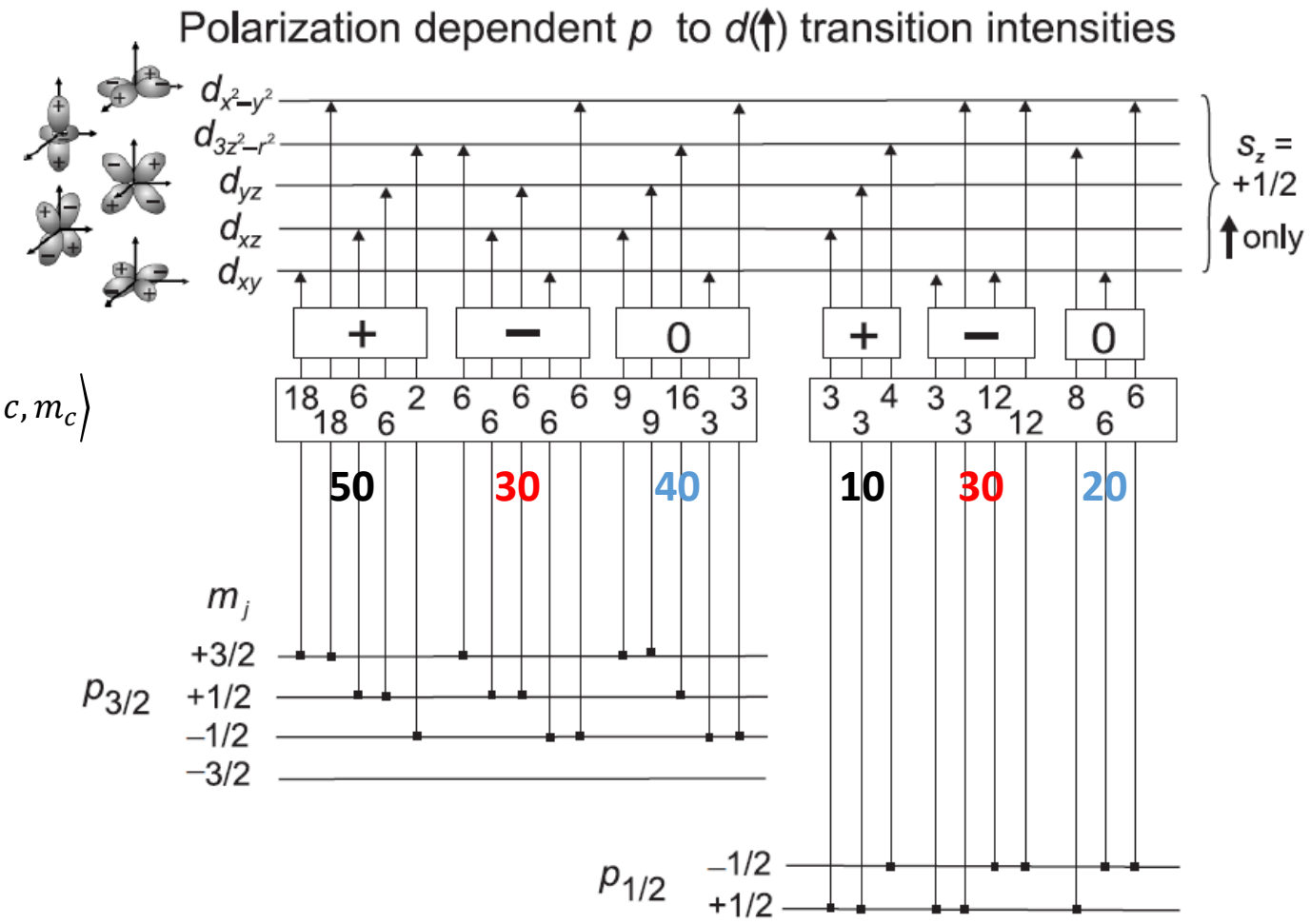

J. Stöhr and H. C. Siegmann, *Magnetism: From Fundamentals to Nanoscale Dynamics*

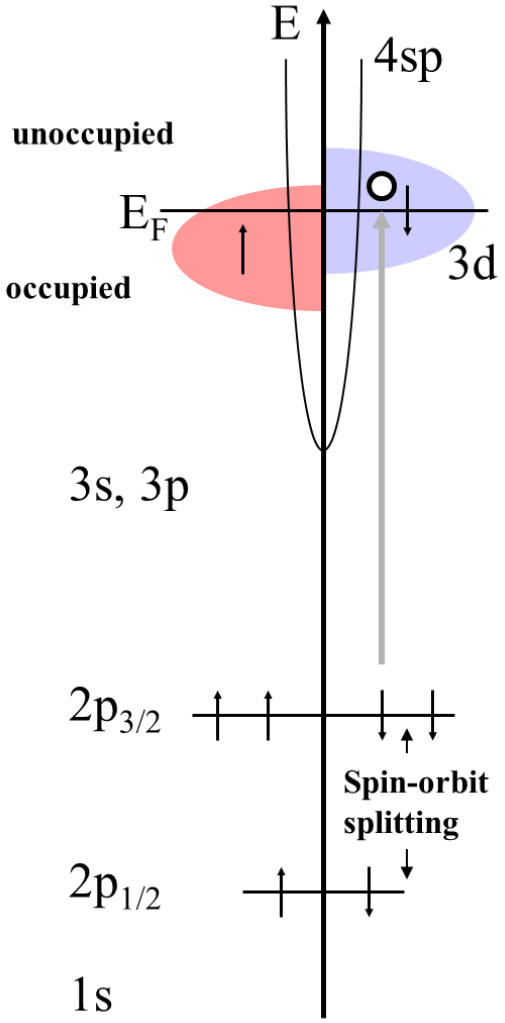

Fermi's golden rule :

$\mu^{\pm} \propto |\langle f|\varepsilon.p|i\rangle|^2 \rho^{\pm}(E)$, dipole transition

Dipole selection rules:

ΔL	=	-1, +1	(p $\rightarrow$ **s,d)**
ΔJ	=	-1, 0, +1	
ΔM_J	=	-1, 0, +1	
Polarization q		+1, 0, -1 (σ^+, π, σ^-)	
L_2:		$2p_{1/2} \rightarrow 4s, 3d_{3/2}$	
L_3:		$2p_{3/2} \rightarrow 4s, 3d_{3/2}, 3d_{5/2}$	

In a solid, an absorbing atom is surrounded by neighbouring ions (ligands). These neighbours create a highly directional electrostatic field that breaks the spherical symmetry of the isolated atom. This splits the degenerate orbitals into different energy levels depending on how they align with the surrounding ions.

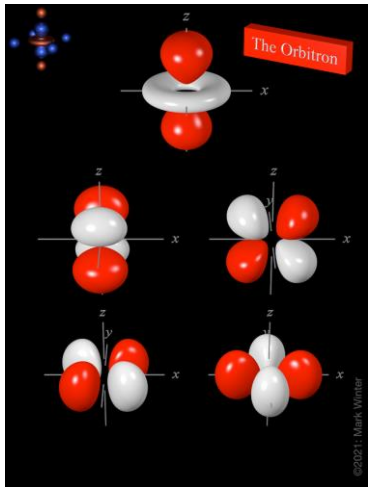

The Crystal Field Hamiltonian:

$$H_{CF} = -e\sum V(\mathbf{r_i}) \qquad V(\mathbf{r}) = \sum A_L^M r^L Y_L^M(\theta,\phi)$$

$$V^{oct} = \left(\frac{7}{2}\right)D_4\left[Y_4^0 + \sqrt{\frac{5}{14}}(Y_4^4 + Y_4^{-4})\right] + \left(\frac{3}{4}\right)D_6\left[Y_6^0 - \sqrt{\frac{7}{2}}(Y_6^6 + Y_6^{-6})\right]$$

Lifts Degeneracy: Orbitals pointing directly at negatively charged ligands are pushed to higher energies due to electrostatic repulsion (e.g., the e_g vs. t_{2g} split in octahedral complexes).

Dictates Line Shape: Because the final states are now split in energy, a single atomic absorption line will branch into multiple distinct peaks.

Determines Ground State: The crystal field strength dictates whether the material is high-spin or low-spin, fundamentally changing the initial state $|i\rangle$

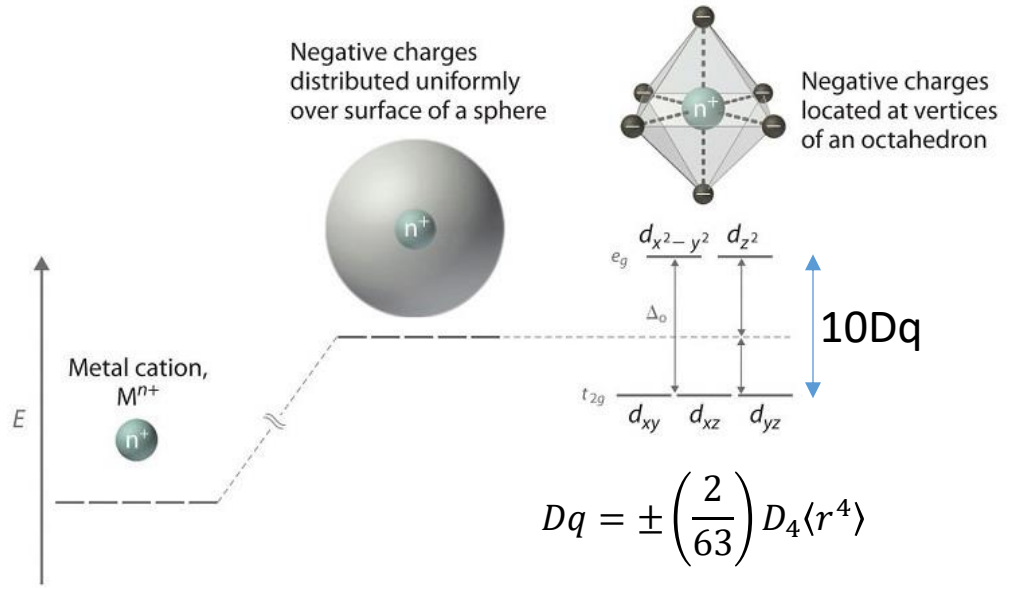

$$Dq = \pm\left(\frac{2}{63}\right)D_4\langle r^4\rangle$$

$$D_4 = \left(\frac{35}{4}\right)Ze^2/a^6$$

See Magnetism: from atoms to solids H. Herper ESM 2026 for further detail

For ground states that are **A or E terms** (e.g., d^3, d^8, high-spin d^4), the angular momentum is completely quenched to first order.

For ground states that are **T terms** (e.g., d^1, high-spin d^6, d^7), the t_{2g} orbitals are asymmetrically filled. Because d_{xy}, d_{xz}, and d_{yz} can be rotated into one another by the angular momentum operator, a small amount of "circulation" is still possible, meaning they retain some intrinsic, unquenched orbital angular momentum.

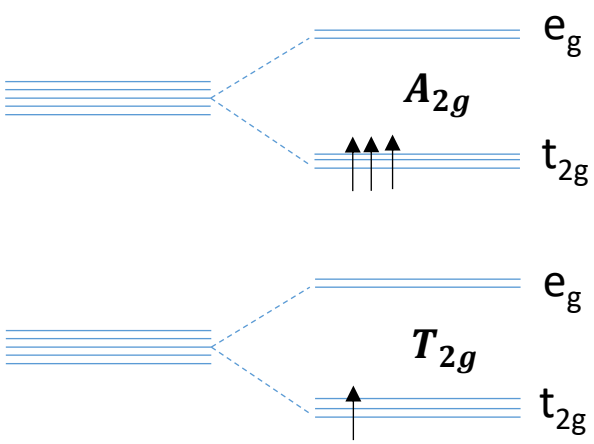

Addition of Spin – Orbit Coupling

Consider a system where the ground state is completely quenched, such as the A_{2g} ground state of a $Ni^{2+}(d^8)$ion. On its own, this state has no orbital angular momentum.
However, the spin-orbit coupling operator ($H_{SO} = \lambda \mathbf{L} \cdot \mathbf{S}$) acts as a perturbation. It takes an excited state with non-zero orbital angular momentum - like the T_{2g} state - and mixes it to the A_{2g} ground state.
The new ground state $|\psi_{gs}\rangle$ becomes:

$$|\psi_{gs}\rangle = |A_{2g}\rangle - \frac{2\lambda}{E_T - E_A}|T_{2g}\rangle$$

Because this new ground state now contains a small percentage of the T_{2g} character, the expectation value of the orbital angular momentum $\langle \mathbf{L} \rangle$ is no longer exactly zero. The quenching has been **partially lifted**.

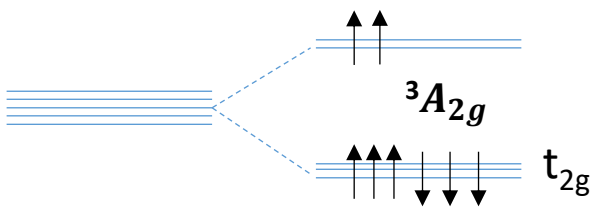

S = 1

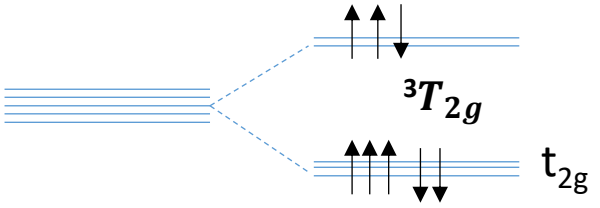

S = 1

So far, we have only considered isolated cations (insulator). What happens when we have an itinerant system such as BCC Fe?

1: BCC Fe has 8 nearest neighbours: configuration $[Ar]3d^6 4s^2$

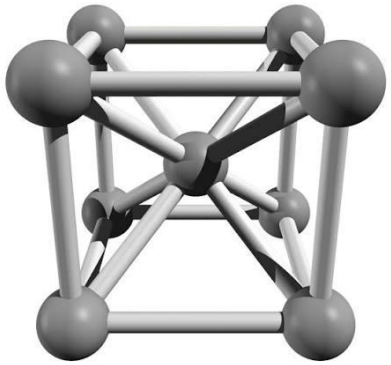

https://commons.wikimedia.org/wiki/File:Iron_bcc.png

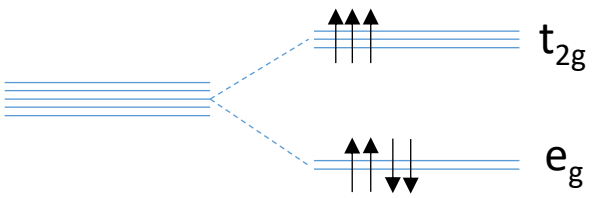

broadening + exchange

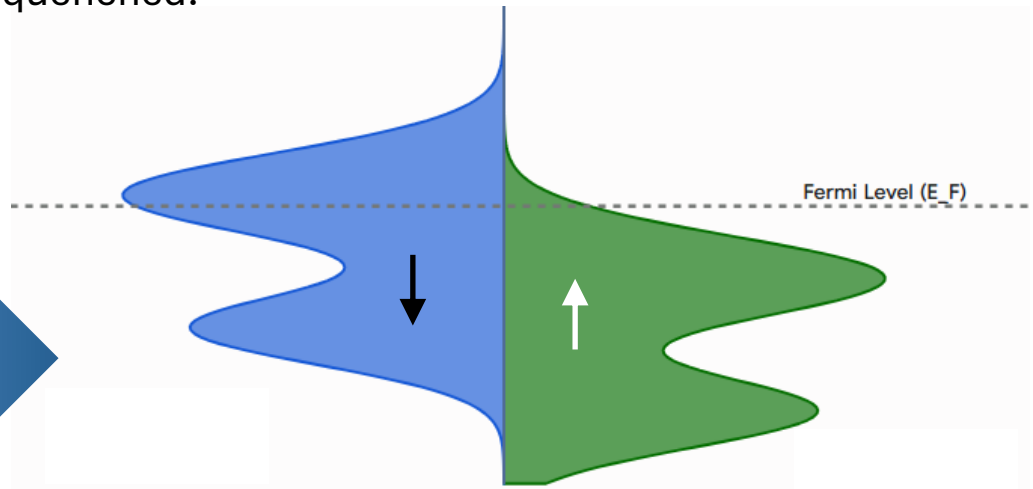

$\langle L \rangle = 0$

As this is a metallic system the number of electrons in the d-band is 7.4 (≈7). In the atomic picture (d^7 high spin case) the e_g orbitals are completely filled, the t_{2g} have 3 electrons (1/2 filled). $\langle L \rangle = 0$

However, in metallic FM systems the orbitals are broadened and exchange split. Therefore, for spin up electrons, the e_g and t_{2g} orbitals are filled (and spin down e_g) and the Fermi level sits in the spin down t_{2g}. The orbital moment is only partially quenched.

Many body effects – Multiplet Theory

When an x-ray ejects a core electron, it leaves behind a localized, positively charged "core hole."
The remaining valence electrons interact with this core hole (especially if the overlap of wavefunctions is large) and with each other.
We must treat the initial and final states as total multi-electron configurations (e.g., transition from $3d^n$ to $2\mathrm{p}^5 3\mathrm{d}^{\mathrm{n}+1}$).

The Electron-Electron Interaction Hamiltonian:

$$H_{ee} = \sum_{i<j} \frac{e^2}{4\pi\epsilon_0 |\mathbf{r_i} - \mathbf{r_j}|}$$

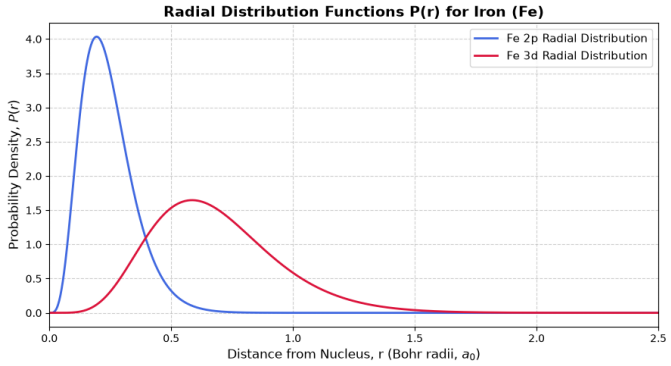

To solve, the Coulomb repulsion and quantum Exchange interactions are parameterised into **Slater Integrals**:

- **F^k (Direct Coulomb):** The classical electrostatic repulsion between electron clouds.
- **G^k (Exchange):** The purely quantum effect arising from the Pauli exclusion principle, stabilizing states with parallel spins.

Key Takeaways for XAS:

- **Multiplet Splitting:** The strong Coulomb (*U*) and Exchange (*J*) interactions between the core hole and valence electrons modify the simple orbital picture into many highly specific energy levels (multiplets).
- **Domination of L- and M-edges:** Many-body effects dominate the X-ray Absorption for transition metal L-edges and rare-earth M-edges.
- **Failure of Single-Particle DFT:** Standard Density Functional Theory (DFT) often fails here; simulating these spectra requires specialized Charge Transfer Multiplet (CTM) calculations.

See Magnetism: from atoms to solids H. Herper ESM 2026 for further detail

Core – hole interactions

The core hole interactions include:

κ1: the core-hole potential.

κ2: the core-hole lifetime and its associated broadening.

κ3: the core-hole spin–orbit coupling.

κ4: core-hole-induced screening effects, including charge transfer

κ5: the core hole–valence hole exchange interaction.

κ6: the higher order term of the core hole–valence hole exchange interaction.

κ7: core hole–valence hole multipole interactions

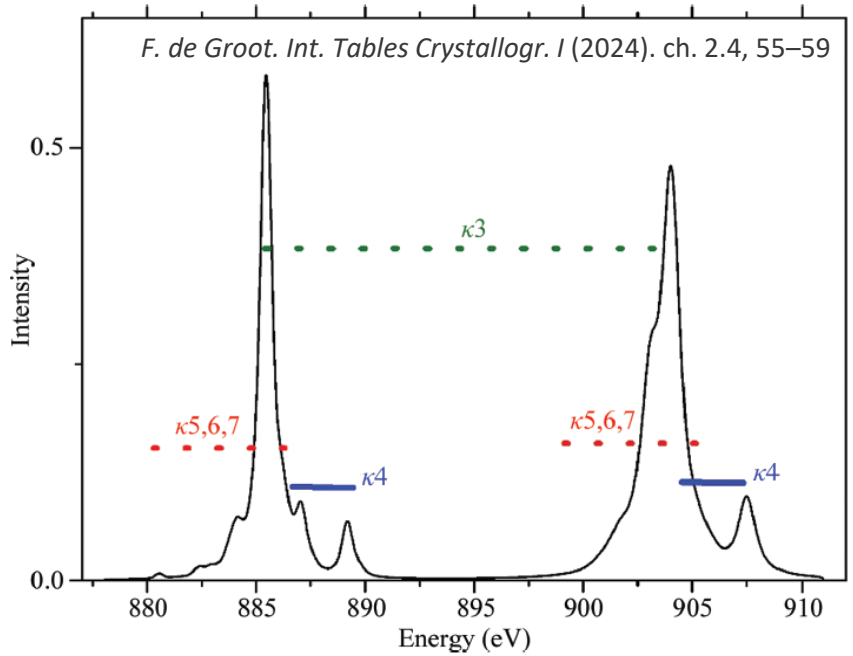

In the case of 1s X-ray absorption (K-edge) there are no multiplet effects and a single-particle density-functional theory or two-particle Bethe– Salpeter calculation is sufficient.

Multiplet theory is only important when (i) you have an open-shell system and (ii) the core hole contains an orbital moment

Magnetism is due to open *d* (Fe, Co, Ni) or *f* –shell systems (Gd). To probe them *directly* in XAS (dipole transition) we have L-edges (p → d) or M-edges (d → f). In these transitions the core hole contains an orbital moment. **Multiplet theory is key.**

Charge Transfer Multiplet Theory

To simulate real-world spectra (such as 2p → 3d transition at a metal L-edge), the total Hamiltonian is built as a sum of three core interactions:

$$H_{\mathrm{CTM}} = H_{\mathrm{atomic}} + H_{\mathrm{CF}} + H_{\mathrm{CT}}$$

$$H_{\mathrm{atomic}} = \sum_{i<j} \frac{e^2}{4\pi\epsilon_0 |\mathbf{r_i} - \mathbf{r_j}|} + \sum_i \zeta_i \mathbf{l_i} \cdot \mathbf{s_i}$$

$$H_{\mathrm{CF}} = \sum_i V_{\mathrm{CF}}(\mathbf{r_i})$$

$$H_{\mathrm{CT}} = \sum_k V_k \left(d_k^\dagger c_k + c_k^\dagger d_k \right)$$

Covalent mixing allows electrons to hop between metal and ligand orbitals. CTM expands initial $|\Psi_i\rangle$ and final $|\Psi_f\rangle$ states over a linear combination of configuration states involving ligand holes L

$$|\Psi_i\rangle = \alpha|3d^n\rangle + \beta|3d^{n+1}L\rangle + \gamma|3d^{n+2}L^2\rangle$$

$$|\Psi_f\rangle = \alpha'|2p^5 3d^{n+1}\rangle + \beta'|2p^5 3d^{n+2}L\rangle + \gamma'|2p^5 3d^{n+3}L^2\rangle$$

Energy Diagonalization and Spectra Generation

To construct the diagonal terms of the CTM interaction matrix, three scalar energy parameters are defined:

1.Charge Transfer Energy (Δ): Energy needed to transfer an electron between ligand valence band and metal d-shell:

$$\Delta = E(3d^{n+1}L) - E(3d^n)$$

2.On-site d-d Coulomb Repulsion (U_{dd}): Electrostatic penalty for double-occupying d-orbitals

3.Core-Hole Attraction (U_{dc}): Electrostatic pull exerted by the 2p core hole on the 3d shell in the final state.

In the final state, the presence of the core hole pulls the 3d energy levels downward, altering the effective charge transfer energy to:

$$\Delta_{\mathrm{f}} = \Delta + U_{dd} - U_{dc}$$

Charge Transfer Multiplet Theory

Software, such as Quanty or CTM4XAS, diagonalize H_{CTM} to find the exact multi-electron eigenvectors and energy eigenvalues, which are then evaluated using Fermi's Golden Rule to output the absorption spectrum:

$$I(\omega) = \sum_f \left|\langle \Psi_f | \epsilon \cdot r | \Psi_i \rangle\right|^2 \delta(E_f - E_i - \hbar\omega)$$

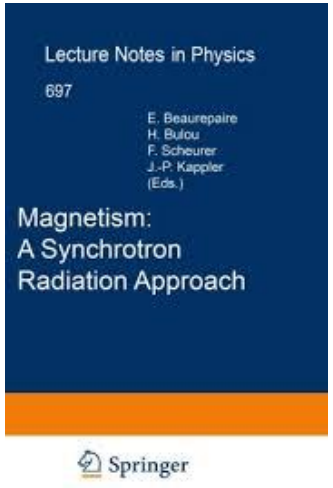

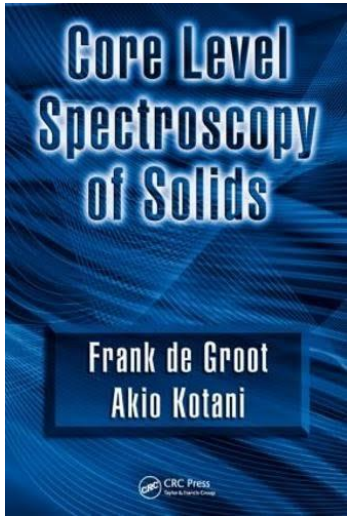

References

1: G. van der Laan. Hitchhikers Guide to Multiplet Calculations
2: G. van der Laan *et al*. X-ray magnetic circular dichroism - A versatile tool to study magnetism
3: F. de Groot. Core level Spectroscopy of Solids
4: J. Stöhr and H. C. Siegmann, *Magnetism: From Fundamentals to Nanoscale Dynamics*

X-ray Magnetic Circular Dichroism (XMCD)

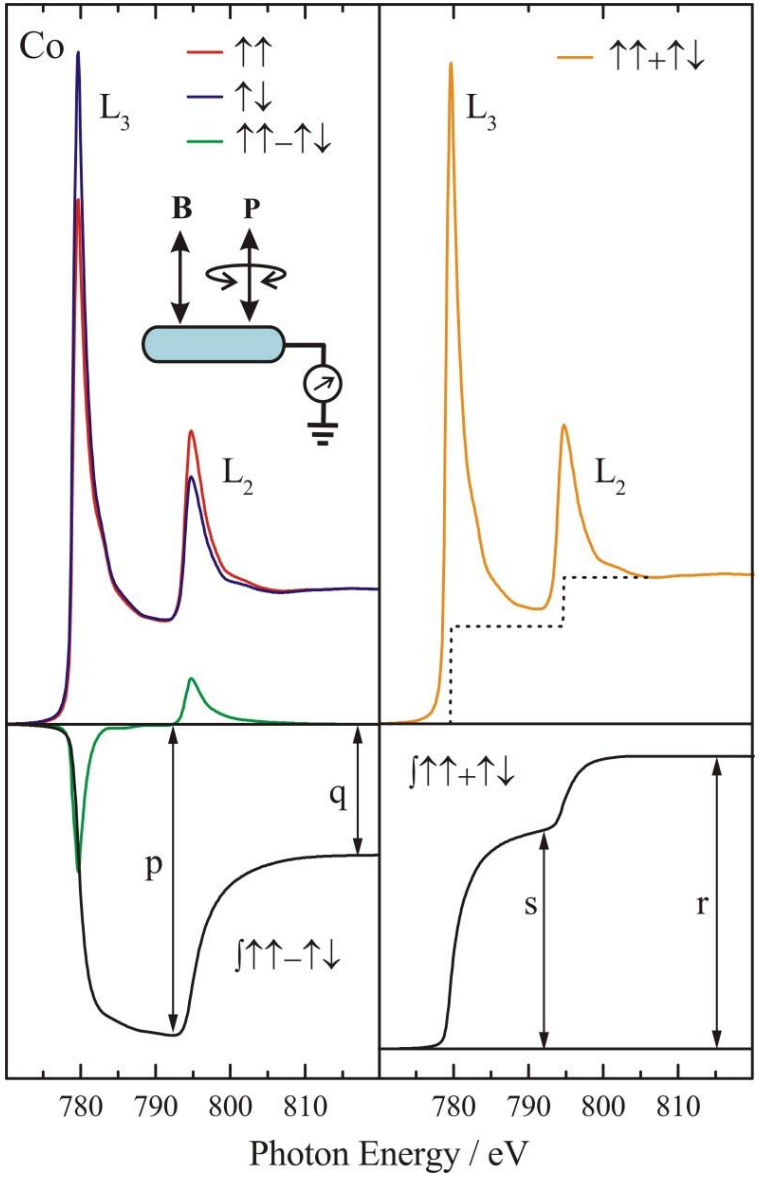

$$\mathrm{XMCD} = I^{\uparrow\downarrow} - I^{\uparrow\uparrow}$$

$$\Delta I_{L_3} = \mathcal{A}R^2 \sum_{n,m_j} \left|\left\langle d_n, \chi^+ \left| C^{(1)}_{-1} \right| p_{3/2}, m_j \right\rangle\right|^2 - \left|\left\langle d_n, \chi^+ \left| C^{(1)}_{+1} \right| p_{3/2}, m_j \right\rangle\right|^2 = -\frac{2}{9} AR^2 \qquad \mathcal{A} = 4\pi^2 \alpha_f \hbar\omega$$

The *two-step model* of XMCD:

• In the *first step*, circularly polarized X-rays generate photoelectrons with a spin and/or orbital momentum from a localized atomic inner shell.

• In the *second step*, the 3*d* shell serves as the detector of the spin or orbital momentum of the photoelectron. For maximum effect, the photon spin needs to be aligned with the magnetization direction.

Sum Rules

Number of *d*-holes $n_h \propto r$

Branching ratio $\langle \boldsymbol{l} \cdot \boldsymbol{s} \rangle / n_h = 2\text{-}3s/r$

Orbital moment $\langle \boldsymbol{L} \rangle = -4\, q\, n_h / 3r$

Spin moment $\langle \boldsymbol{S} \rangle + {}^7/_2 \langle \boldsymbol{T} \rangle = -(3p\text{-}2q)\, n_h / r$

Ratio $m_{orb} / m_{spin} = 2q / (9p - 6q)$

nature reviews methods primers
https://doi.org/10.1038/s43586-025-00397-9

Primer

Check for updates

X-ray magnetic circular dichroism

C. A. F. Vaz[1], G. van der Laan[2], S. A. Cavill[3], H. A. Dürr[4], A. Fraile Rodríguez[5,6], F. Kronast[7], W. Kuch[8], Ph. Sainctavit[9], G. Schütz[10], H. Wende[11], E. Weschke[12] & F. Wilhelm[13]

$$\left\langle f \left| P_q^{(1)} \right| i \right\rangle = \delta(m_s', m_s) \langle R_{n',l}(r) | r | R_{n,c}(r) \rangle \sum_{m_c, m_l} e_\alpha^q \left\langle l, m_l \left| C_{\mathrm{q}}^{(1)} \right| c, m_c \right\rangle$$

$$\mathrm{R} = \langle R_{n',l}(r) | r | R_{n,c}(r) \rangle$$

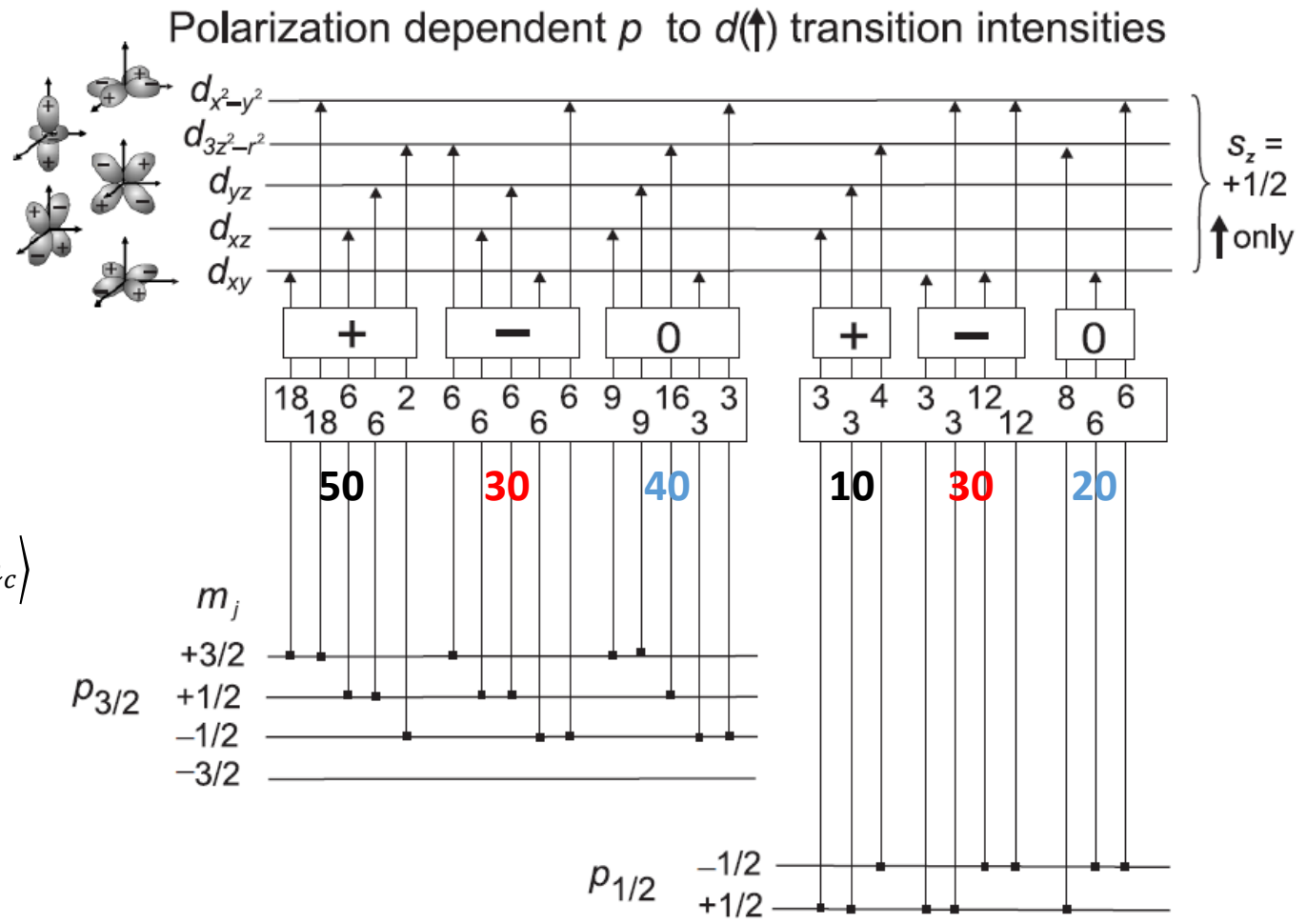

J. Stöhr and H. C. Siegmann, *Magnetism: From Fundamentals to Nanoscale Dynamics*

X-ray Magnetic Circular Dichroism (XMCD)

VOLUME 75, NUMBER 1 PHYSICAL REVIEW LETTERS 3 JULY 1995

Experimental Confirmation of the X-Ray Magnetic Circular Dichroism Sum Rules for Iron and Cobalt

C. T. Chen,[1] Y. U. Idzerda,[2] H.-J. Lin,[1,*] N. V. Smith,[1,†] G. Meigs,[1] E. Chaban,[1] G. H. Ho,[3,*] E. Pellegrin,[1] and F. Sette[1,‡]

High precision, $L_{2,3}$-edge photo-absorption and magnetic circular dichroism spectra of iron and cobalt were measured in transmission with in-situ grown thin films, eliminating experimental artifacts encountered by the indirect methods used in all previous measurements. The magnetic moments determined from the integrals of these spectra are found to be in excellent agreement (within 3%) for the orbital to spin moment ratios, and in good agreement (within 7%) for the individual moments, with those obtained from Einstein - de Haas gyromagnetic ratio measurements.

$$\mu x = -\ln(T) = -\ln\left(\frac{I_t}{I_0}\right)$$

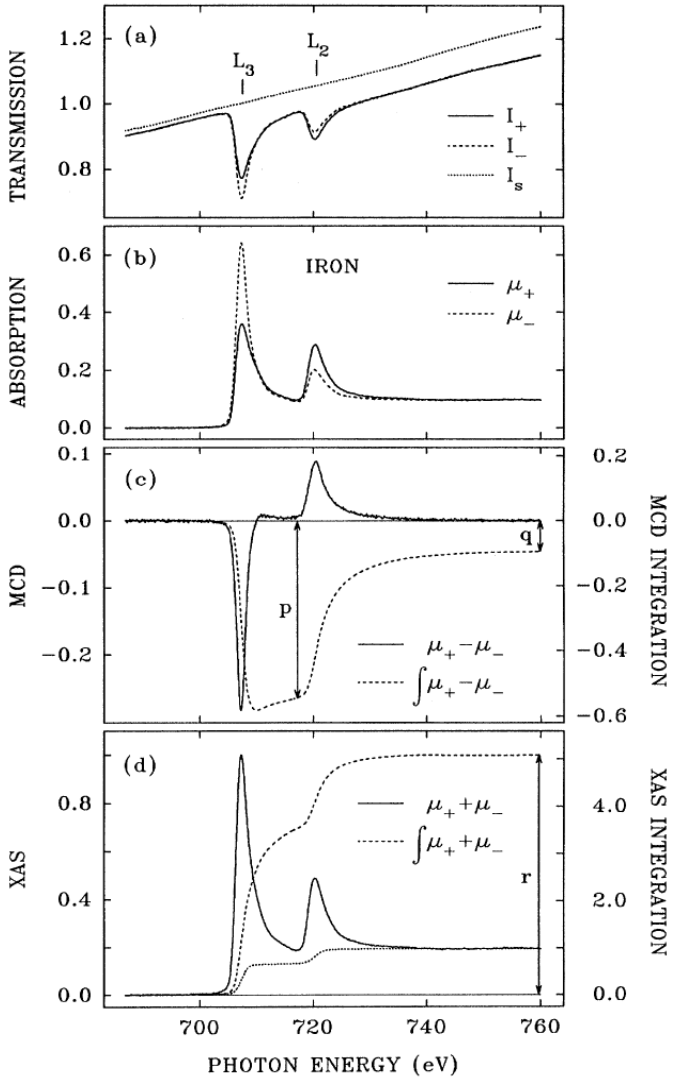

X-ray Magnetic Linear Dichroism (XMLD)

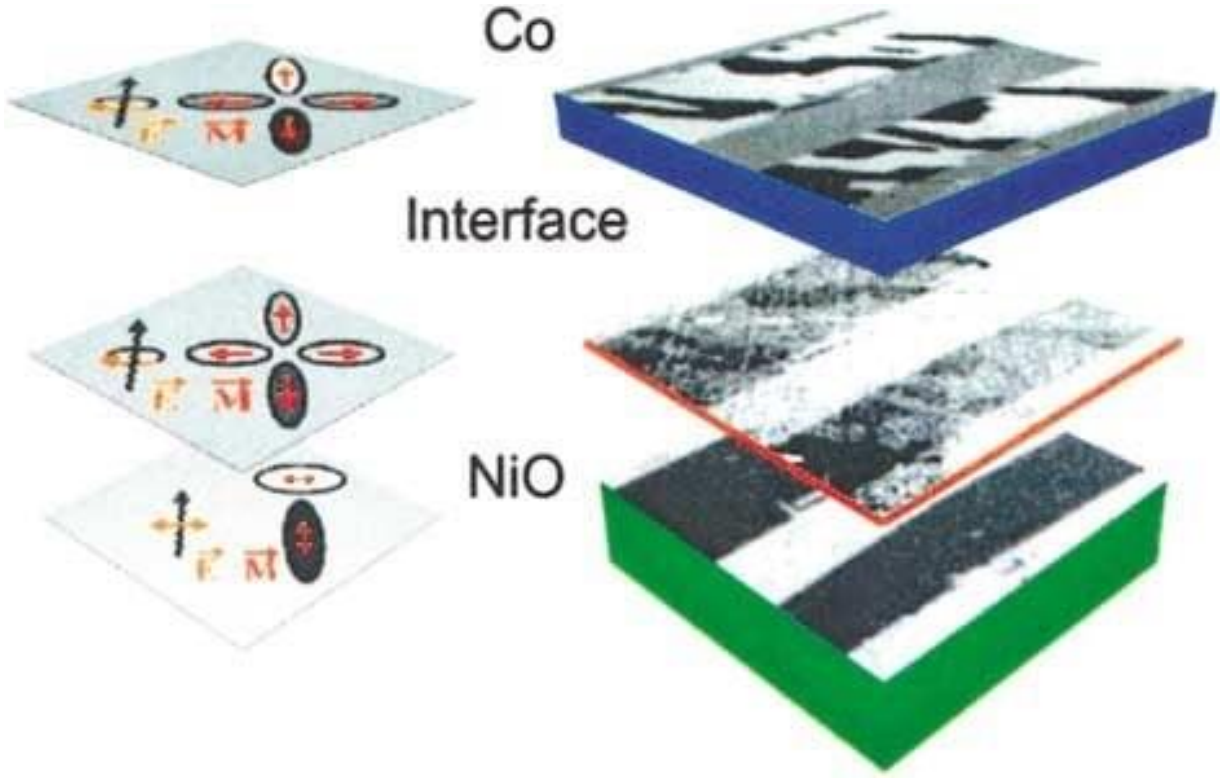

Phys. Rev. Lett. **87**, 247201 (2001)

Wigner-Eckart Expansion for Linear Polarization ($\Delta m = 0$)

The general transition matrix element is given by factoring out the geometric dependence (the 3-j symbol) from the fundamental physical properties of the atomic shells (the reduced matrix element):

$$\left\langle l', m \left| C_0^{(1)} \right| l, m \right\rangle = (-1)^{l'-m} \begin{pmatrix} l' & 1 & l \\ -m & 0 & m \end{pmatrix} \left\langle l' \left|\left| C^{(1)} \right|\right| l \right\rangle$$

Transition Type	Angular Matrix Element $\langle Y_{l',m\|}\cos\theta\|Y_{l,m}\rangle$	Intensity Factor (Matrix Element Squared)	Physical Implication for XMLD
$\Delta l = +1$ (e.g., 2p $\rightarrow$3d)	$\sqrt{\frac{(l-m+1)(l+m+1)}{(2l+1)(2l+3)}}$	$\frac{(l+1)^2 - m^2}{(2l+1)(2l+3)}$	Intensity is maximum for empty m=0 orbitals (d_{z^2}) and minimal for high m orbitals.

The m^2 dependence in the numerator of the intensity factors is the mathematical heart of XMLD. Because the intensity depends on m^2 rather than m, linear polarization cannot distinguish between $+m$ and $-m$ states (which is why XMLD does not require a net magnetization and works for antiferromagnets). Instead, it probes the unequal thermal population or energy splitting of different $|m|$ states caused by the crystal field and spin-orbit coupling.

X-ray Magnetic Linear Dichroism (XMLD)

Cartesian Orbital	Symmetry Group (Octahedral)	Linear Combination of |l=2,m⟩	Predominant |m| State	Probed by Polarization
d_{z^2}	e_g	$\|0\rangle$	m = 0	**E** ∥ z (Out-of-plane)
$d_{x^2-y^2}$	e_g	$\frac{1}{\sqrt{2}}(\|2\rangle + \|-2\rangle)$	|m| = 2	**E** ⊥ z (In-plane x, y)
d_{xz}	t_{2g}	$\frac{1}{\sqrt{2}}(\|-1\rangle - \|1\rangle)$	|m| = 1	**E** along x or z
d_{yz}	t_{2g}	$\frac{i}{\sqrt{2}}(\|-1\rangle + \|1\rangle)$	|m| = 1	**E** along y or z
d_{xy}	t_{2g}	$\frac{i}{\sqrt{2}}(\|-2\rangle - \|2\rangle)$	|m| = 2	**E** ⊥ z (In-plane x, y)

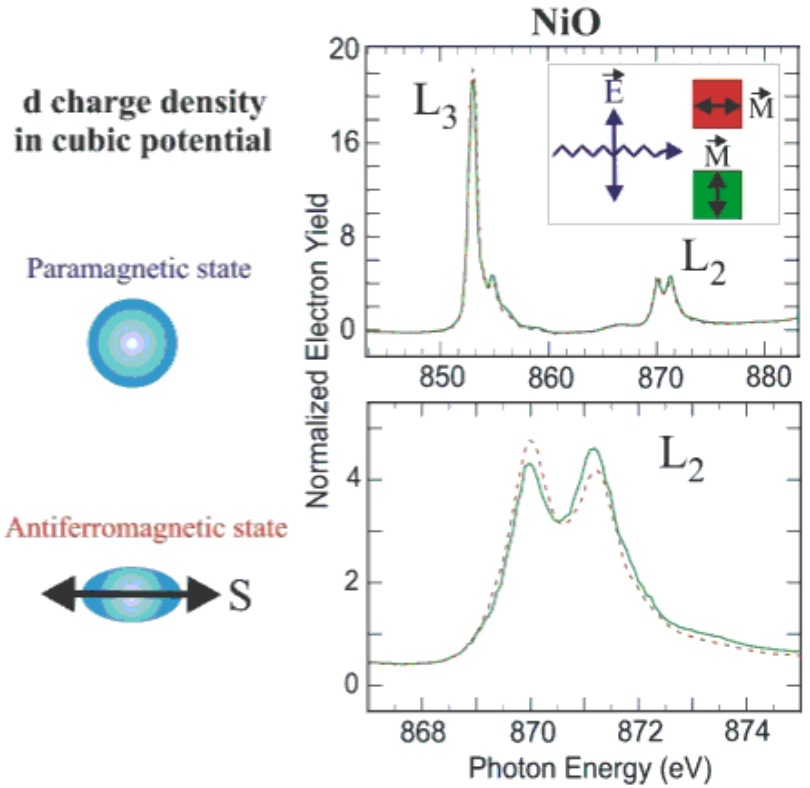

J. Stöhr and H. C. Siegmann, *Magnetism: From Fundamentals to Nanoscale Dynamics* (Springer, Berlin, Heidelberg, 2006).

The Physical Mechanism of XMLD in Crystals

1.Spatial Overlap: The transition probability is maximized when the electric field vector of the X-ray is parallel to the spatial lobes of the orbital.

2.Generating the Dichroism Signal: To extract the XMLD signal, you measure the absorption intensity with polarization parallel to a specific axis ($I_{\parallel}$) and then subtract the intensity with polarization perpendicular to it ($I_{\perp}$).

3.Measuring Anisotropy: If we define z as the magnetic or symmetry axis, the dichroism $I_{XMLD} = I_{\parallel} - I_{\perp}$ essentially measures the difference in electron hole population (or energy splitting) between the out-of-plane d_{z^2} orbital (m = 0) and the in-plane $d_{x^2-y^2}/d_{xy}$ orbitals (|m| = 2).
If the material is perfectly isotropic, these states are equally populated and $I_{\parallel} = I_{\perp}$, yielding zero XMLD. If spin-orbit coupling or strain breaks this symmetry, the XLD signal emerges.

The orbital moment in Fe_3O_4

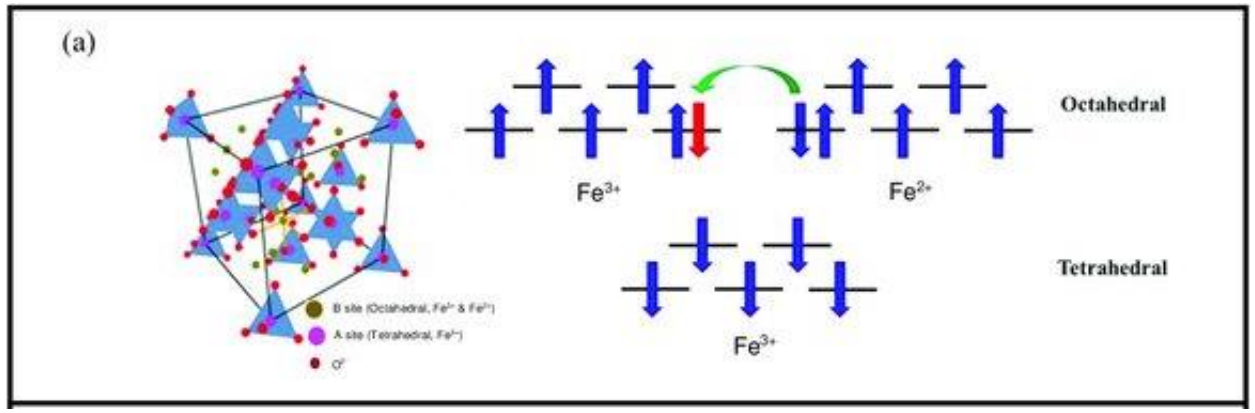

$$Fe_A^{3+}[Fe^{2+}Fe^{3+}]_B O_4$$

Nanomaterials 6(11):211 (2016)

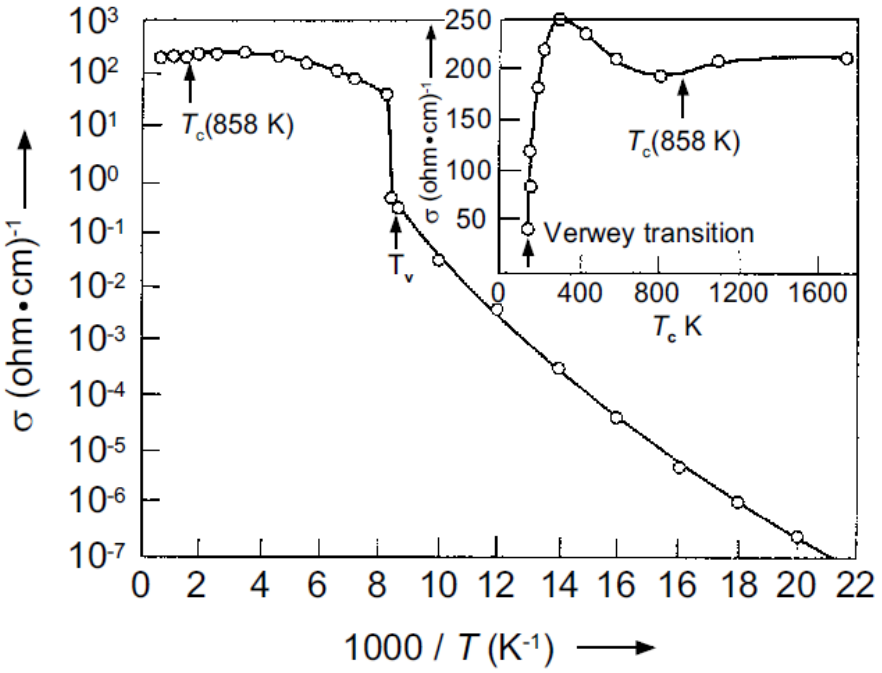

Miles P A, Westphal W B and Hippel V A 1957 Rev. Mod. Phys. 29 279

The orbital moment in Fe_3O_4

$m_{orb} = 0\ \mu_B$

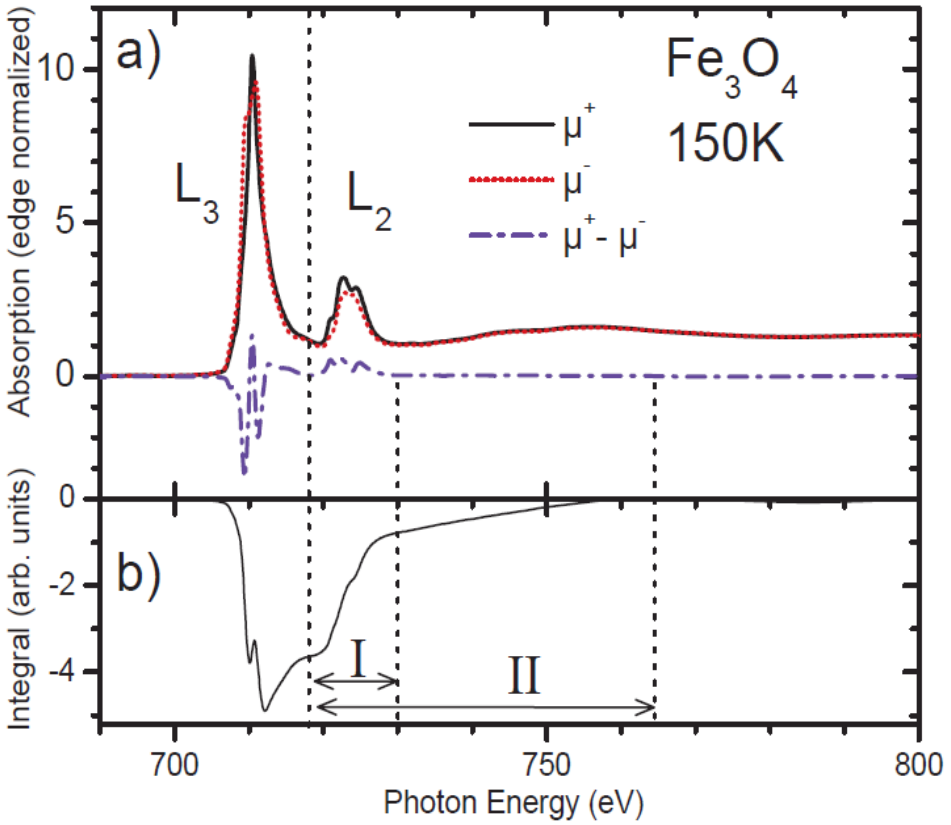

EPL 73, 97 (2005) **0.49:0.21:0.30**

$m_{orb} = 0.65\ \mu_B$

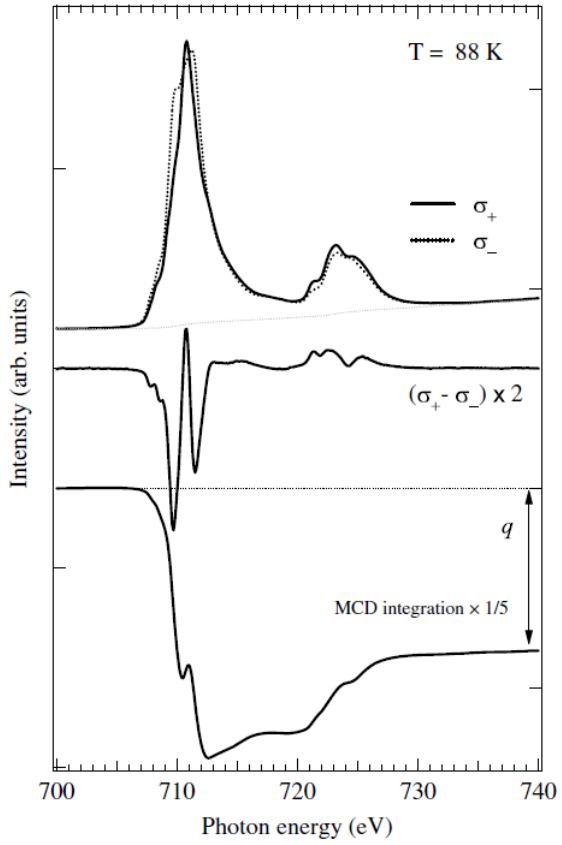

PRL 93, 077204 (2004) **0.53:0.13:0.34**

The orbital moment in Fe_3O_4

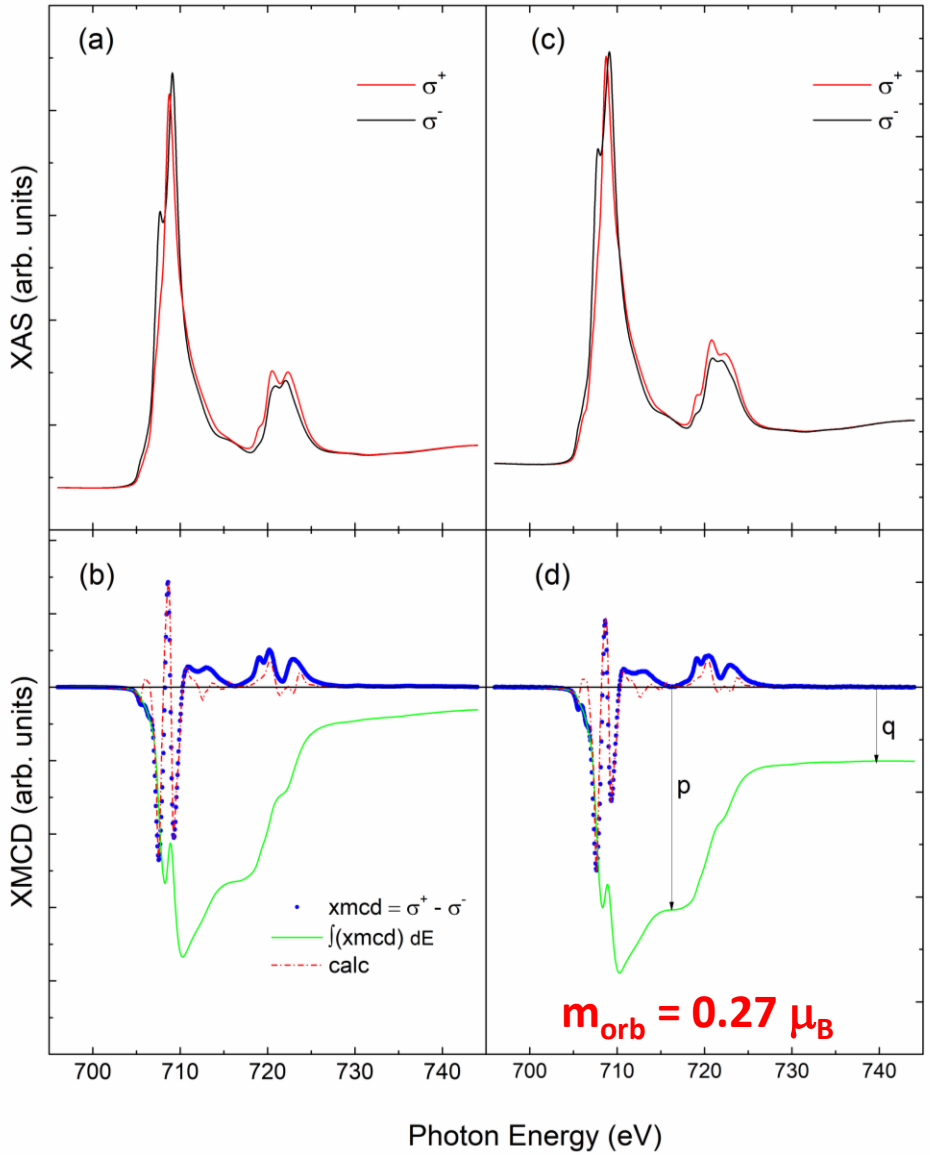

m_{orb} = 0.27 μ_B

$$g = 2\left(1 + \frac{m_l}{m_s}\right)$$

C. J. Love *et al.*, Phys. Rev. B **107**, 064414 (2023)

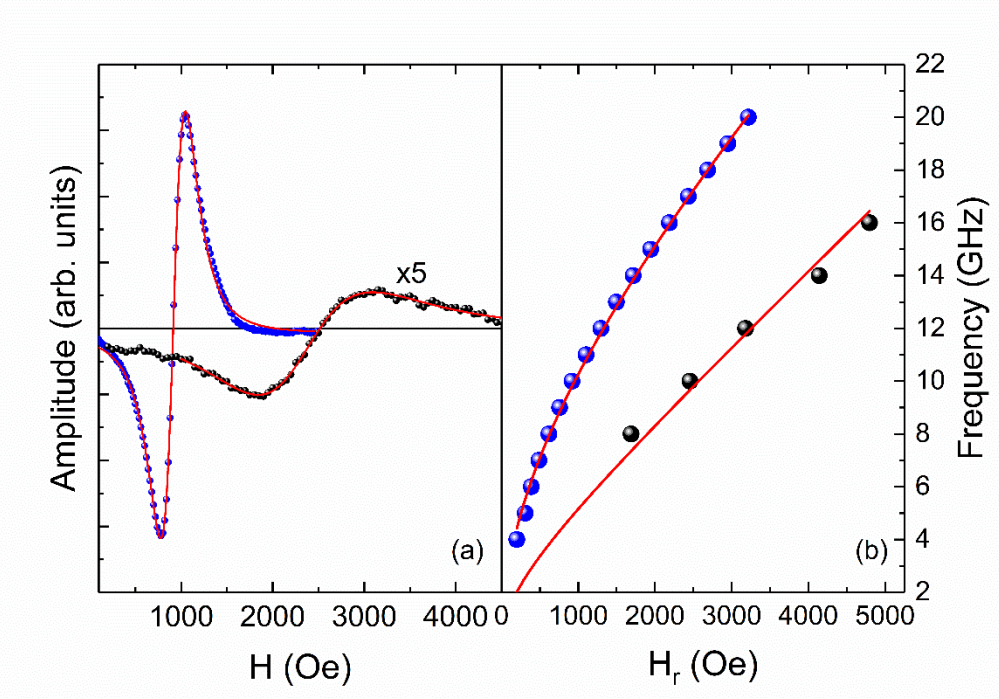

Fits to the FMR give g = 2.19 ± 0.01 → Orbital moment

XMCD: $m_{orb} / m_{spin} = 0.094$ ∴ g = 2.19

K-edge XMCD m_{orb} = 0.26 per unit formula PRL **123**, 2072021 (2019)

0.01 ML of Co on Pt(111)

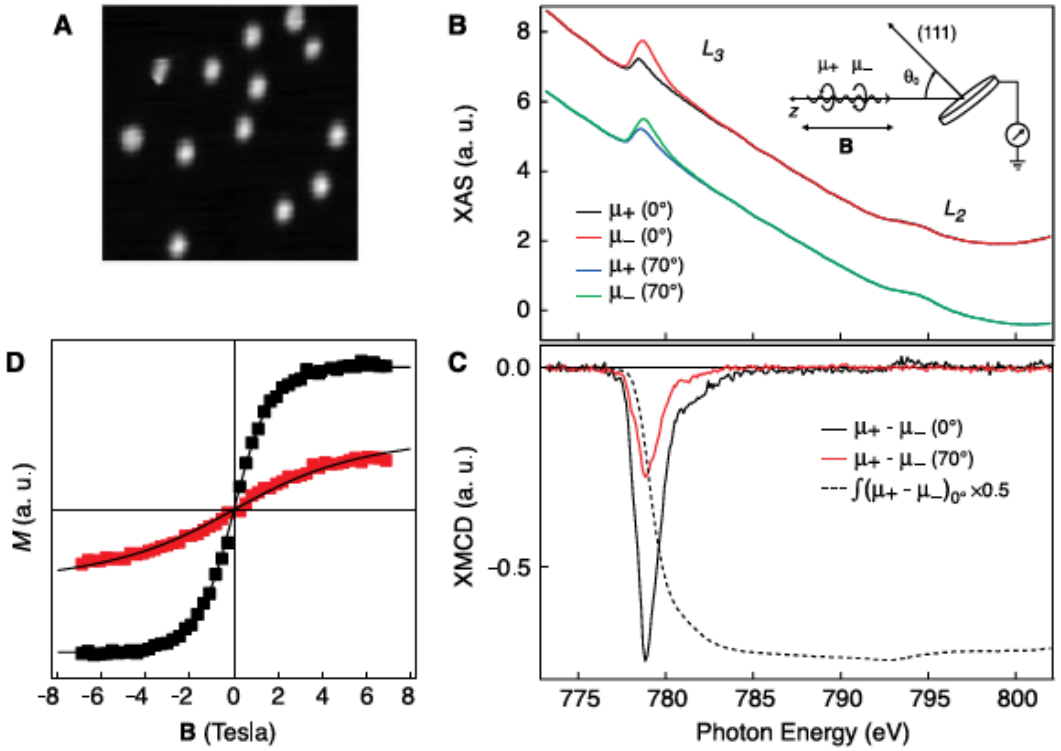

Hund's limit for d^7 ion: $m_L/m_S = 1$

Bulk Co hcp: $m_L/m_S = 0.1$

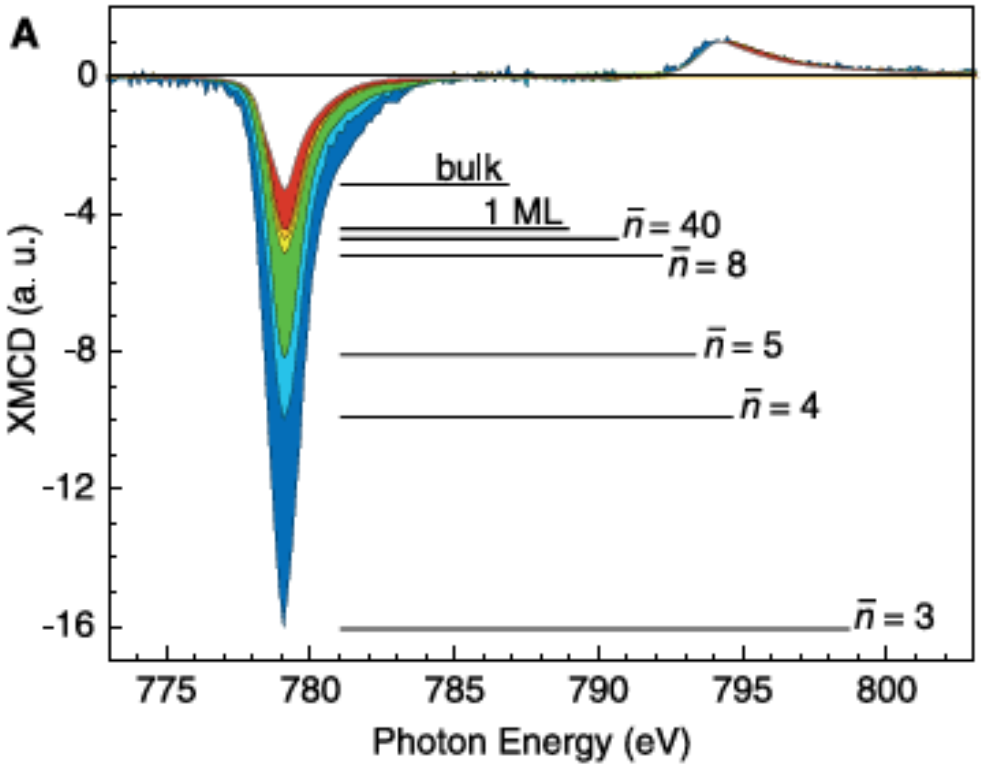

P. Gambardella *et al.*, Science **300**, 1130 (2003)

Orbital Moment vs n

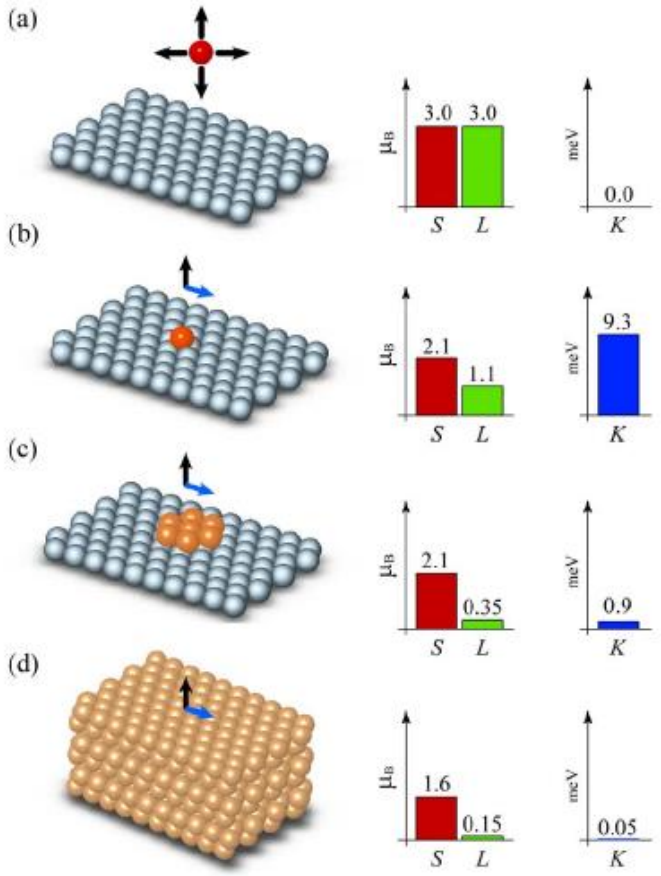

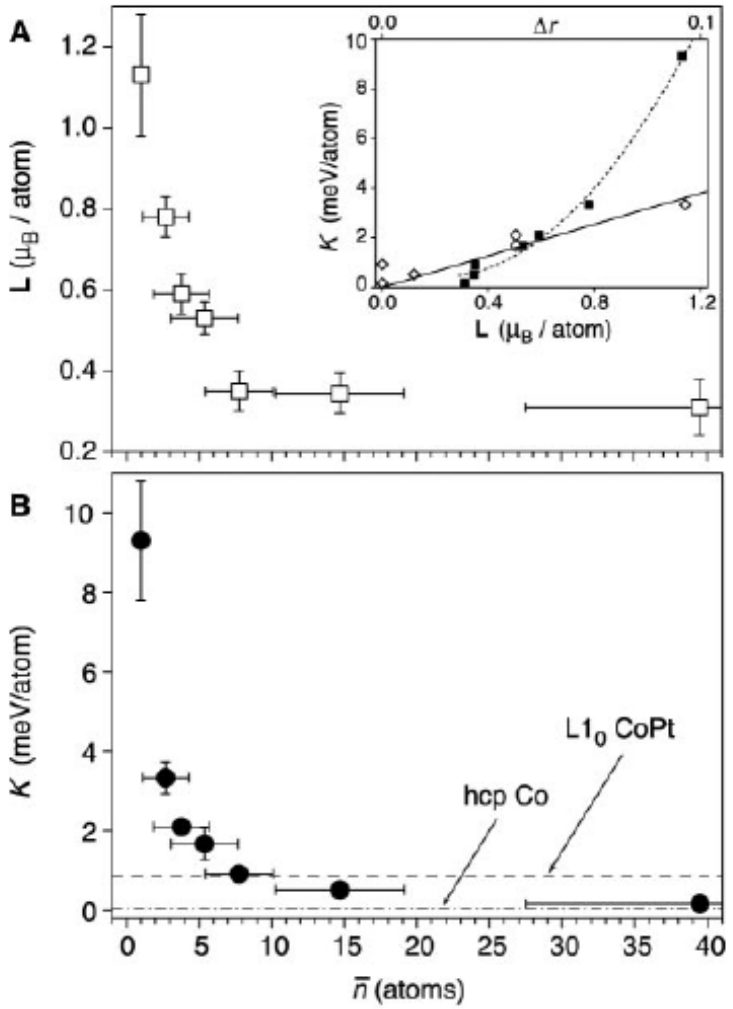

P. Gambardella *et al.*, Science **300**, 1130 (2003)

Magnetic lengthscales

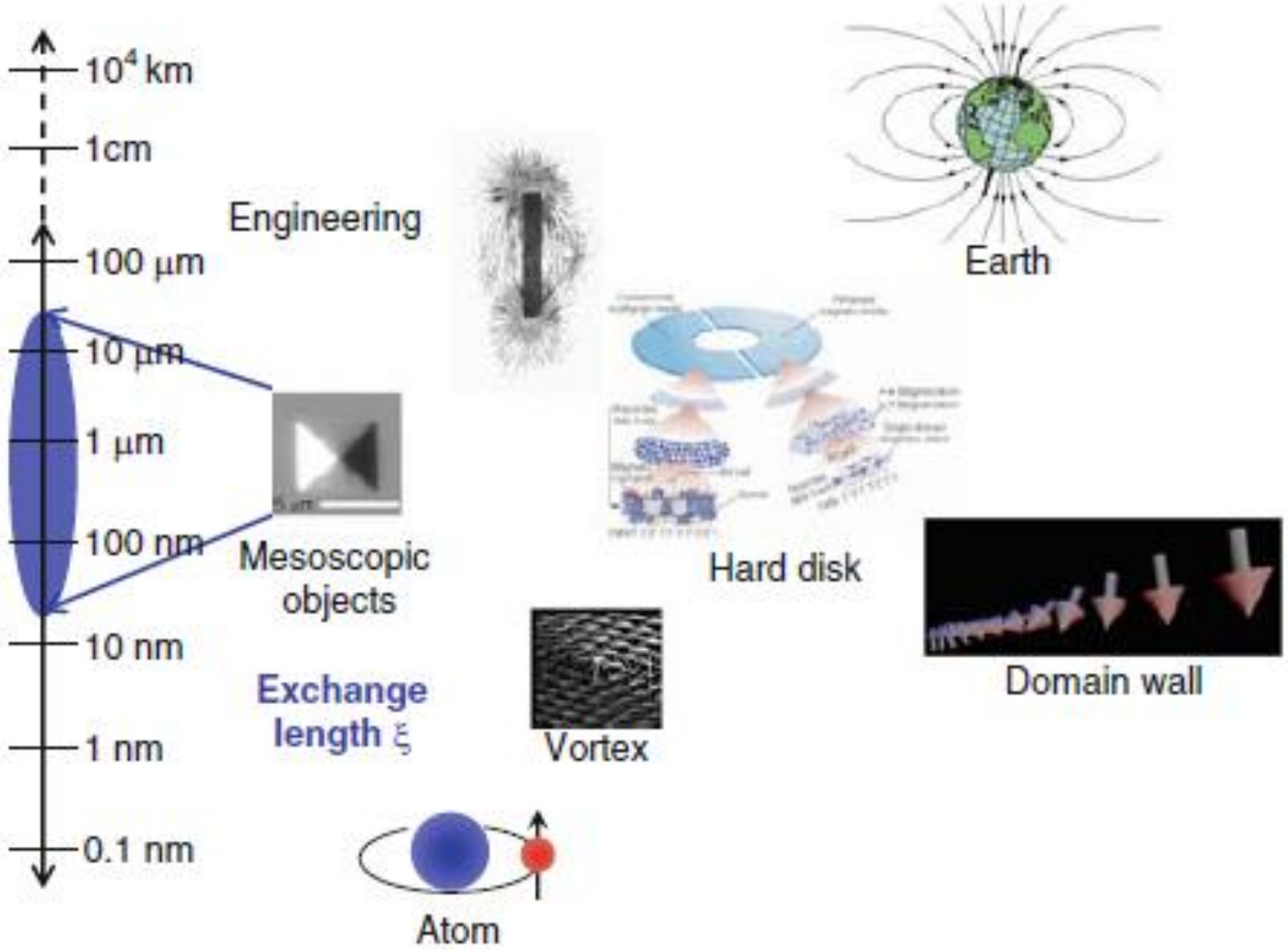

Courtesy of C. Quitmann,

XPEEM

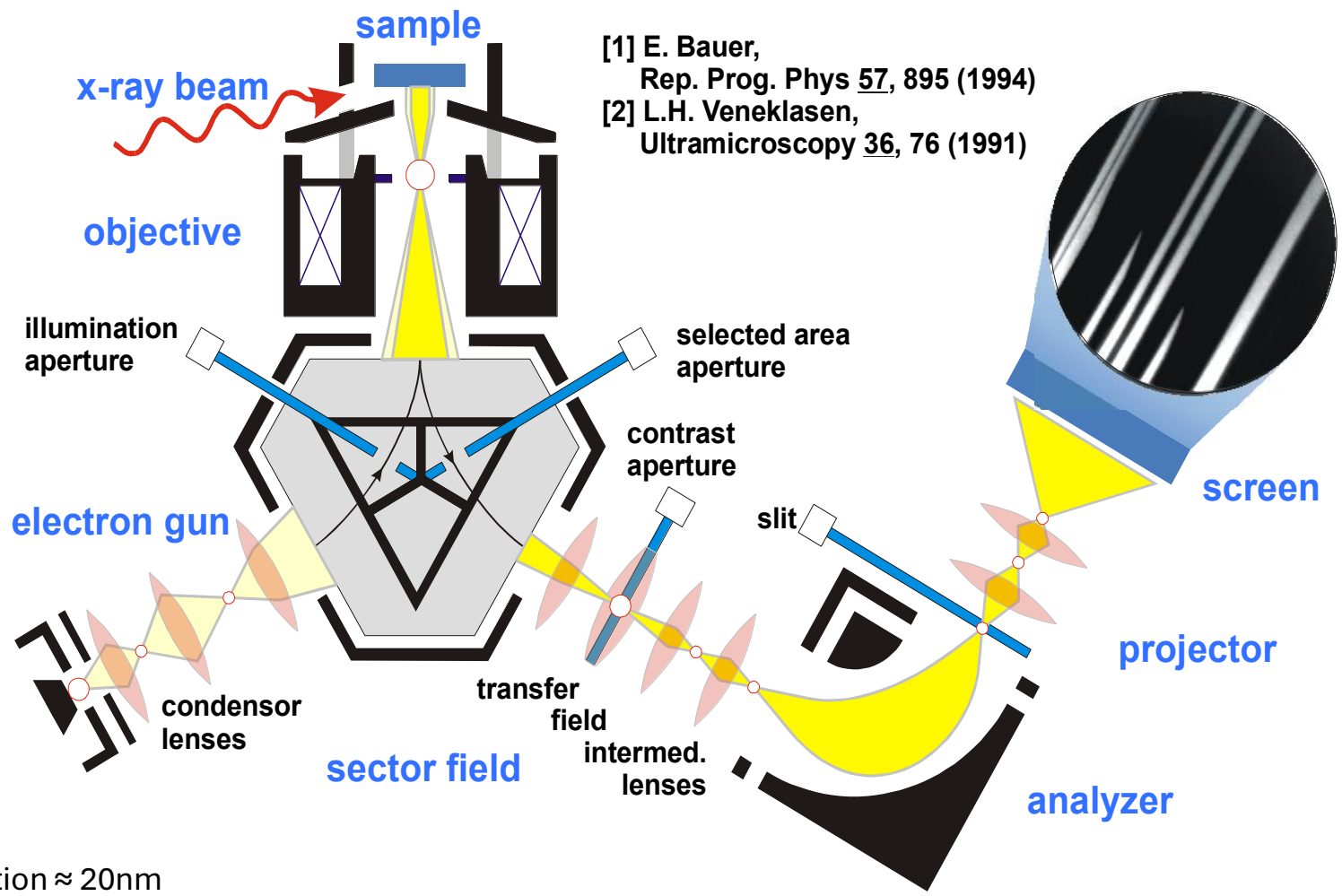

[1] E. Bauer, Rep. Prog. Phys 57, 895 (1994)
[2] L.H. Veneklasen, Ultramicroscopy 36, 76 (1991)

Full Field Microscope : Resolution ≈ 20nm
Temperature: 30K < T < 1200K
Azimuthal rotation. XMCD $\propto$ Mqcosθ

XPEEM + XMCD = Magnetic imaging with chemical specificity

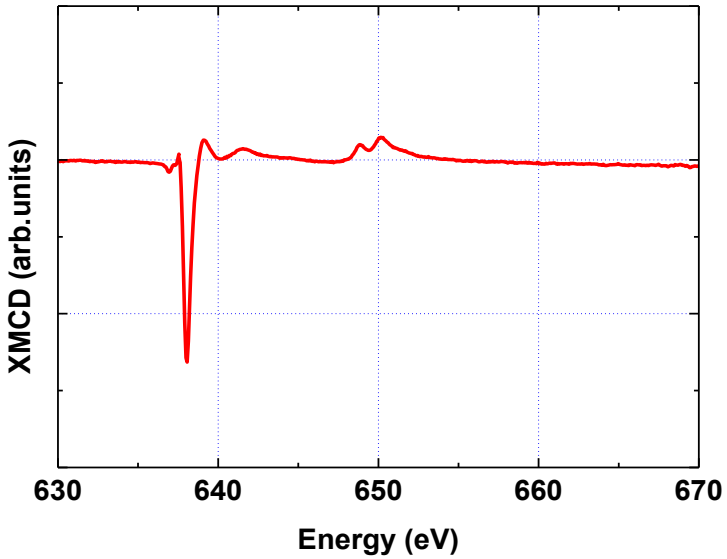

$$I(x,y) = \left[I^{L3}_{\sigma+} \Big/ I^{PE}_{\sigma+} - I^{L3}_{\sigma-} \Big/ I^{PE}_{\sigma-} \right]_{x,y}$$

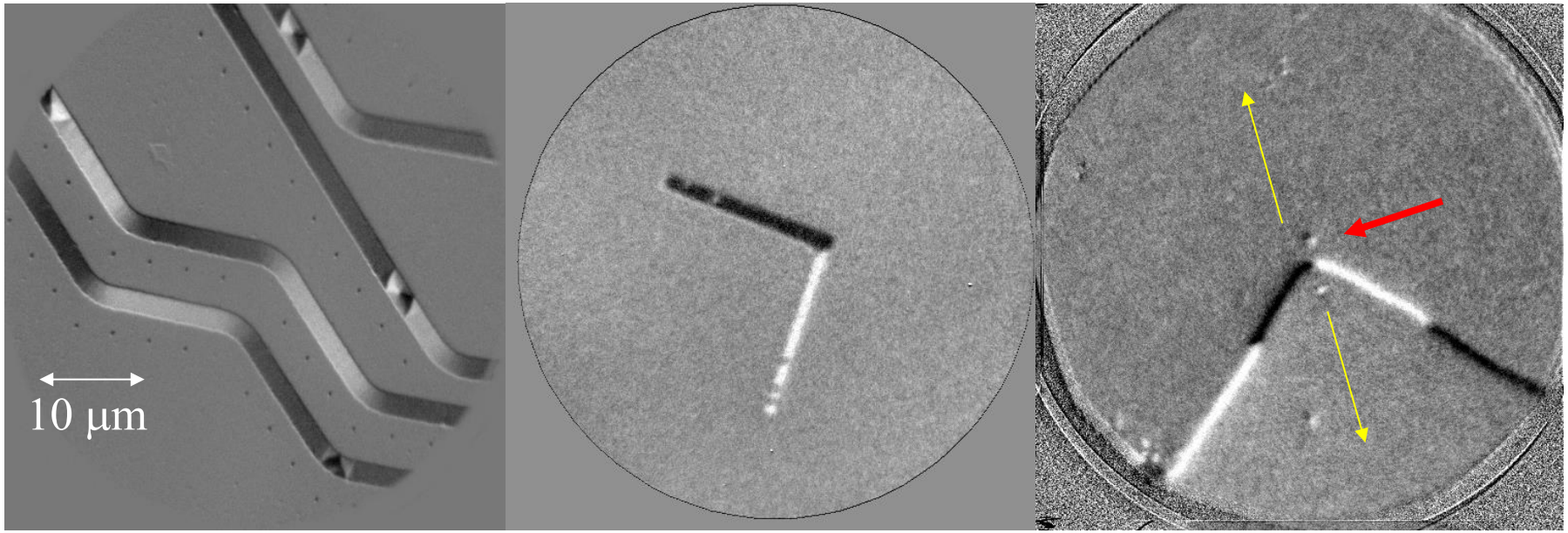

FeGa structures on PZT

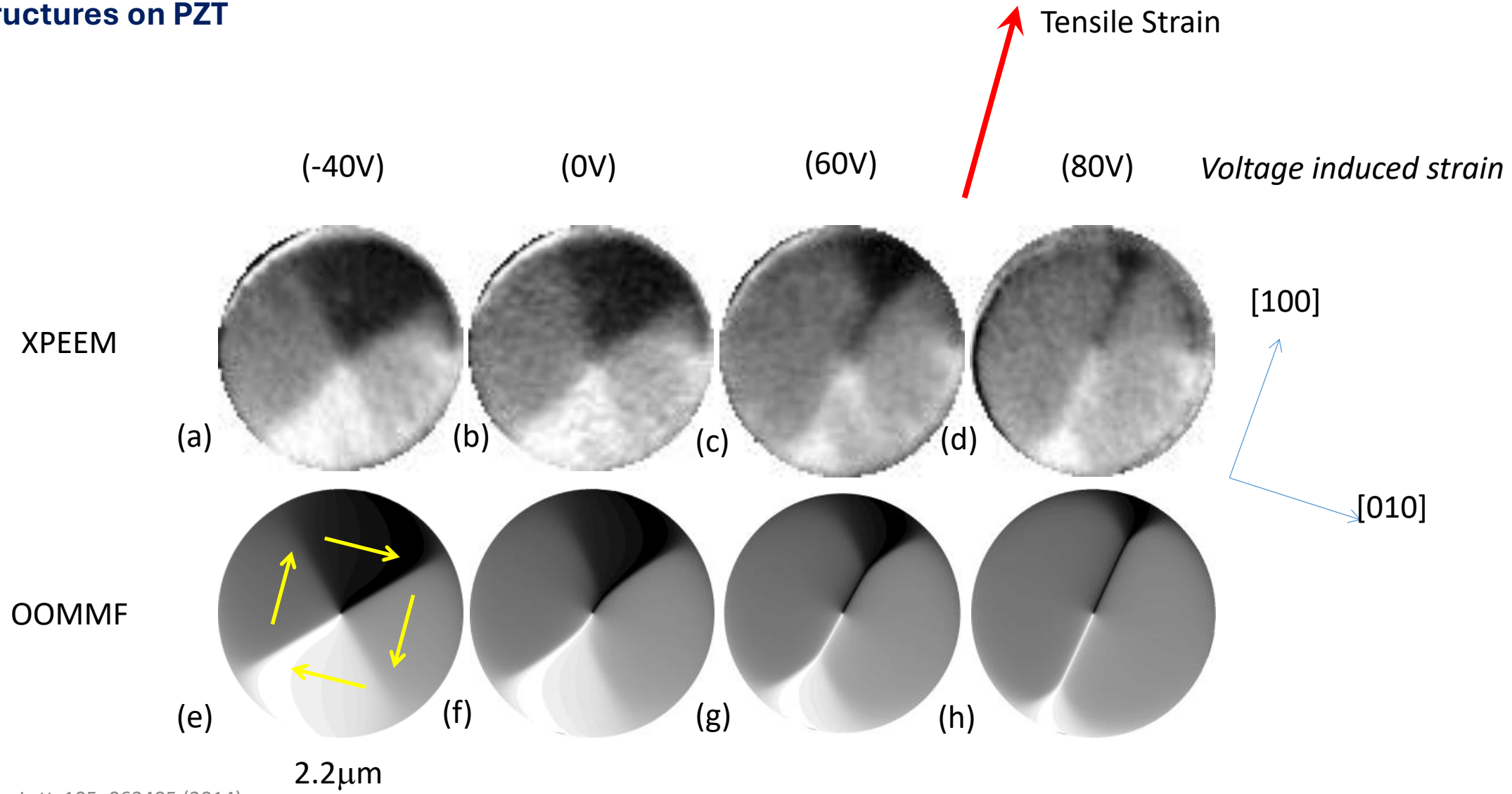

Appl. Phys. Lett. 105, 062405 (2014)

Scanning Transmission X-ray Microscopy (STXM)

Pros:

•**True Bulk Sensitivity:** STXM probes the entire volume and thickness of the sample.

•**High Magnetic Field Compatibility:** X-ray photons are not deflected by magnetic fields. This allows STXM to measure samples in-situ while applying strong external magnetic fields (up to several Tesla), making it ideal for studying magnetic reversal.

•**Immune to Charging Effects:** Because it relies on detecting photons rather than electrons, insulating samples do not suffer from the image-distorting electrostatic charging effects common in electron microscopy.

Cons:

•**Requires X-Ray Transparent Samples:** Samples must be thin enough for soft X-rays to pass through (typically < 100–200 nm thick) and must be grown or mounted on delicate X-ray transparent membranes (like silicon nitride). Bulk crystals or opaque substrates cannot be used.

•**Slower Acquisition Time:** It is a scanning technique that builds the image pixel-by-pixel

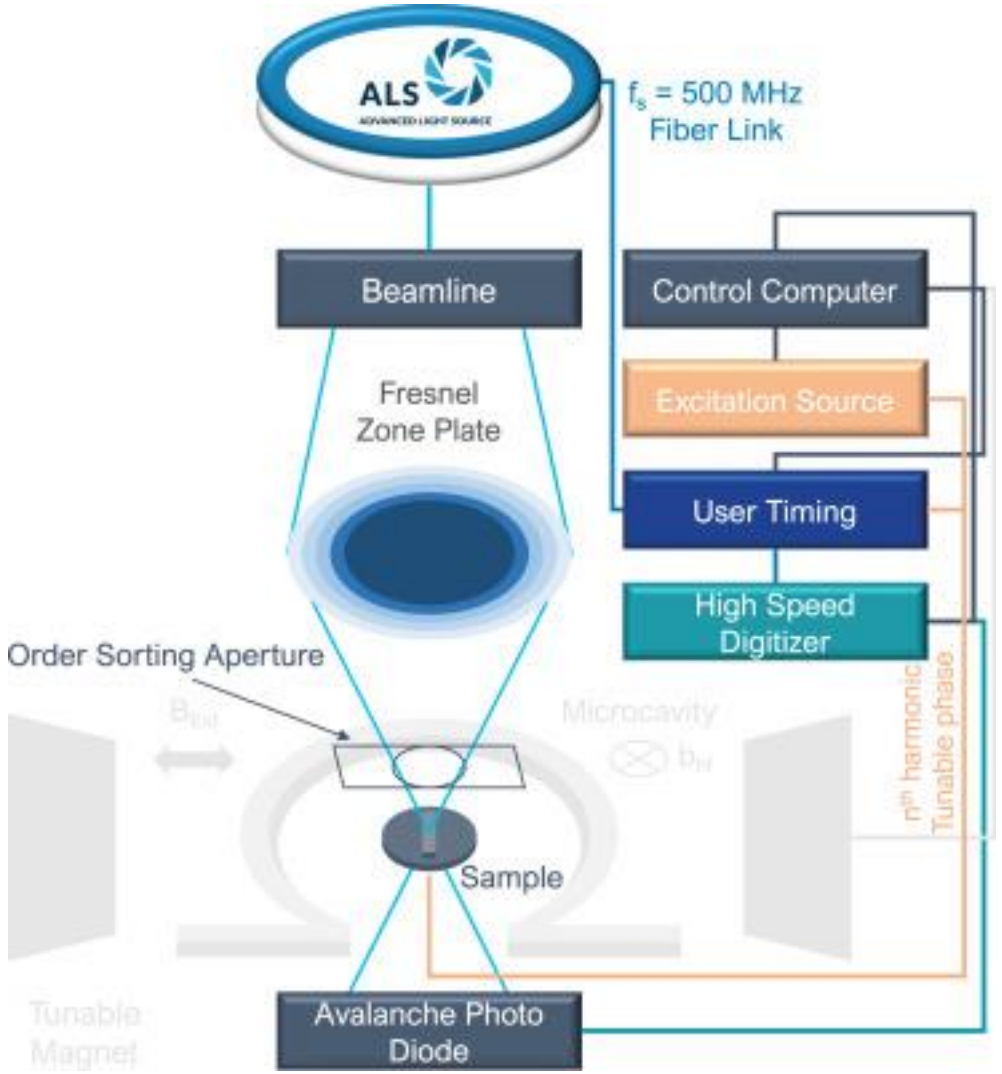

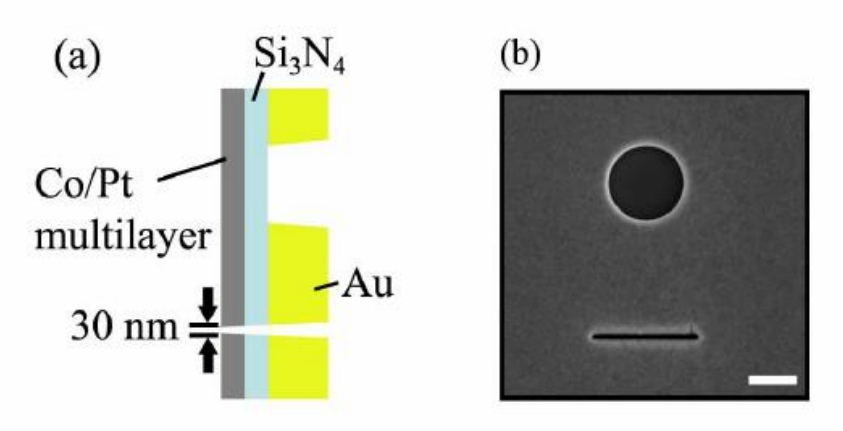

Holography with Extended Reference And Linear Differential Operator

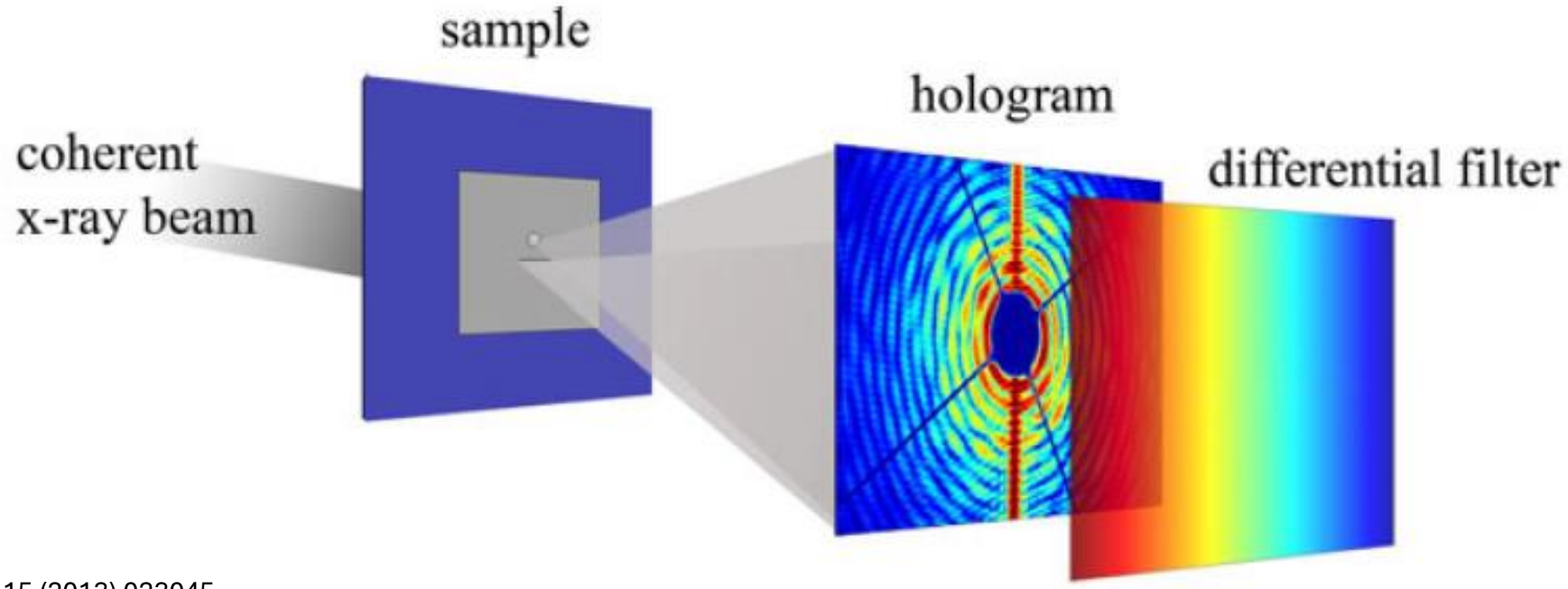

New Journal of Physics 15 (2013) 023045

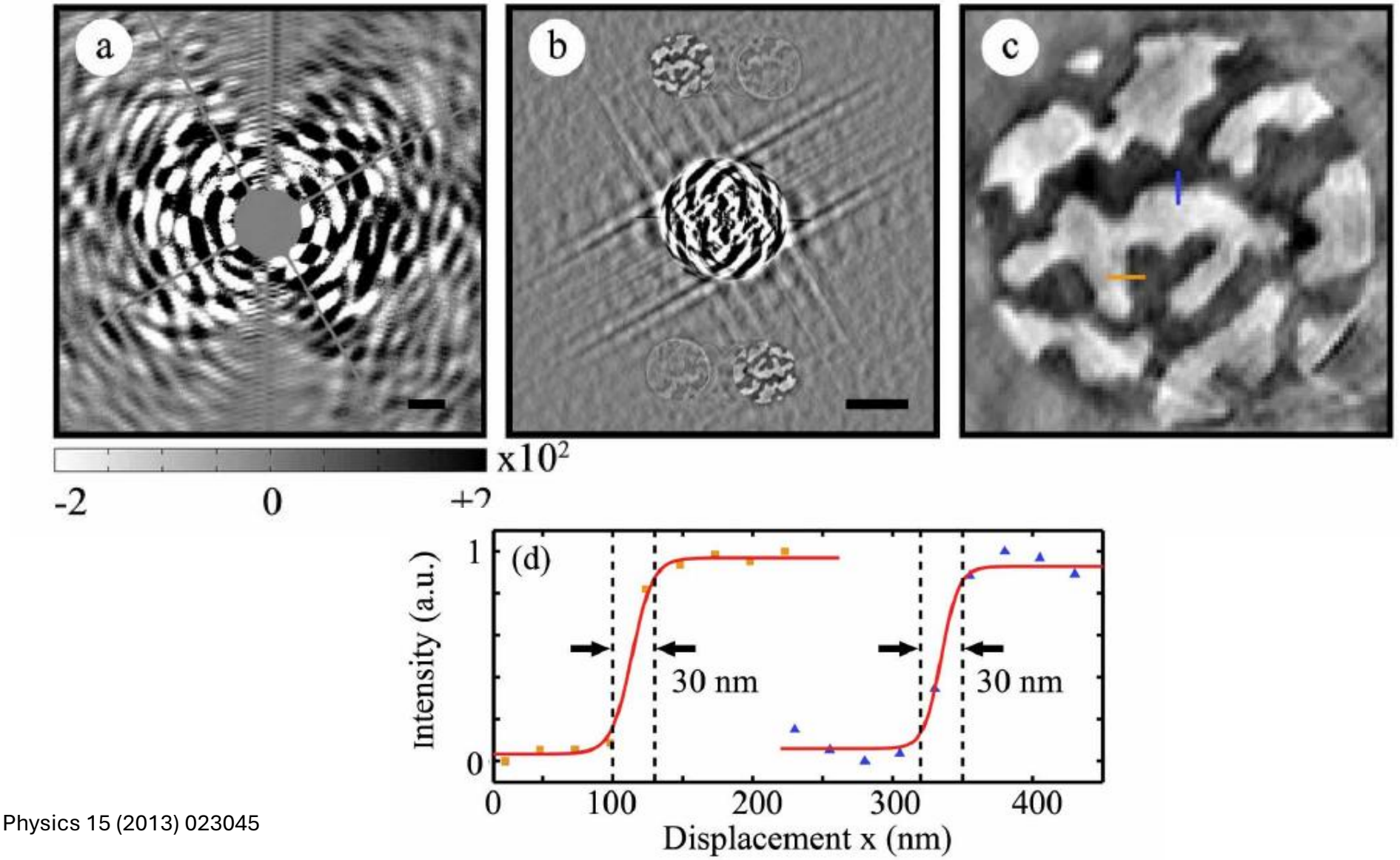

New Journal of Physics 15 (2013) 023045

Magnetic timescales

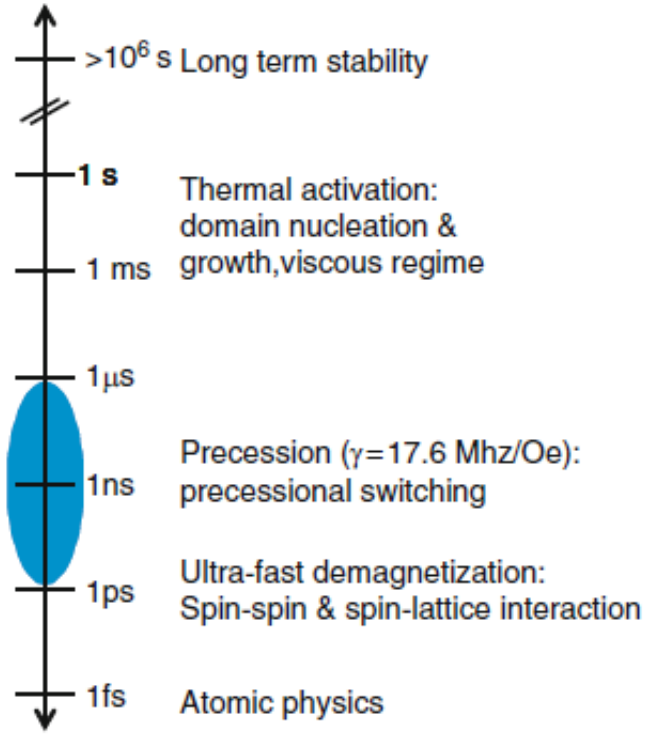

During reversal dM/dt transferred to lattice

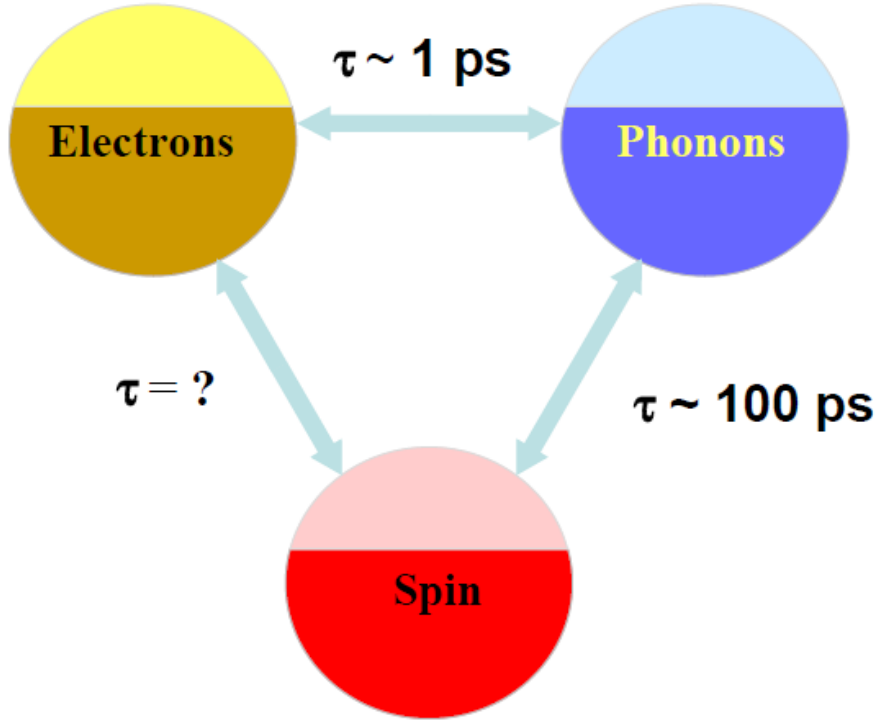

Gerrits, Th et al. Ultrafast precessional magnetization reversal by picosecond magnetic field pulse shaping. *Nature* ***418, 509–512 (2002).***

Tudosa, I. *et al. The ultimate speed of magnetic switching in granular recording media*. *Nature* ***428,*** 831–833 (2004).

Beaurepaire, E *et al*. Ultrafast spin dynamics in ferromagnetic nickel. *Phys. Rev. Lett*. ***76, 4250–4253 (1996).***

Stamm. C *et al*. Femtosecond modification of electron localization and transfer of angular momentum in nickel. Nature. Mater, 6, 740 (2007)

Time resolved XMCD-PEEM: Magnetisation Dynamics

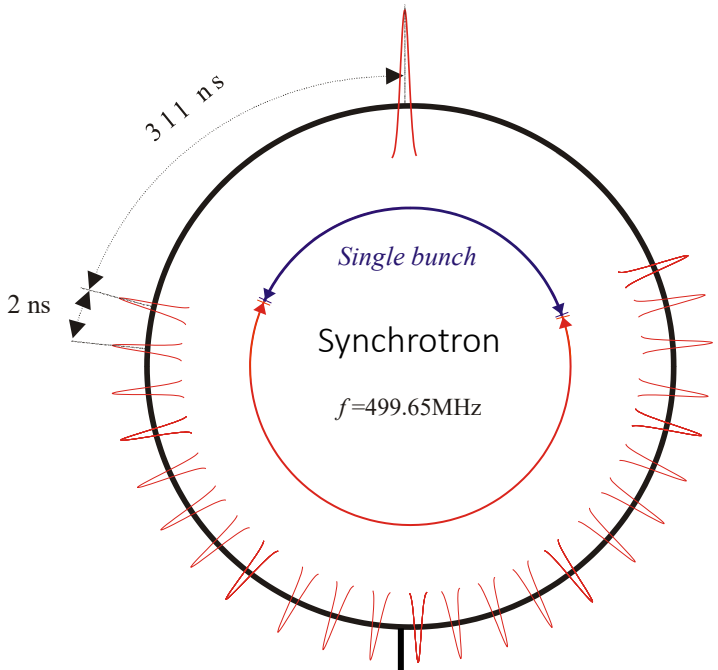

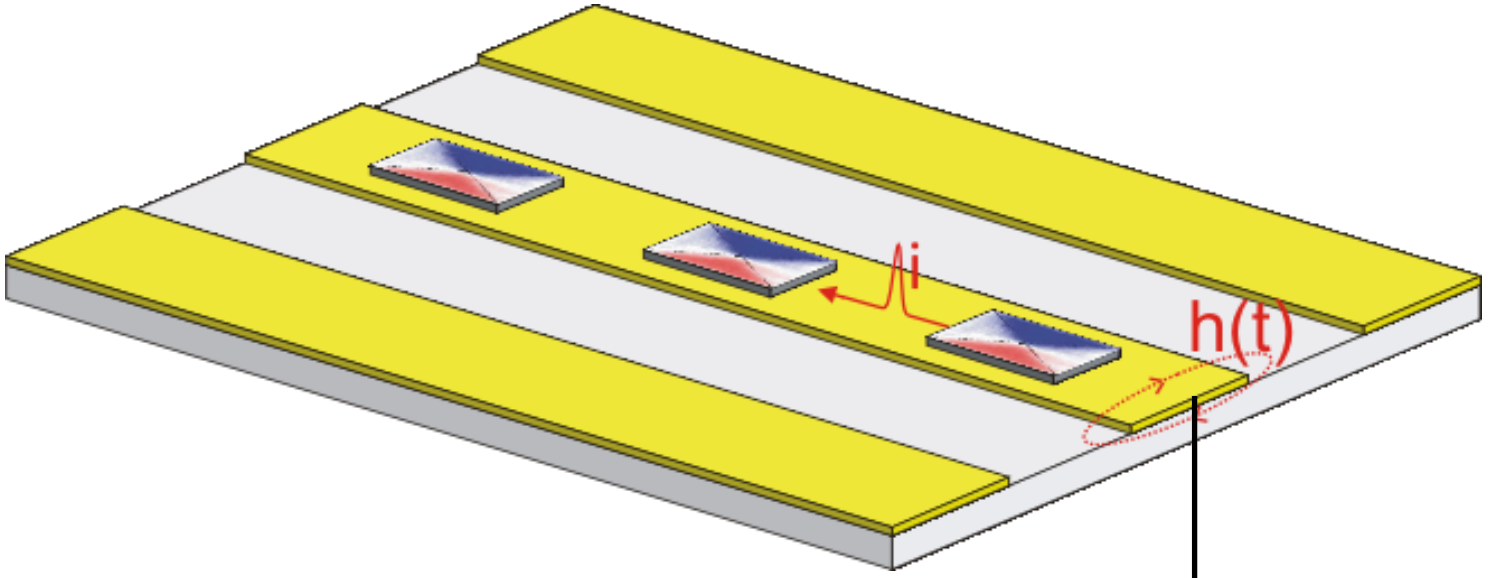

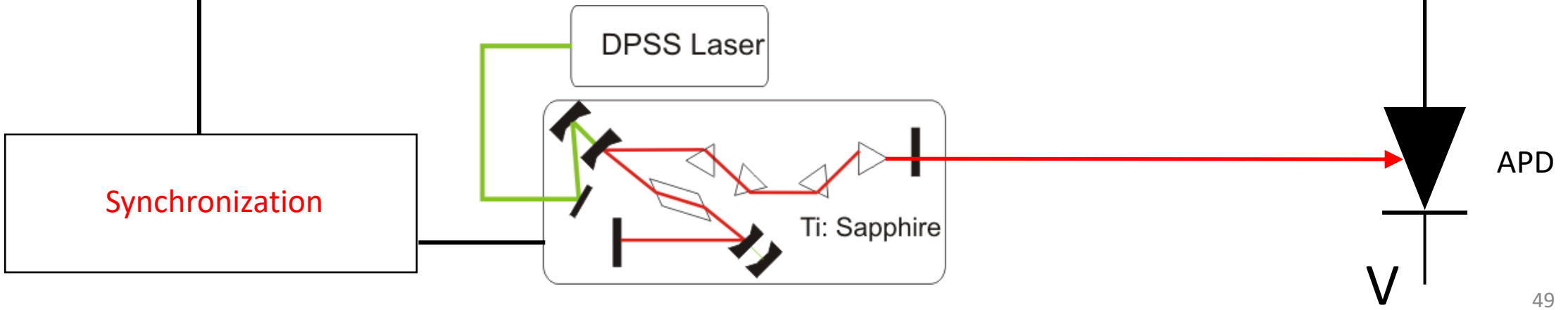

Time resolution of the synchrotron

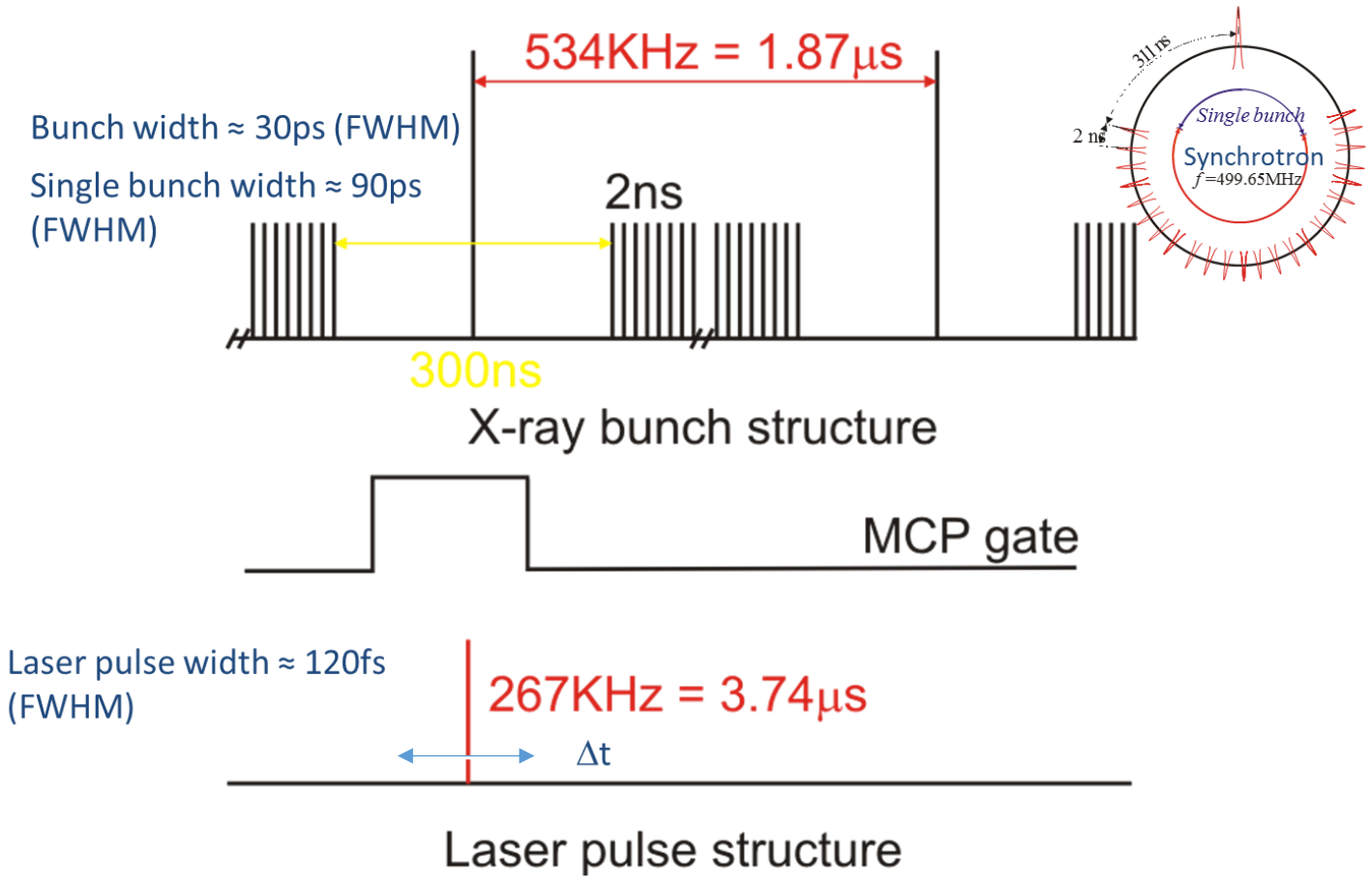

Time resolved XMCD-PEEM: Magnetisation Dynamics

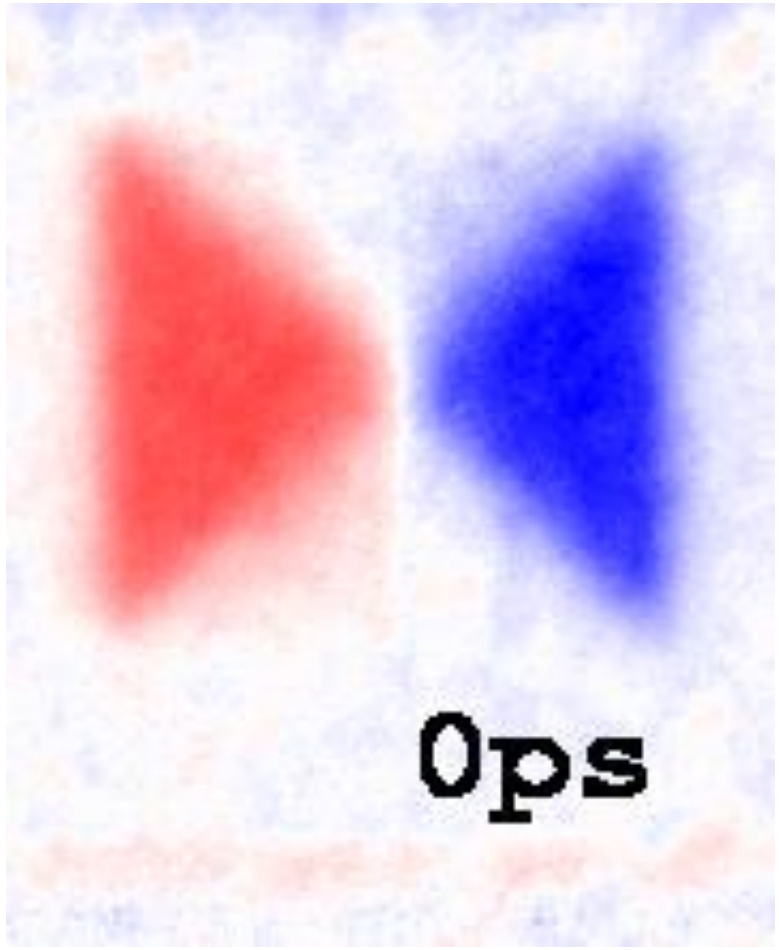

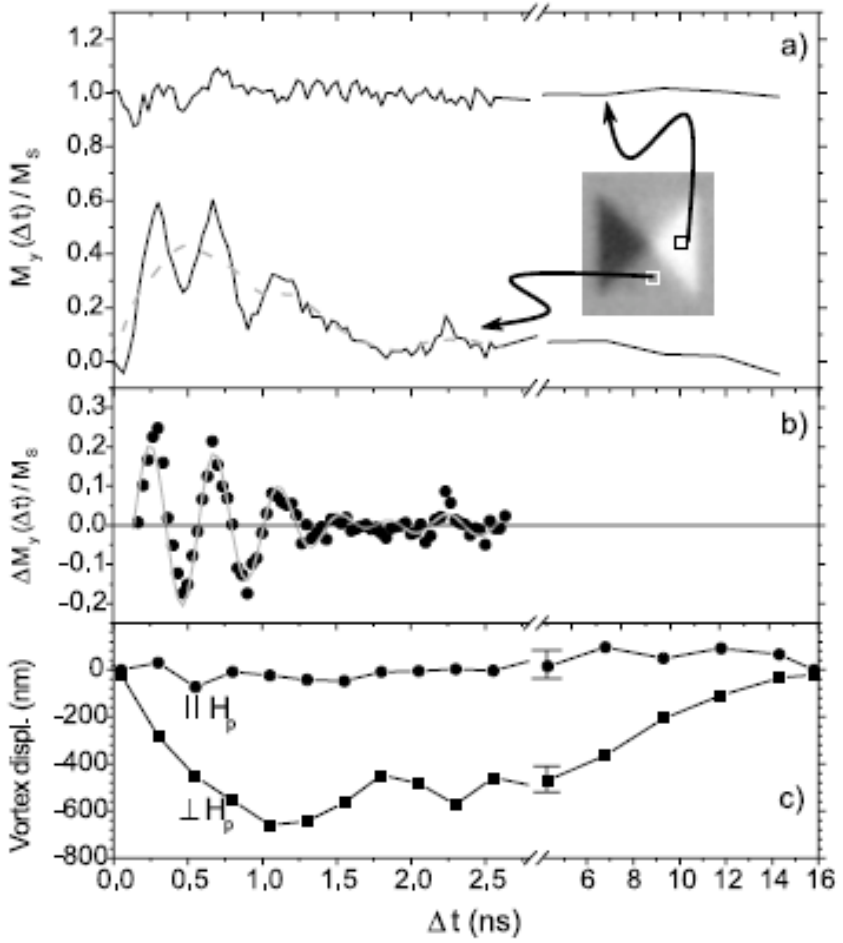

PRL 94, 217204 (2005)
NUCL INSTRUM METH A 588 (2008) 494–501

Courtesy of C. Quitmann

XFMR: Magnetisation Dynamics

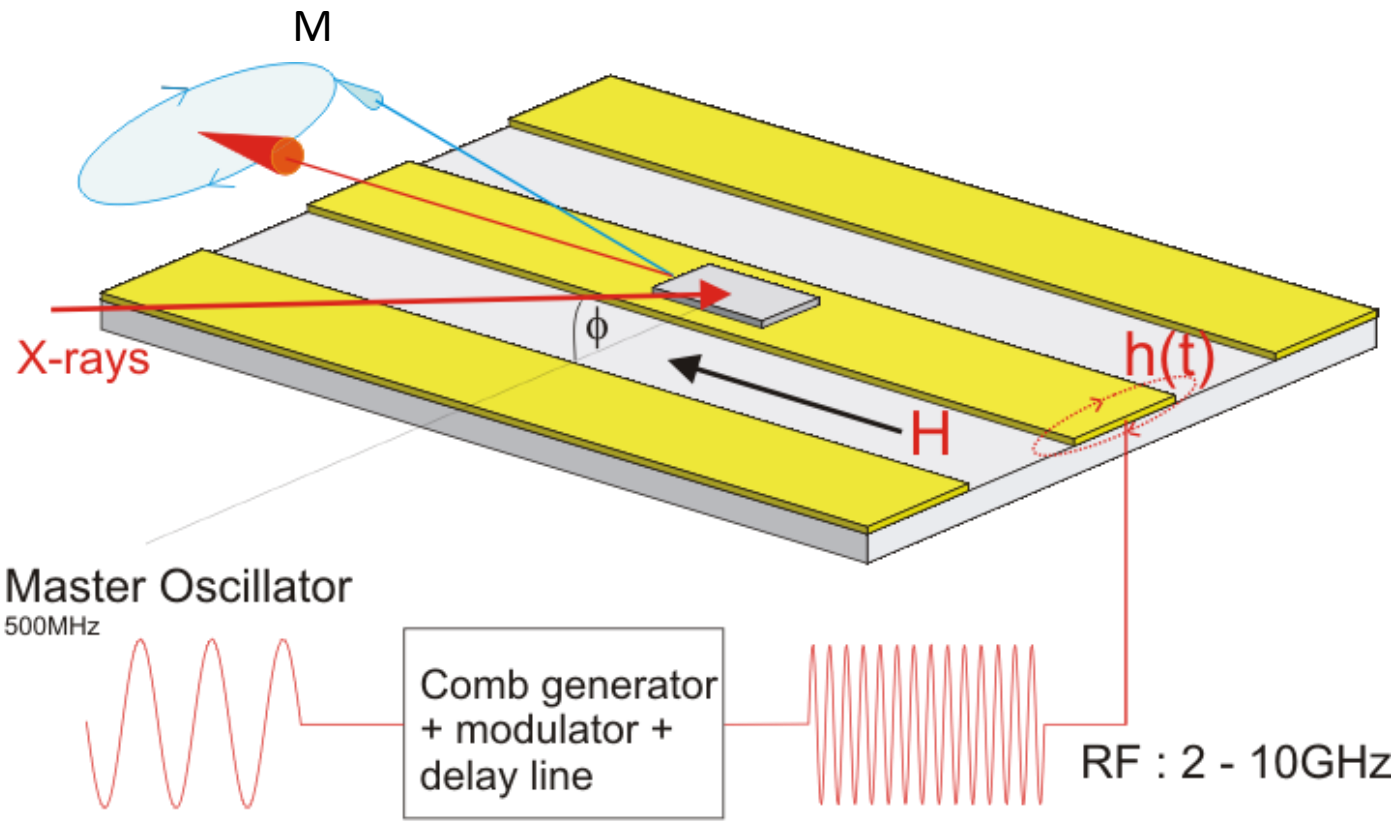

M. Marcham et. al. J. Appl. Phys, **109**, 07D353 (2011) , G. Boero *et al.*, Appl. Phys. Lett. **87**, 152503 (2005), D. A. Arena *et al.*, Phys. Rev. B **74**, 064409 (2006)

X-ray detected ferromagnetic resonance (XFMR)

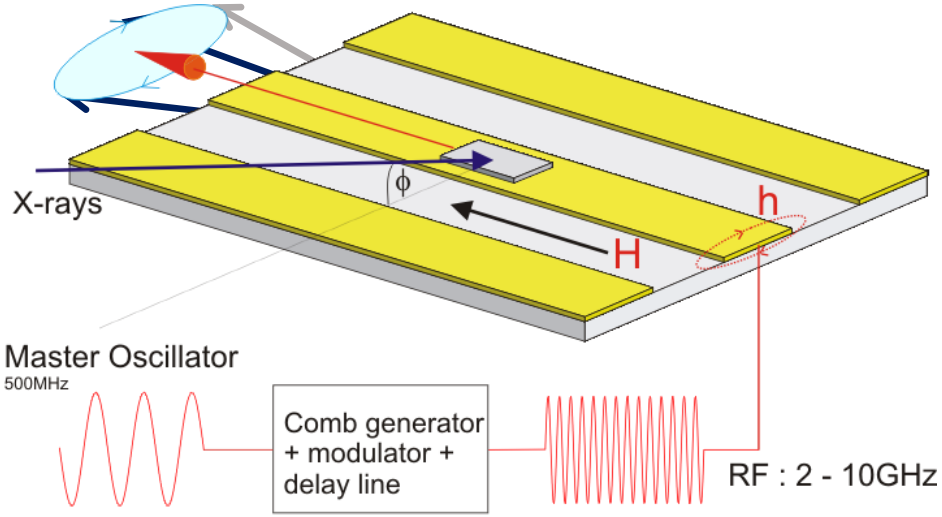

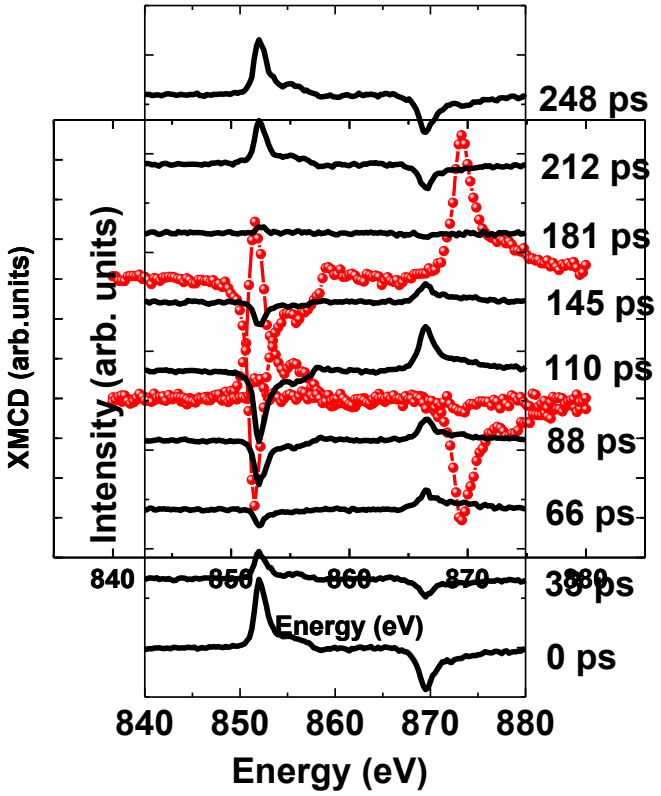

Stroboscopic Measurement

Able to make use of all bunches – no special fill pattern needed

X-ray detected ferromagnetic resonance (XFMR)

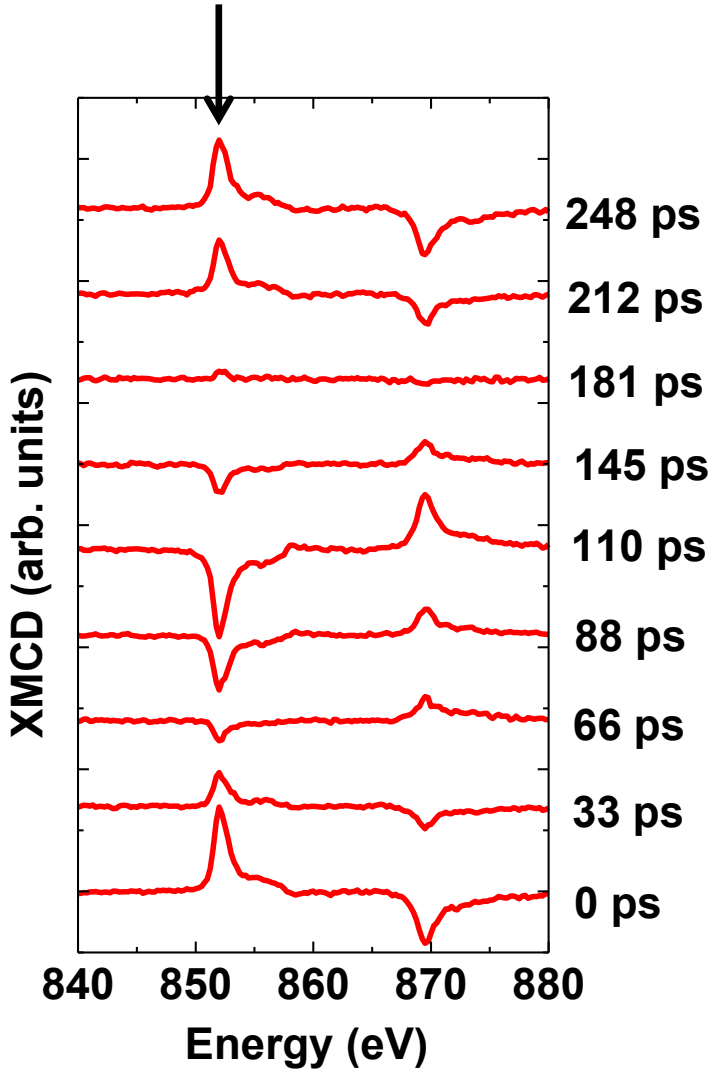

Fe and Ni moments precessing in phase

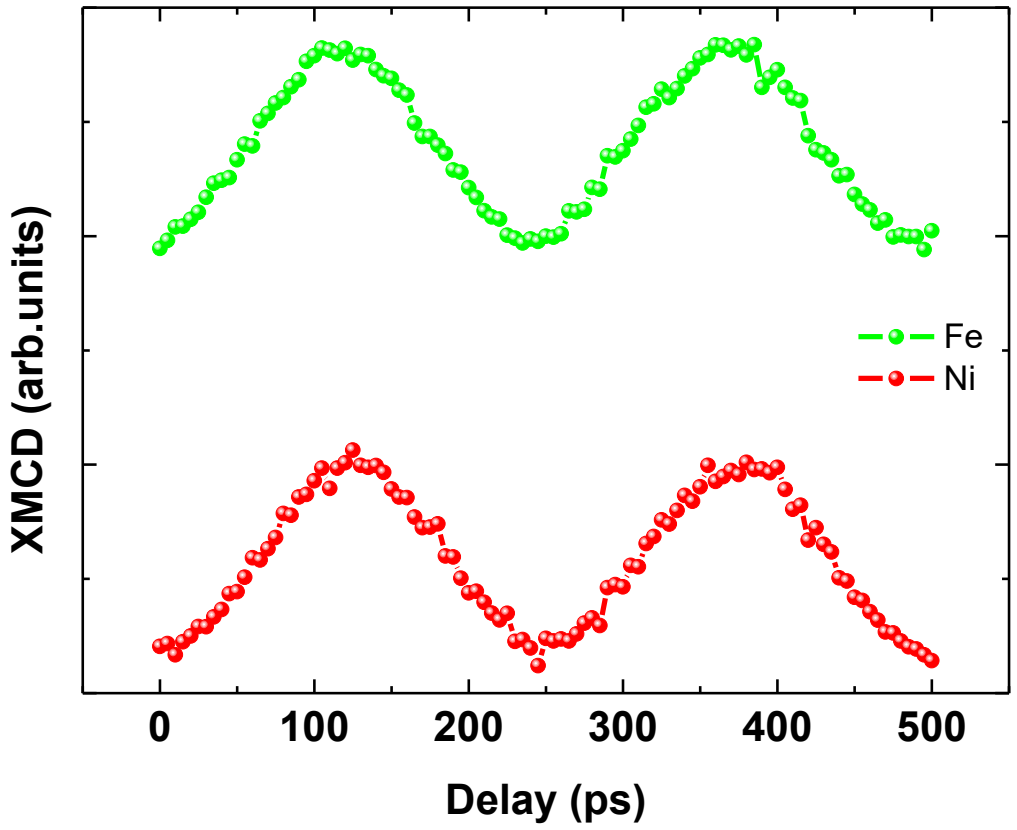

M. Marcham et. al. J. Appl. Phys, **109**, 07D353 (2011)

X-ray detected ferromagnetic resonance (XFMR)

Magnetization dynamics in an exchange-coupled NiFe/CoFe bilayer

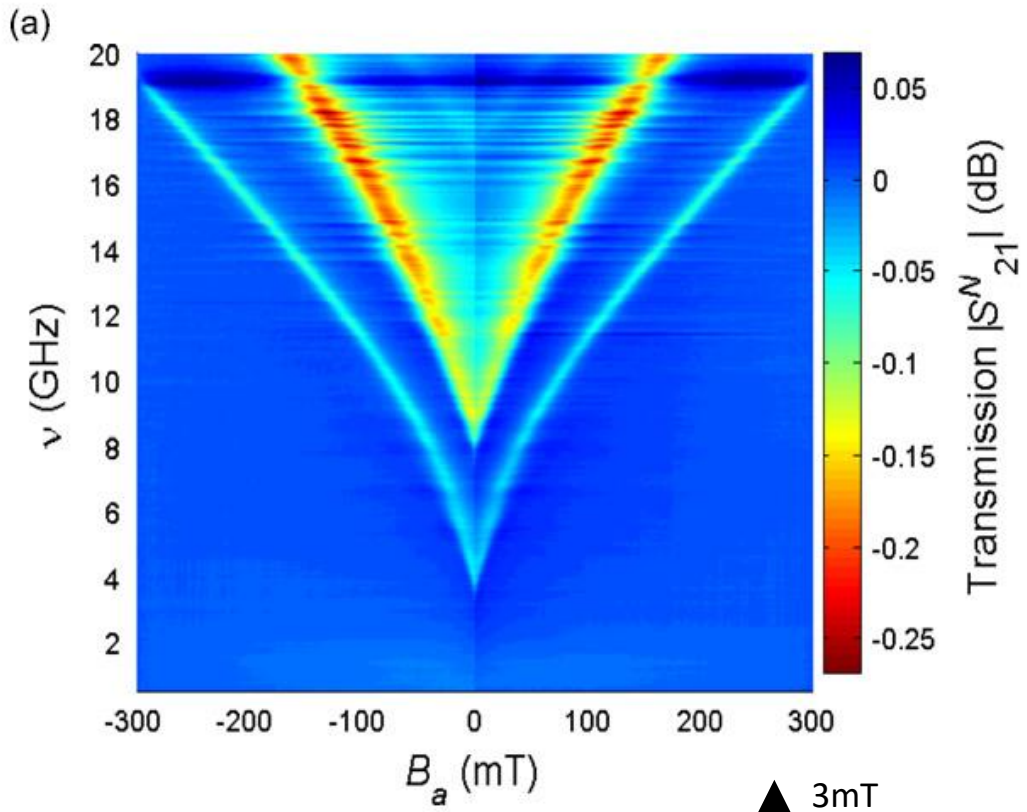

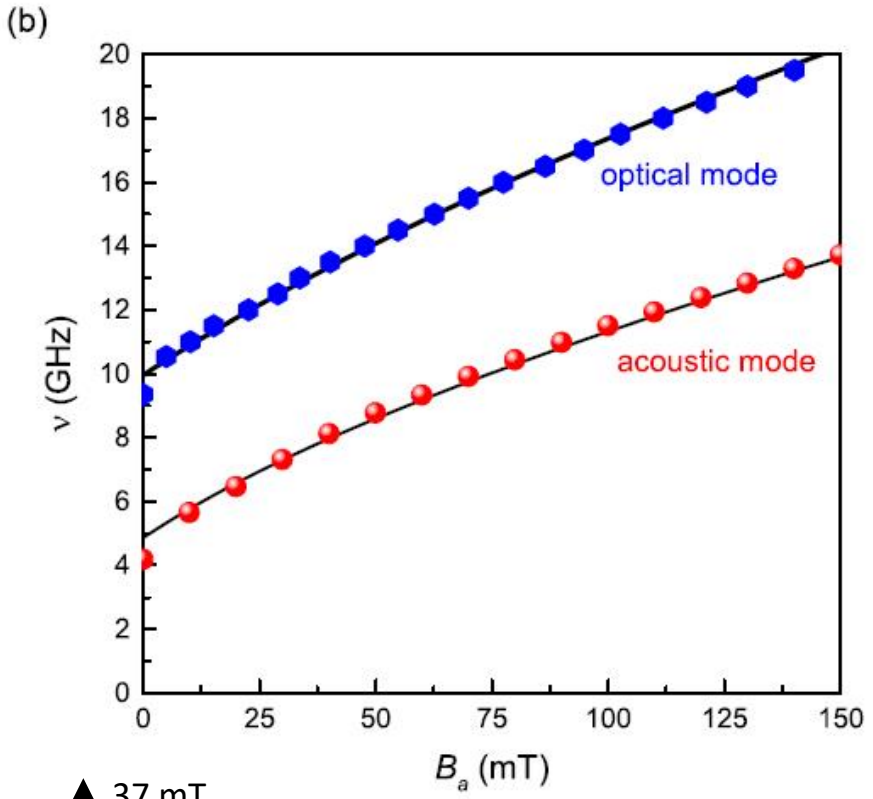

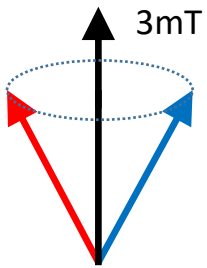

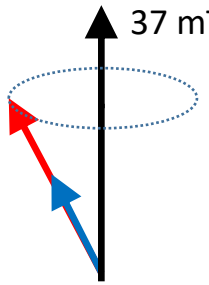

G. Stenning *et. al.* New.J.Phys, **17**, 013019 (2015)

Magnetization dynamics in an exchange-coupled NiFe/CoFe bilayer

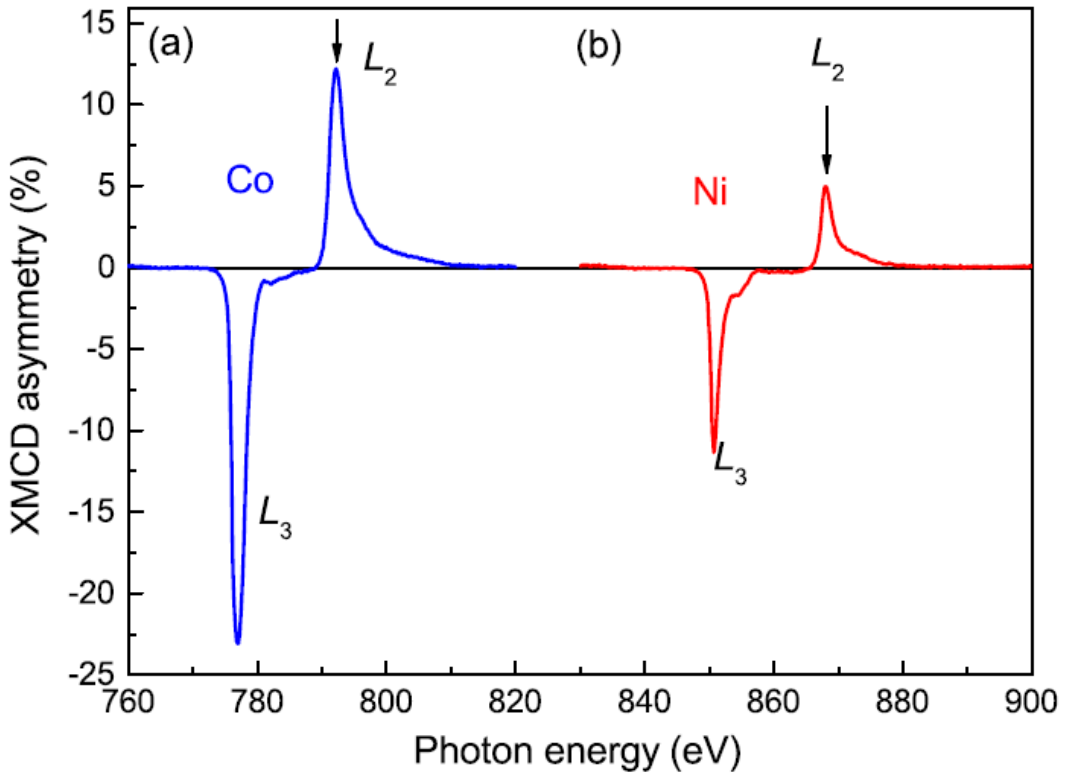

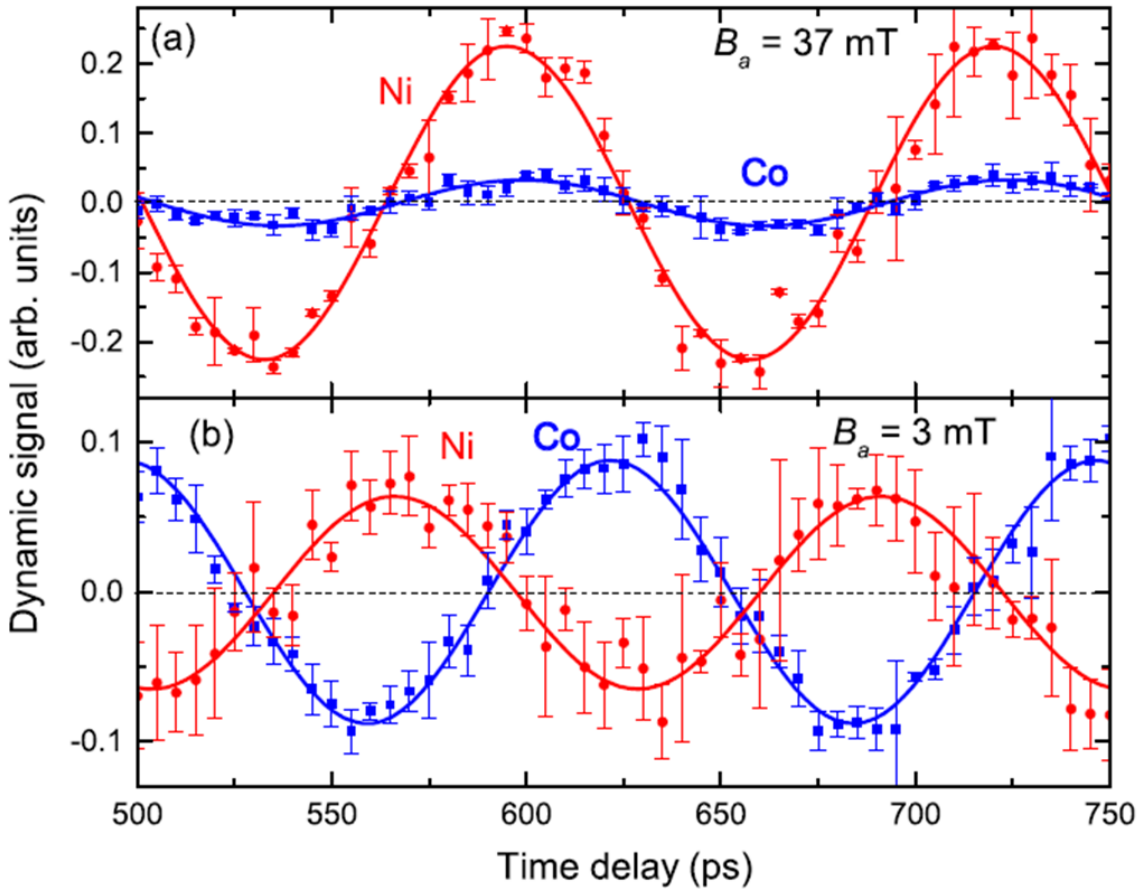

G. Stenning *et. al.* New.J.Phys, **17**, 013019 (2015)

The atomic form factor is a measure of the scattering amplitude of a wave by an isolated atom

$$|Q| = \frac{4\pi}{\lambda} sin\theta$$

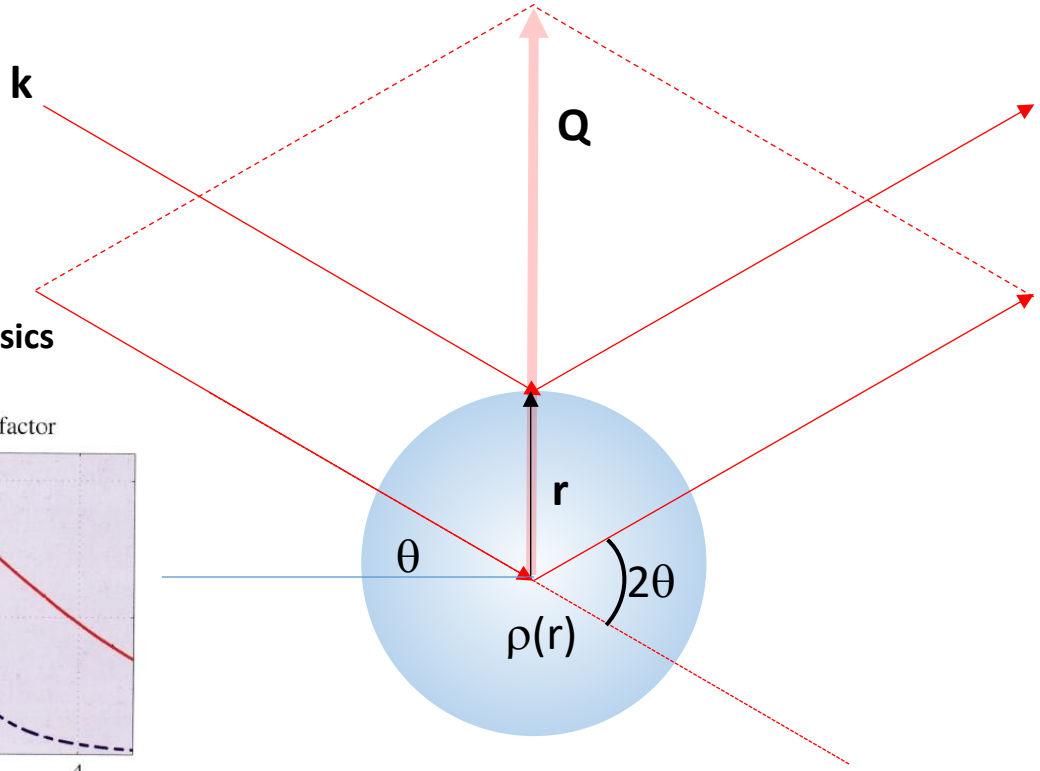

$$\Delta\phi(r) = (\boldsymbol{k'} - \boldsymbol{k}) \cdot \boldsymbol{r} = \boldsymbol{Q} \cdot \boldsymbol{r}$$

Elements of Modern X-ray Physics
D. McMorrow

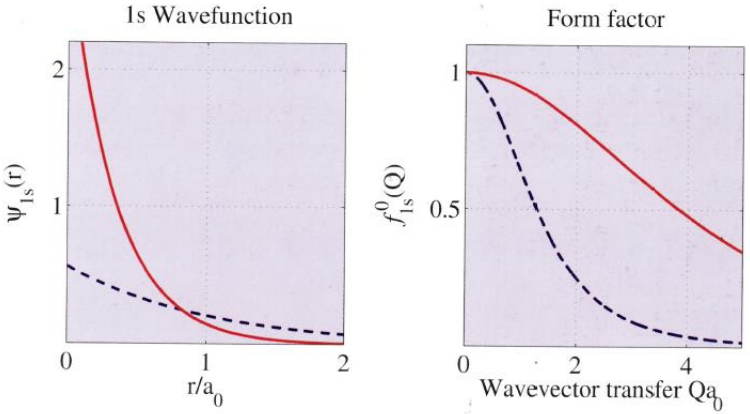

$$f(Q) = \int \rho(r) e^{i\boldsymbol{Q}\cdot\boldsymbol{r}} dr$$

= Z for Q -> 0
= 0 for Q -> ∞

Atomic form factor = Fourier transform of the electron density.
Isotropic for closed shells.

$$f^{crystal}(Q) = \sum_{r_j} f_j(Q) e^{i\boldsymbol{Q}\cdot\boldsymbol{r_j}} \sum_{R_n} e^{i\boldsymbol{Q}.\boldsymbol{R_n}}$$

$$Laue: \boldsymbol{Q} = \boldsymbol{G}$$

$$f(Q,E) = f(Q) + f'(E) + if''(E)$$

$$f(Q) = \int \rho(r) e^{iQ\cdot r} dr$$

Leads to anisotropic tensor of scattering

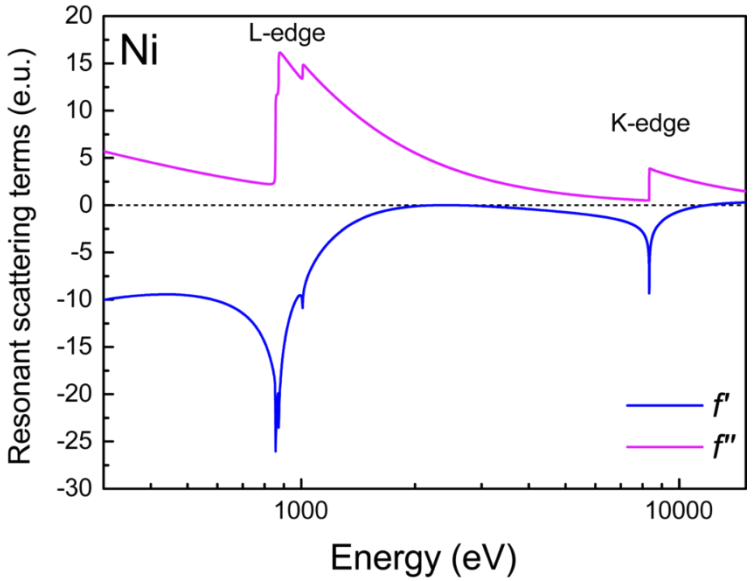

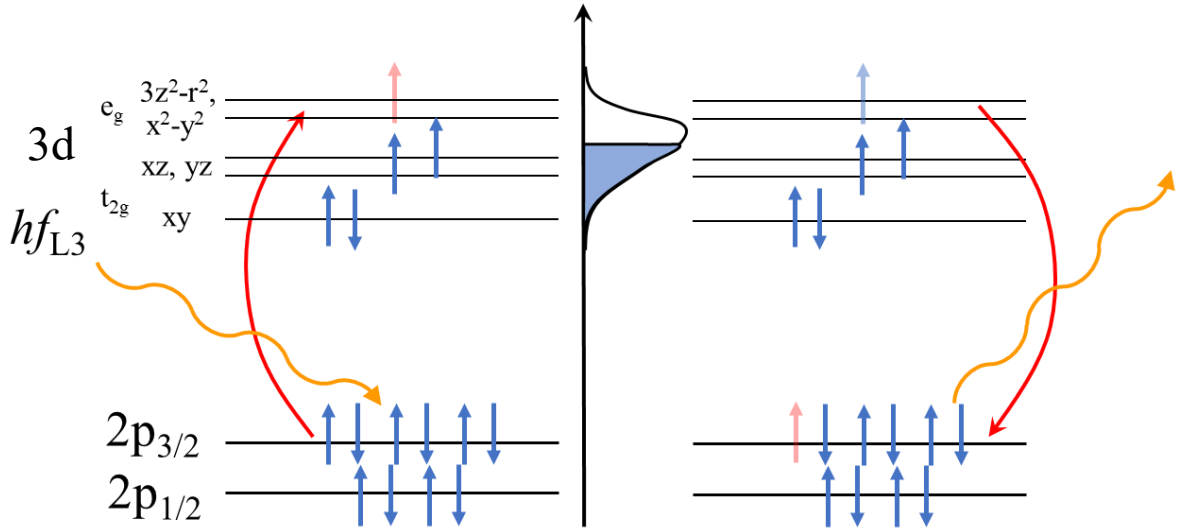

$$f'(E) = \frac{1}{\pi}\mathcal{P}\int_{-\infty}^{\infty} \frac{f''(E')}{(E'-E)} dE'$$

Henke – Gullikson atomic factor

$$f_1(\omega) = Z + \mathrm{f}'(\omega)$$

$$f_2(\omega) = \mathrm{f}''(\omega)$$

At $L_{2,3}$ edges in TM atoms, we probe holes in 3d orbital – **sensitive to magnetism**. Magnetic dichroism in *f''* also present in *f'*

The magnetic propagation vector

The propagation vector describes the periodicity and phase relationship of the magnetic moments within a material relative to its crystallographic unit cell.

$\cos(\vec{k} \cdot \vec{R})$

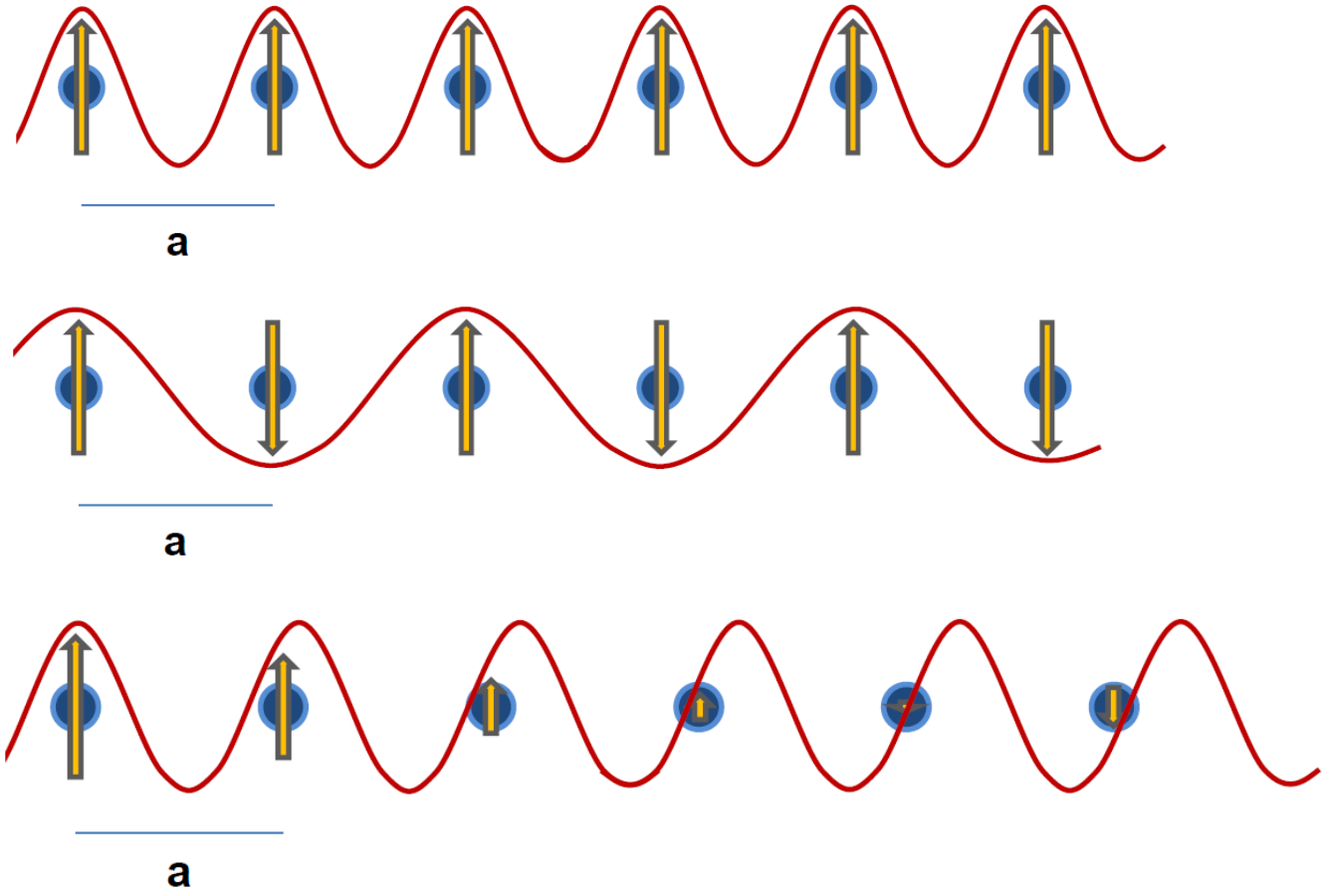

$\vec{k} = [0,0,0]$

$\vec{k} = [\frac{1}{2}, 0,0]$

$\vec{k} = [\tau, 0,0]$

Magnetic ordering – incommensurate cycloid

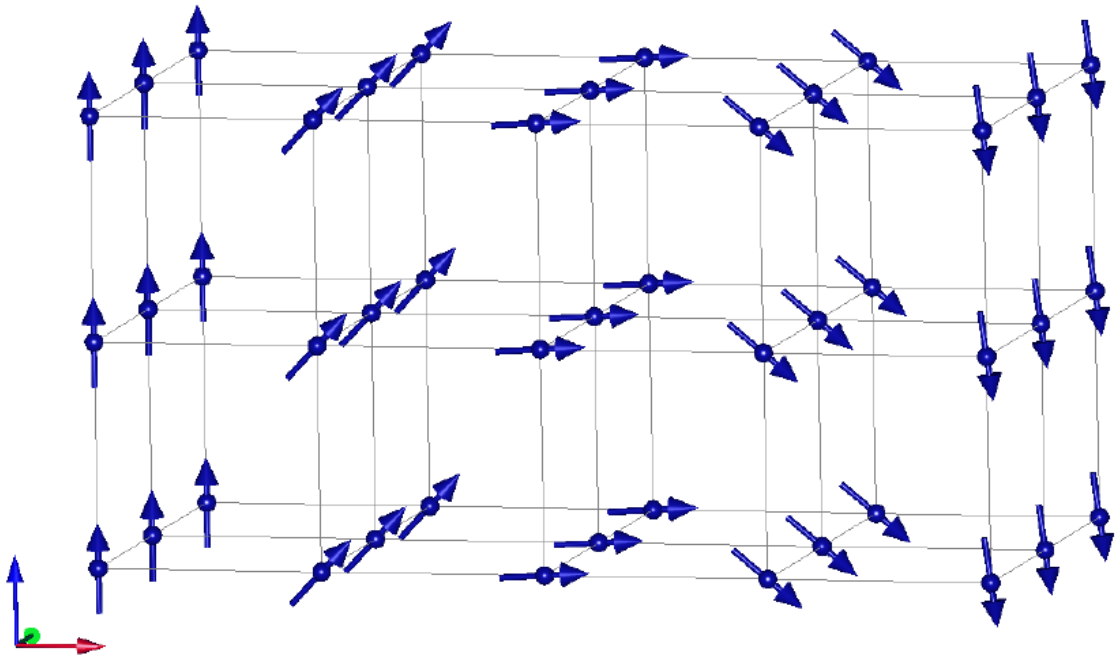

$$\boldsymbol{\mu}_{ld} = \sum_{\boldsymbol{q},n} \boldsymbol{m}_{\boldsymbol{q}d}^{(n)} \exp(-i\boldsymbol{q}.\boldsymbol{l})$$

$$\boldsymbol{m}_{\boldsymbol{q}}^{(1)} = \tfrac{1}{2}[0,0,\mu],\ \boldsymbol{q}^{(1)} = (\delta,0,0)$$

$$\boldsymbol{m}_{\boldsymbol{q}}^{(2)} = \tfrac{1}{2}[i\mu,0,0],\ \boldsymbol{q}^{(2)} = (\delta,0,0)$$

$$\begin{aligned}\boldsymbol{\mu}_{\boldsymbol{l}} &= \boldsymbol{m}_{\boldsymbol{q}}^{(1)}\left(\exp(-2\pi\delta l_x) + \exp(2\pi\delta l_x)\right) \\ &\quad + \boldsymbol{m}_{\boldsymbol{q}}^{(2)}\left(\exp(-2\pi\delta l_x) - \exp(2\pi\delta l_x)\right) \\ &= 2\boldsymbol{m}_{\boldsymbol{q}}^{(1)}\cos(2\pi\delta lx) - 2i\boldsymbol{m}_{\boldsymbol{q}}^{(2)}\sin(2\pi\delta l_x) \\ &= \mu[\sin(2\pi\delta l_x), 0, \cos(2\pi\delta l_x)]\end{aligned}$$

From R. Johnson – “Magnetic diffraction”: Neutron Winter School
(Use of q rather than k)

Polarisation Analysis

- Magnetic unit cell can differ from crystallographic unit cell leading to forbidden reflections
- According to the electric dipole approximation, the scattering amplitude consists of charge, first order magnetic and second order magnetic scattering terms

$$f(E) = -\left(\frac{3}{4\pi \mathrm{k}}\right) F^{(0)}(\varepsilon' \cdot \varepsilon) - i\left(\frac{3}{4\pi \mathrm{k}}\right) F^{(1)}(\varepsilon' \times \varepsilon) \cdot \boldsymbol{M} - \left(\frac{3}{4\pi \mathrm{k}}\right) F^{(2)}(\varepsilon' \cdot \boldsymbol{M})(\varepsilon \cdot \boldsymbol{M})$$

- Polarisation matrices contain four channels:

$$\begin{pmatrix} \sigma'\sigma & \sigma'\pi \\ \pi'\sigma & \pi'\pi \end{pmatrix}$$

- Off diagonal terms only non-zero in the case of magnetic scattering (not strictly true: anisotropic scattering tensor)
- Linearly polarised light allows components to be isolated

$$f(E)_{Linear} = -\left(\frac{3}{4\pi \mathrm{k}}\right)\begin{pmatrix} 1 & 0 \\ 0 & \cos(2\theta) \end{pmatrix} - i\left(\frac{3}{4\pi \mathrm{k}}\right)\begin{pmatrix} 0 & m_i\cos(\theta) - m_k\sin(\theta) \\ -m_i\cos(\theta) - m_k\sin(\theta) & m_j\sin(2\theta) \end{pmatrix}$$

- Circularly polarised light expressed as: $P^{\pm} = \sigma \pm i\pi$

Experimental Methodology

RASOR diffractometer on BLADE beamline

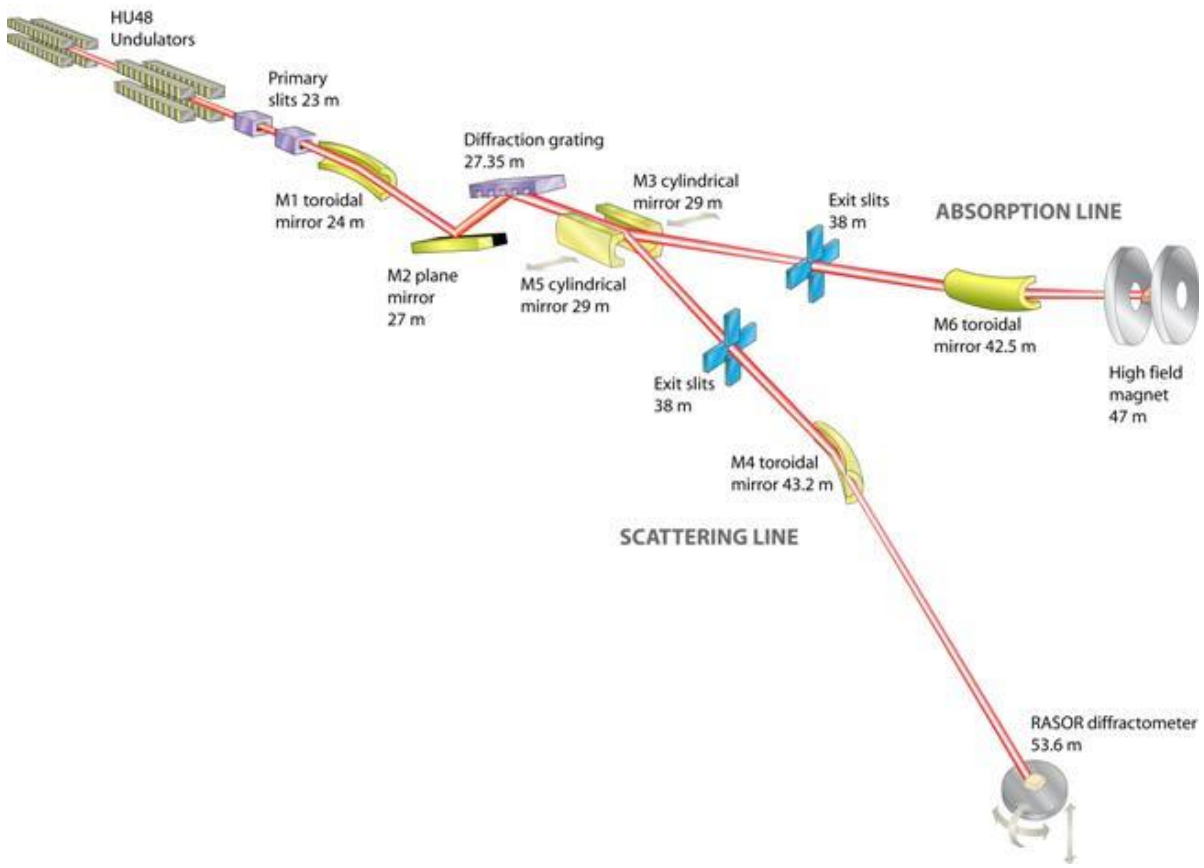

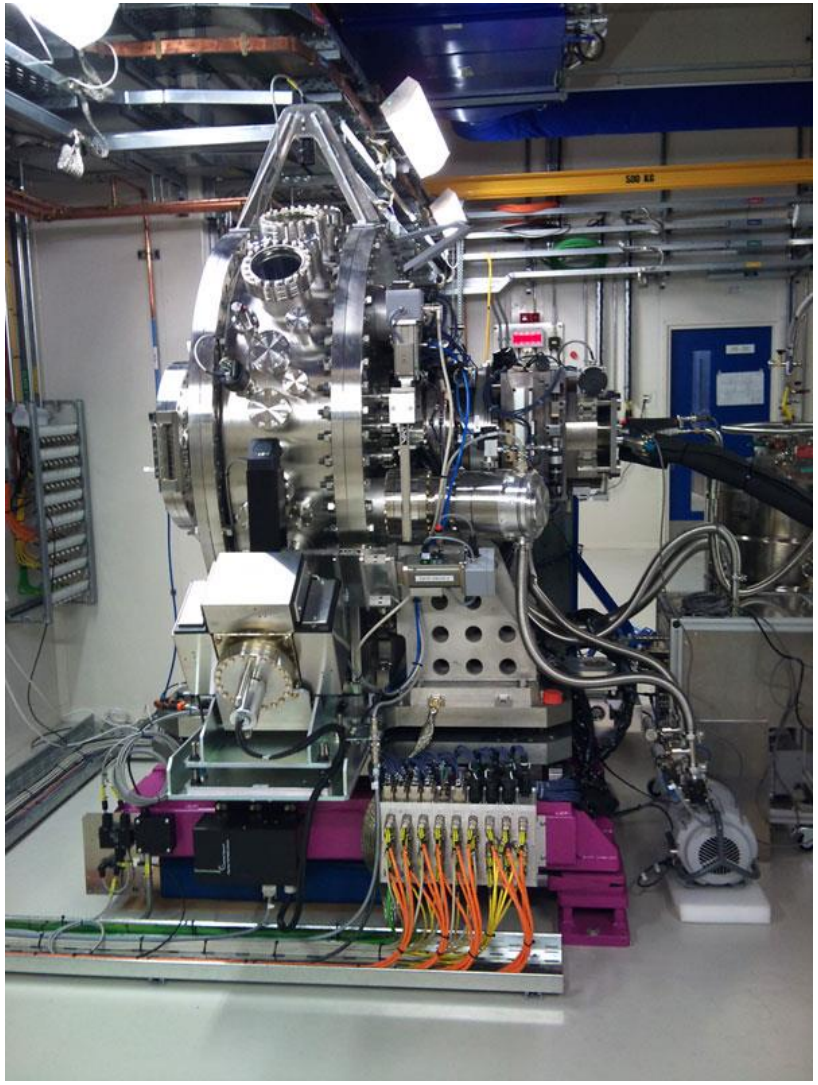

RASOR diffractometer on BLADE beamline

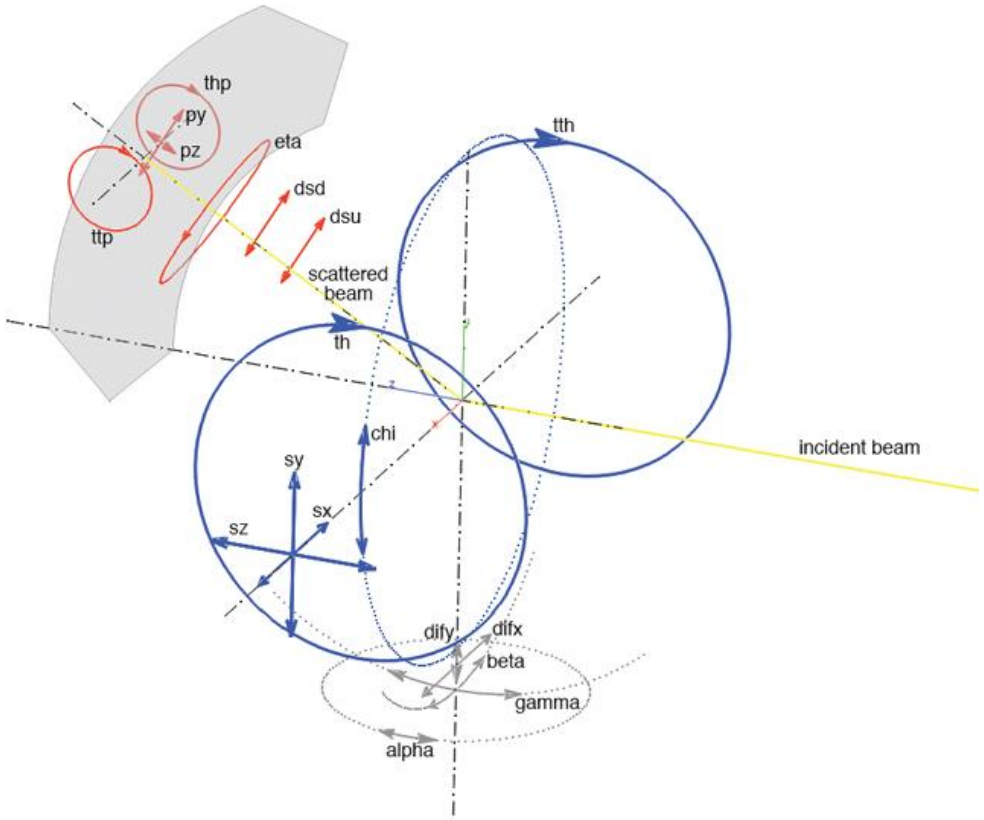

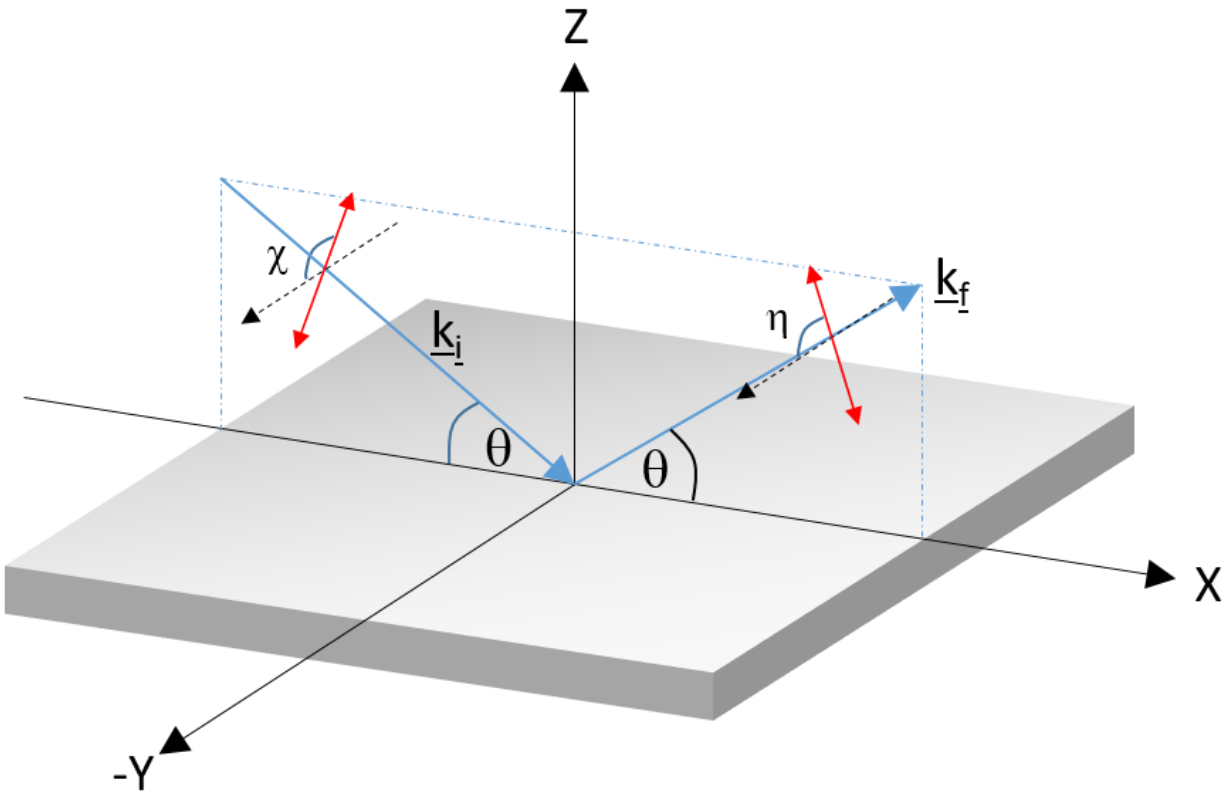

Polarisation Analysis

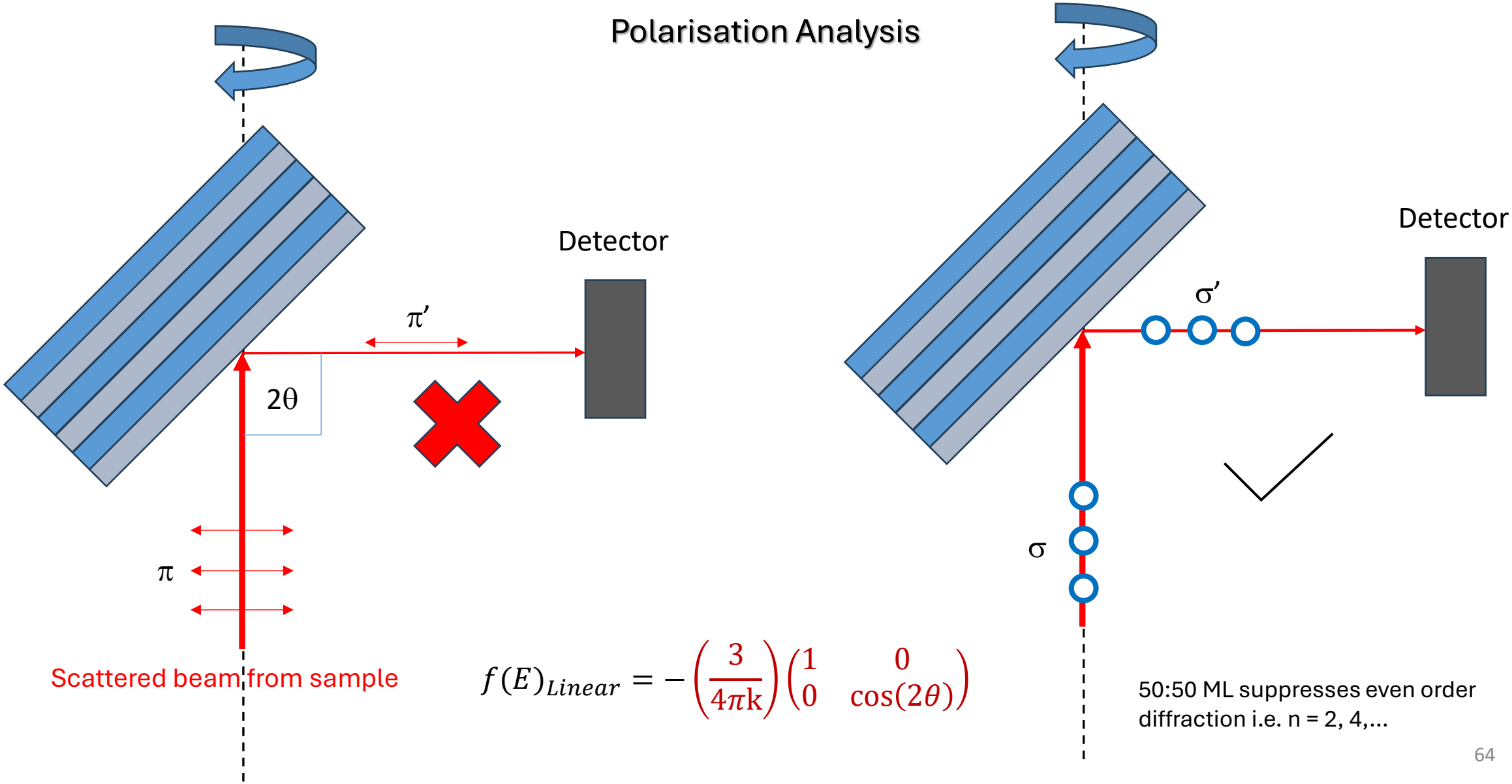

$$f(E)_{Linear} = -\left(\frac{3}{4\pi k}\right)\begin{pmatrix}1 & 0\\ 0 & \cos(2\theta)\end{pmatrix}$$

50:50 ML suppresses even order diffraction i.e. n = 2, 4,…

Resonant Diffraction – "anomalous" diffraction

W-type Hexaferrite ($SrCo_2Fe_{16}O_{27}$)

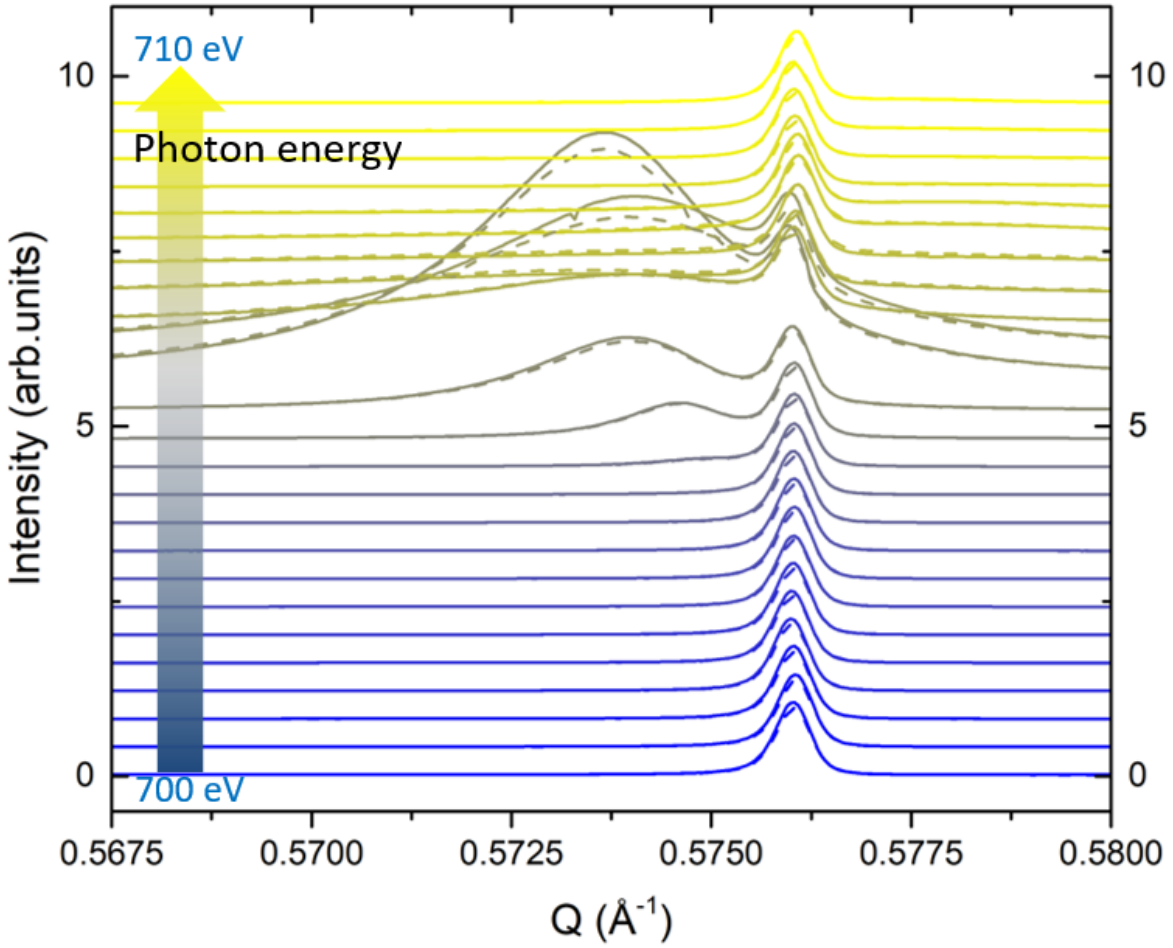

$$\boldsymbol{\varepsilon_i} = \cos(\chi)\,\hat{\boldsymbol{\imath}} + \sin(\chi)\left[\sin(\theta)\,\hat{\boldsymbol{\jmath}} + \cos(\theta)\hat{\boldsymbol{k}}\right]$$

$$\boldsymbol{\varepsilon_f} = \cos(\eta)\,\hat{\boldsymbol{\imath}} + \sin(\eta)\left[-\sin(\theta)\,\hat{\boldsymbol{\jmath}} + \cos(\theta)\hat{\boldsymbol{k}}\right]$$

$$f_m = -i\left(\frac{3}{4\pi q}\right)\left[(\boldsymbol{\varepsilon_f} \times \boldsymbol{\varepsilon_i}) \cdot \boldsymbol{m}\right]\left[F^1_{-1} - F^1_1\right]$$

$$I(\omega, Q) = \left|\sum_n f_{\mathrm{n}}(\omega) exp(i\boldsymbol{Q} \cdot \boldsymbol{r})\right|^2$$

$$\boldsymbol{Q} = \boldsymbol{k_f} - \boldsymbol{k_i}$$

Note: for soft x-rays the Ewald sphere is very small! Need large unit cell and/or small magnetic propagation vectors

Example 1: Multiferroics

- Display both ferroelectric and magnetic orders
- Coupling between electric polarisation (***P***) and magnetisation (***M***) : magnetoelectric effect
- Control of ***M*** via external electric field ***E*** key to development of next generation low power technologies
- Non-collinear spin structures can allow necessary symmetry breaking required for multiferroics
- Search remains for low-cost room temperature ME materials in thin film form

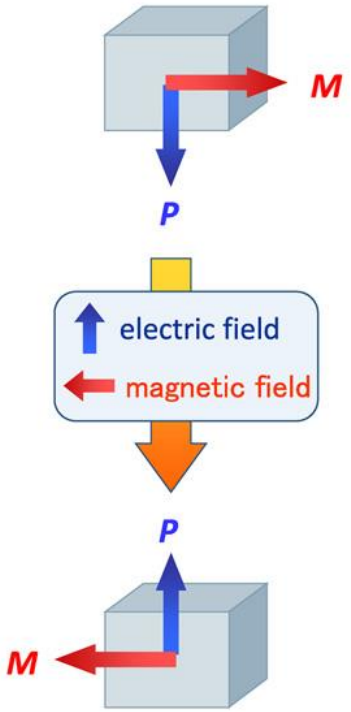

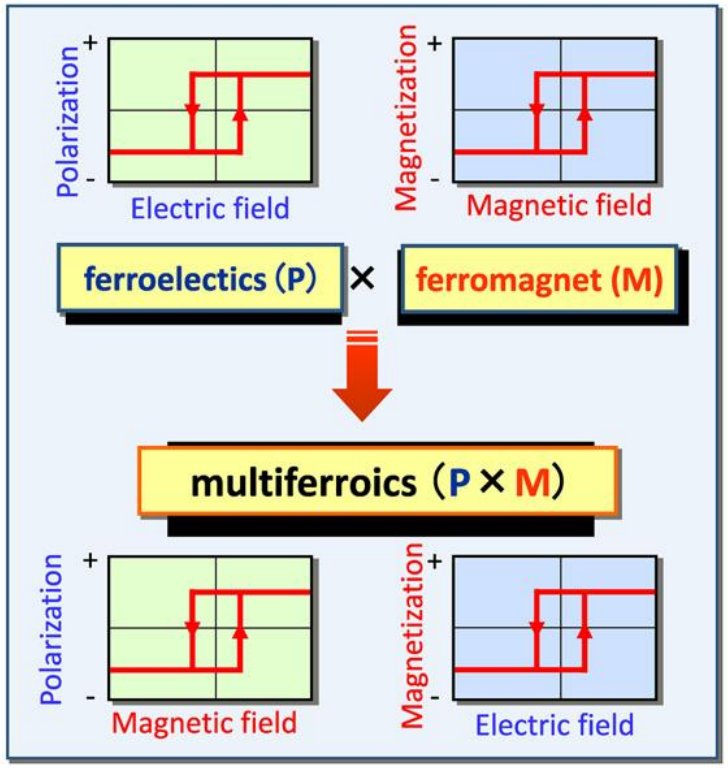

Y. Tokura *et al.* Rep. Prog. Phys. **77** (2014) 076501

Major mechanisms of ferroelectricity of spin origin

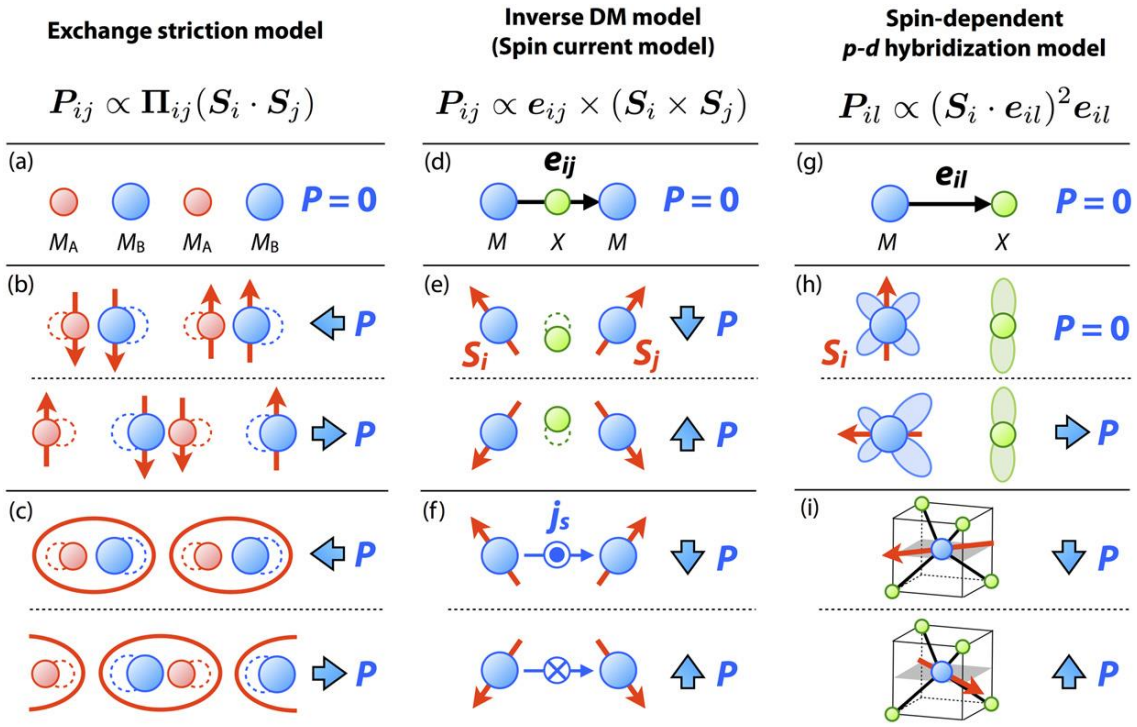

Inverse DM model

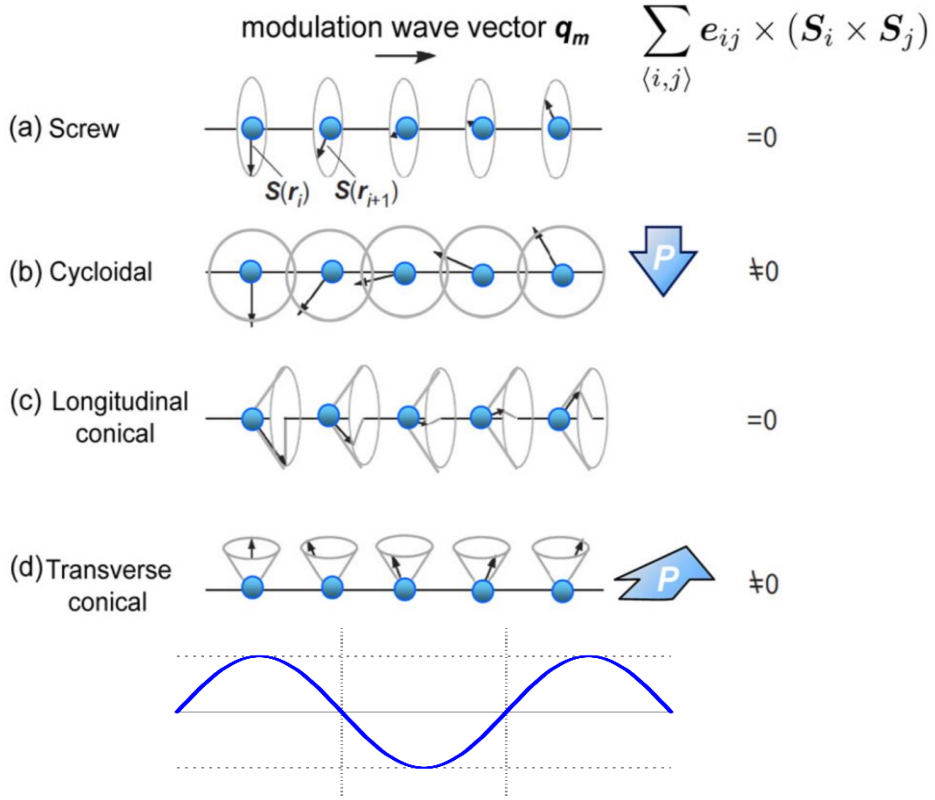

Y. Tokura *et al*. Rep. Prog. Phys. **77** (2014) 076501

Other interests in non collinear spin order - Skyrmions

$BaFe_{12-x-\delta}Sc_xMg_\delta O_{19}$ x = 1.6

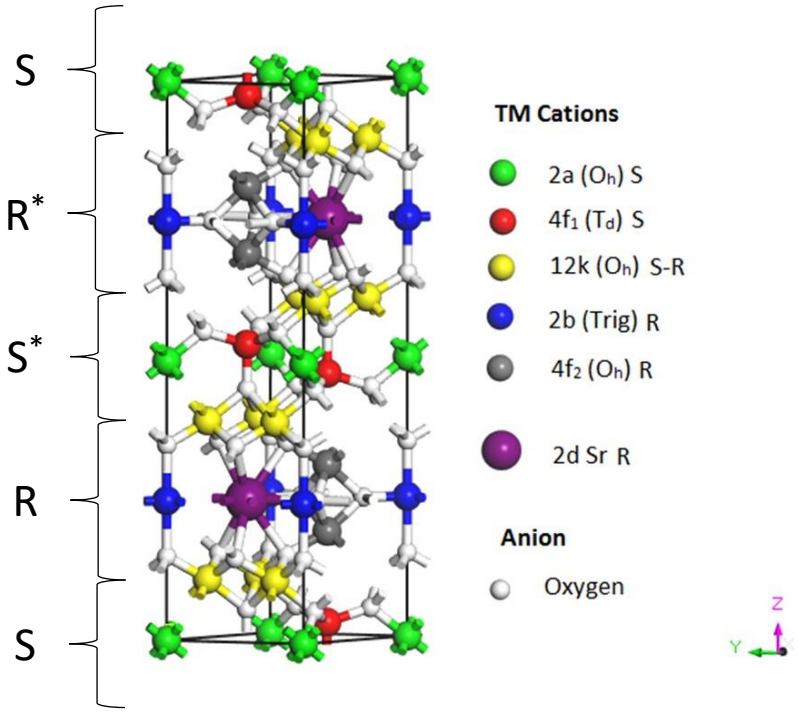

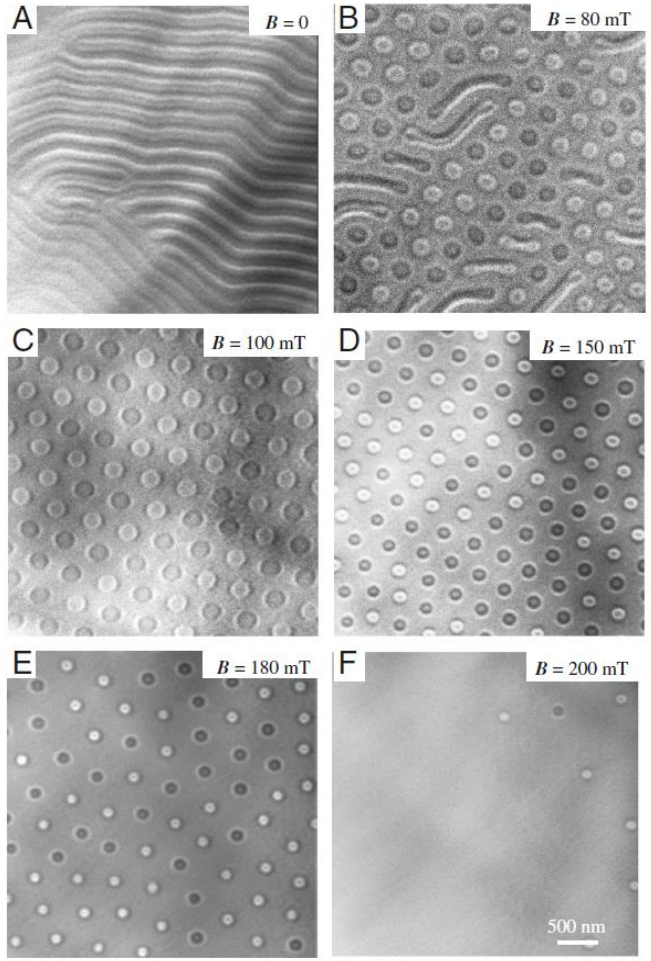

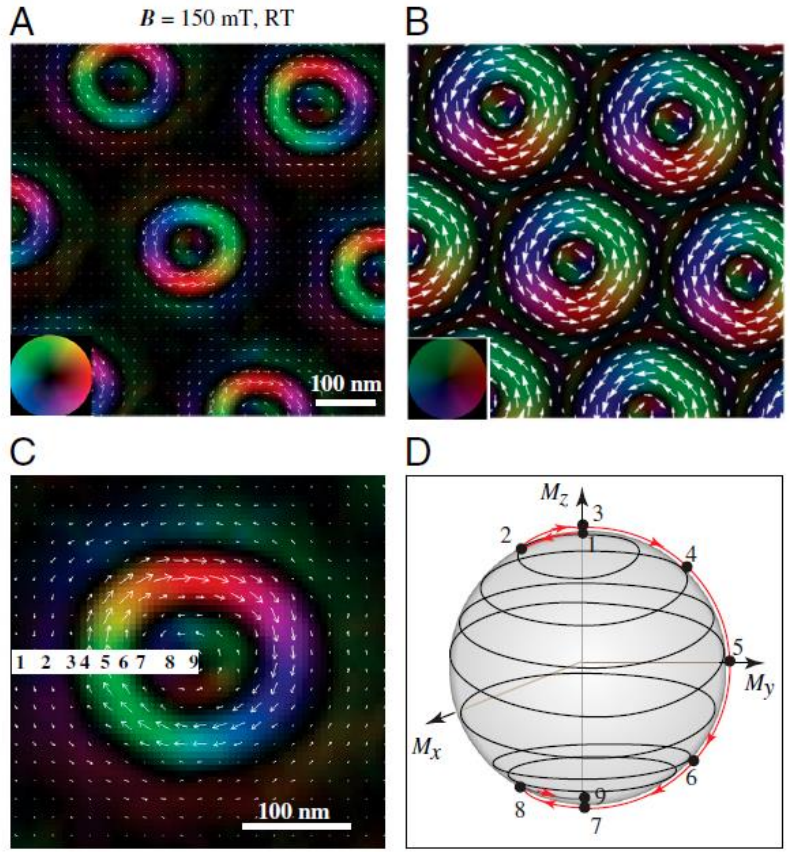

Yu *et al*. PNAS **109**, 8856 (2012)

M-type Hexaferrite

SRS*R*

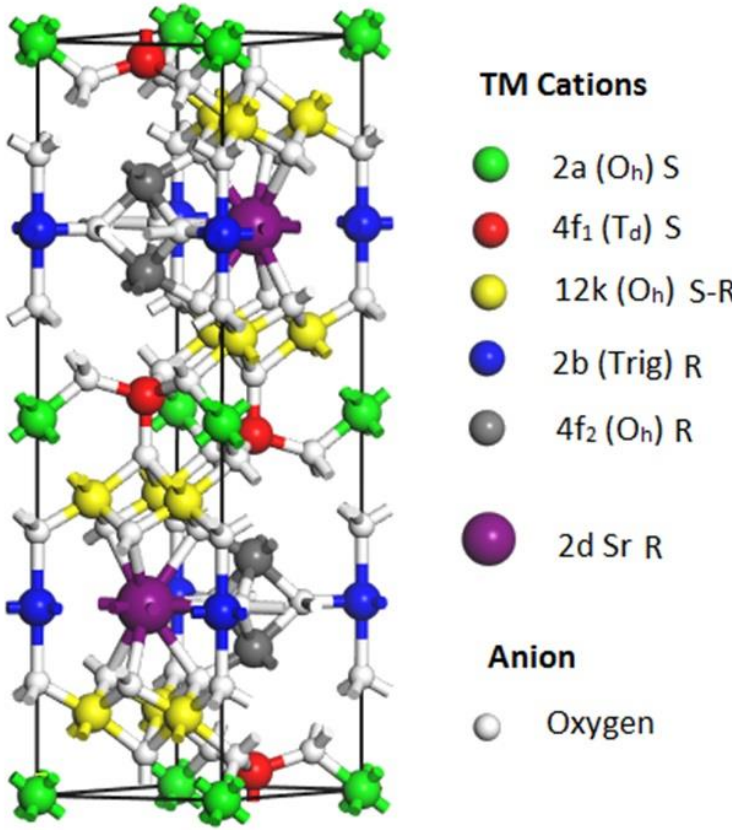

Space group P63/mmc: h + k + l = 2n

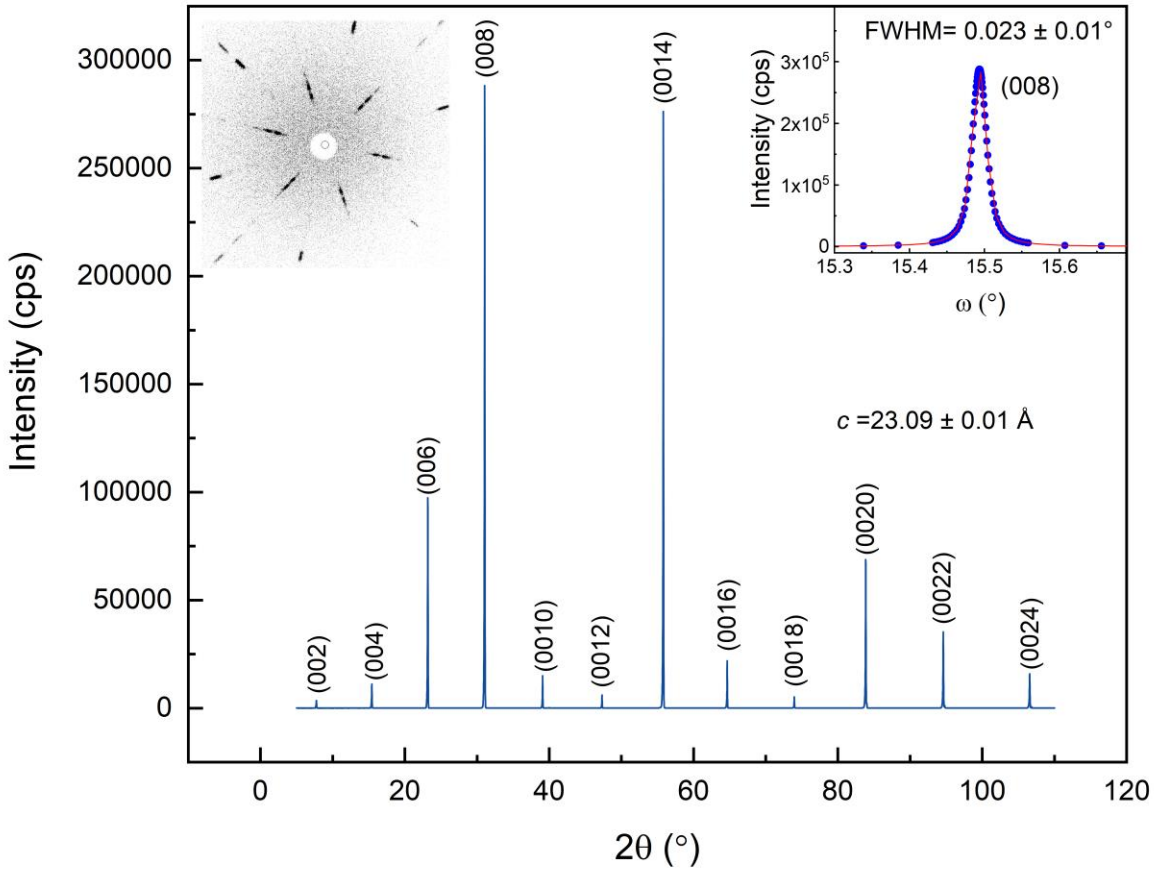

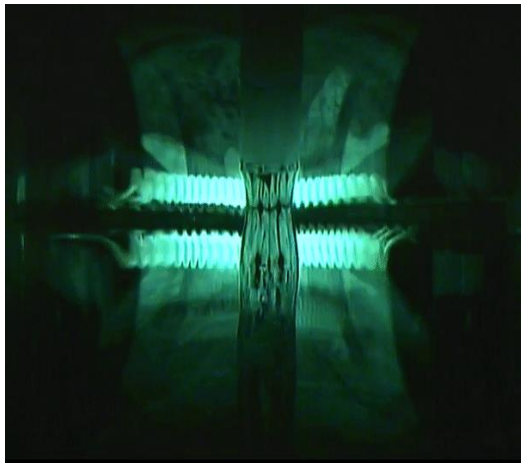

c = 23.09 Å
a = *b* = 5.88 Å

Advanced Physics Research , 2026; 5:e00161
https://doi.org/10.1002/apxr.202500161

- Non-collinear structures feature spins not aligned along same axis
- Longitudinal conical (LC) and transverse conical (TC) feature canted spins rotating about a respective axis
- LC expressed using ferro/ferrimagnetic and spin spiral sublattice components
- TC expressed using ferrimagnetic and cycloidal sublattice components
- LC can be canted in-plane using externally applied field

Transverse Conical

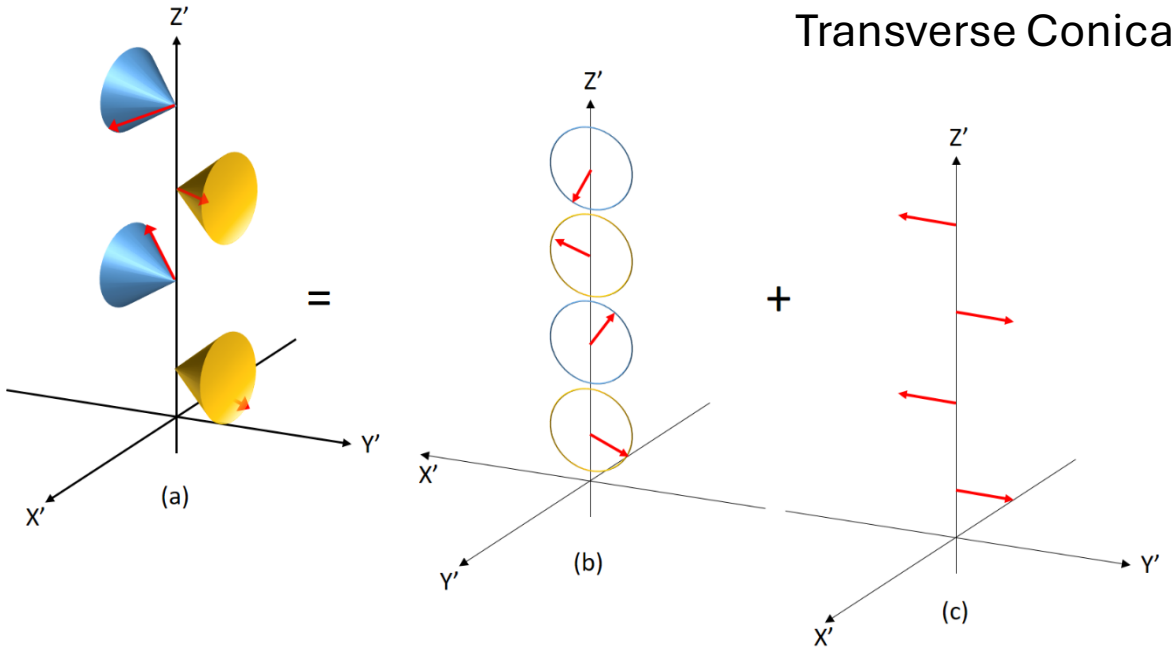

Longitudinal Conical

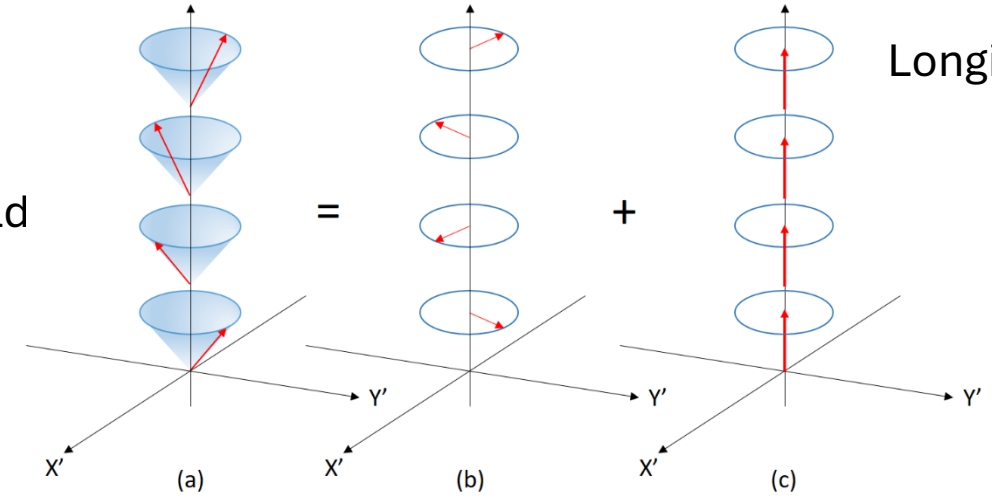

M-type Hexaferrite ($SrCo_{1.2}Ti_{1.2}Fe_{9.6}O_{19}$)

Fe L_3 edge

- Only the (002) Bragg peak accessible at this energy
- At resonance with Fe L_3, a second peak appears Q = (0,0,0.268) $Å^{-1}$ = (0,0,0.98) r.l.u – incommensurate. **d ≈ 23 Å (as seen also in neutron data)**
- **Forbidden in the structural space group.** Templeton – Templeton scattering ruled out; (0 0 1) not allowed for a 6_3 screw axis. Renninger scattering also ruled out as cause of peak.
- Peak is magnetic in nature (dichroic with circular polarised light)

k = [0,0,(2-τ)]

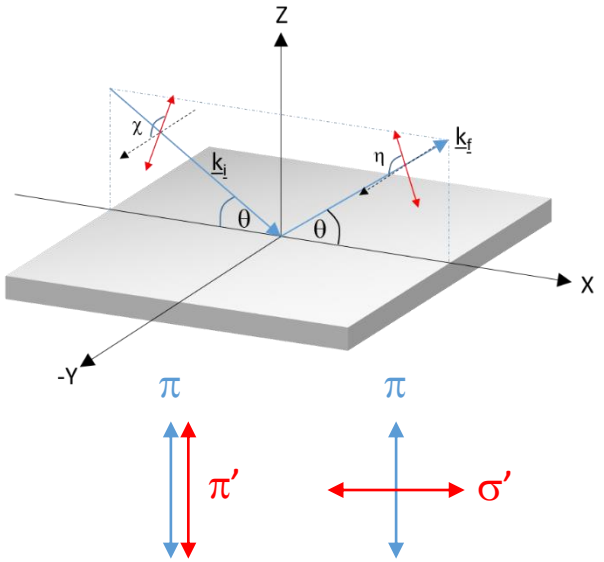

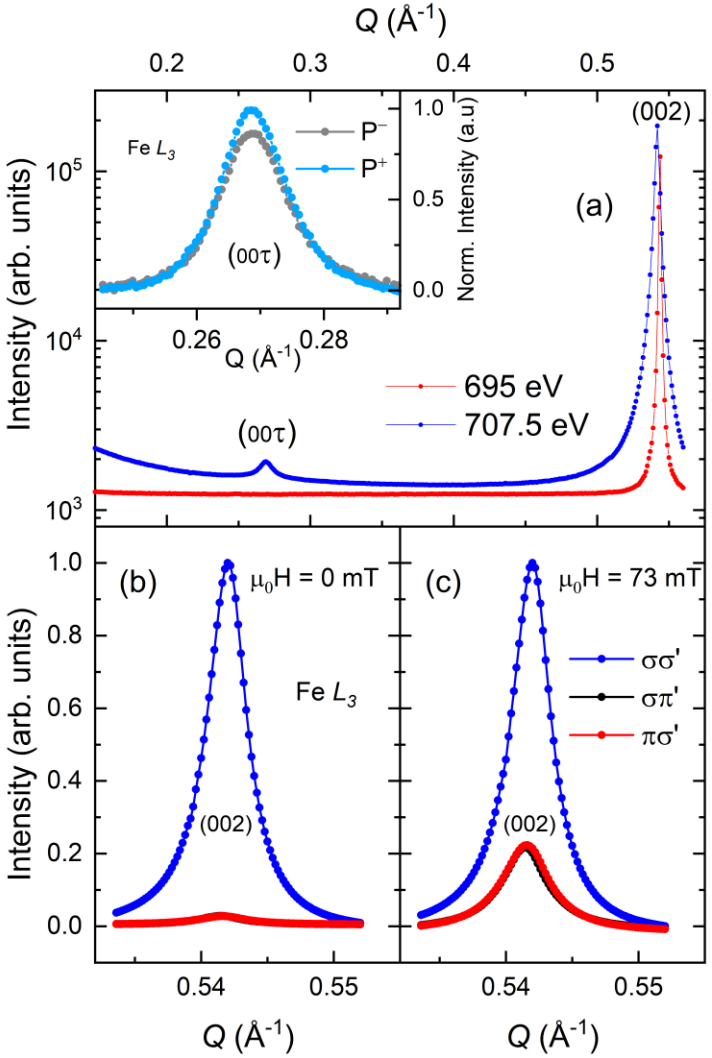

Advanced Physics Research , 2026; 5:e00161
https://doi.org/10.1002/apxr.202500161

Resonant Diffraction – "anomalous" diffraction

M-type Hexaferrite ($SrCo_{1.2}Ti_{1.2}Fe_{9.6}O_{19}$)

Co L_3 edge

- Only the (002) Bragg peak accessible at this energy. Magnetic contribution as seen in (σπ') channel – collinear ferrimagnetic contribution.
- A second peak, forbidden by the SG, appears at Q = (0,0,1) r.l.u. without the polarization analyser. Non collinear magnetism??
- However, peak also seen off resonance with no energy dependence.
- With polarization analyser in, no peak seen for both charge scattering (σσ') or magnetic (σπ') channels. Second order light diffracting from (002) planes (Bragg peak).

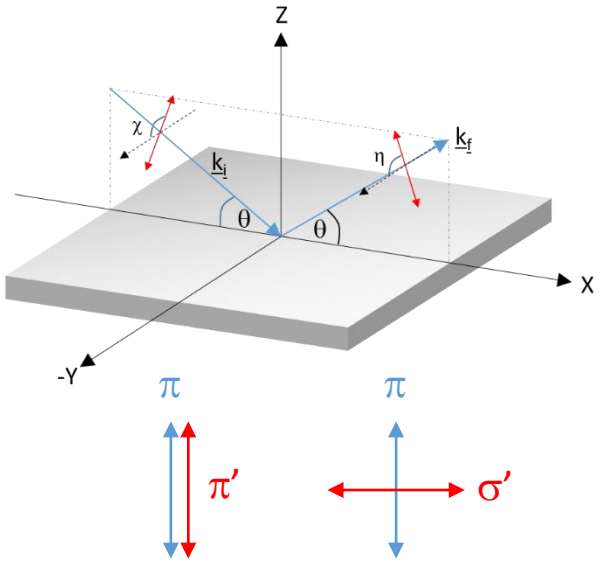

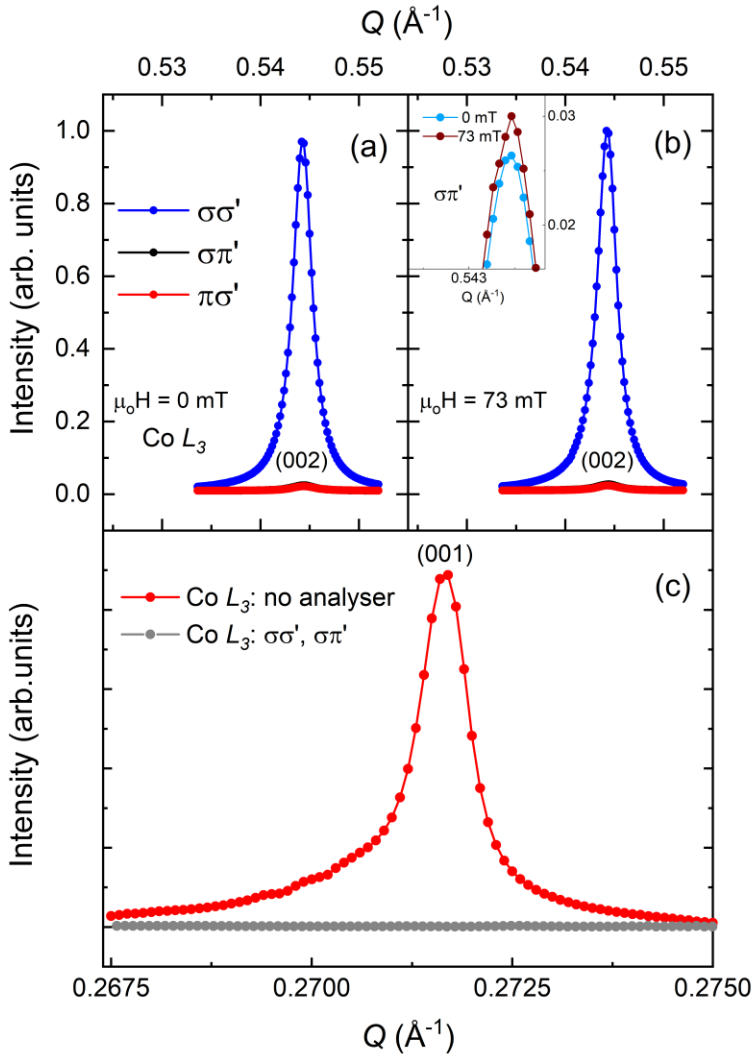

Advanced Physics Research , 2026; 5:e00161
https://doi.org/10.1002/apxr.202500161

Example 2: Photo-induced melting of Antiferromagnetic order in Manganites

Time Resolved Resonant Diffraction

Photoinduced Melting of Antiferromagnetic Order in $La_{0.5}Sr_{1.5}MnO_4$

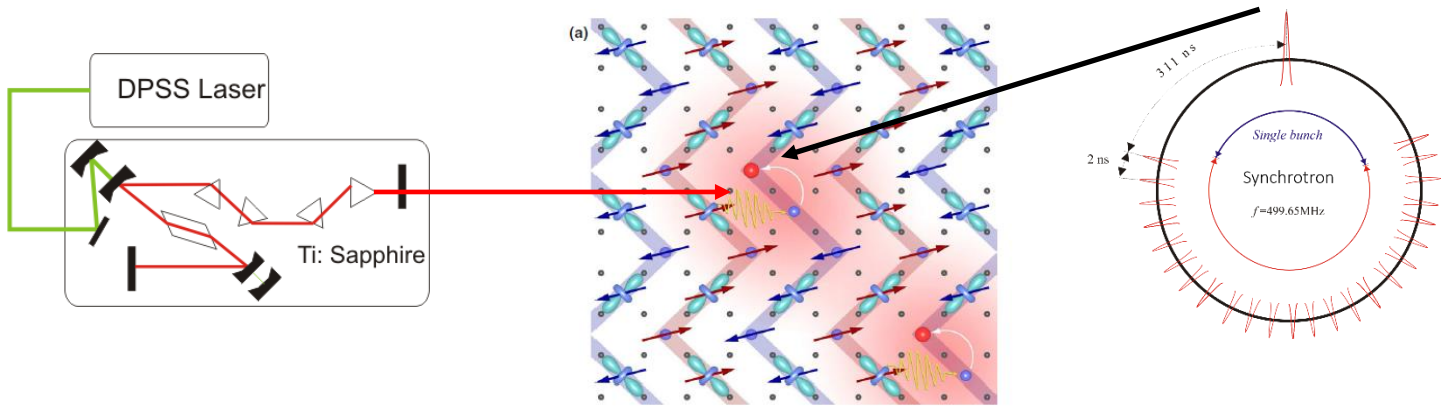

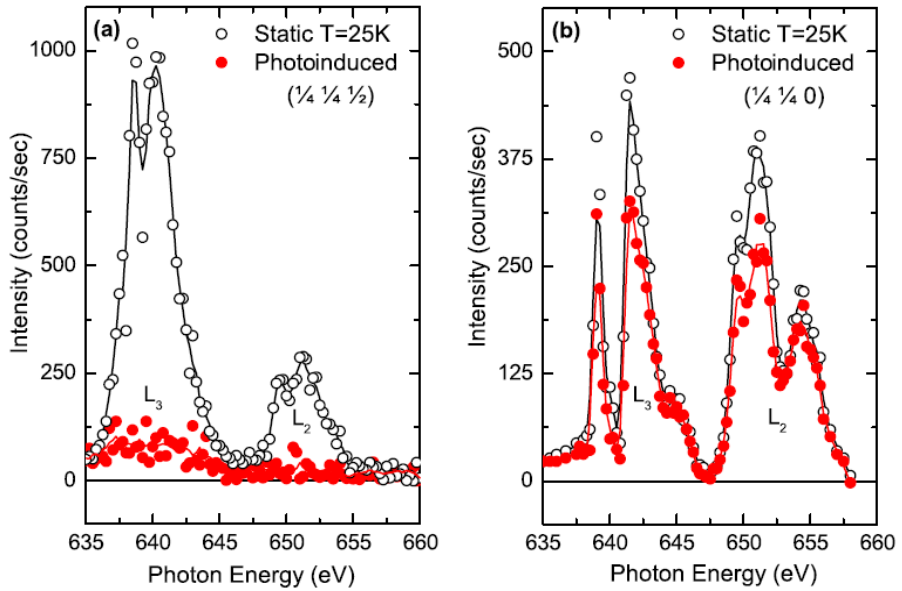

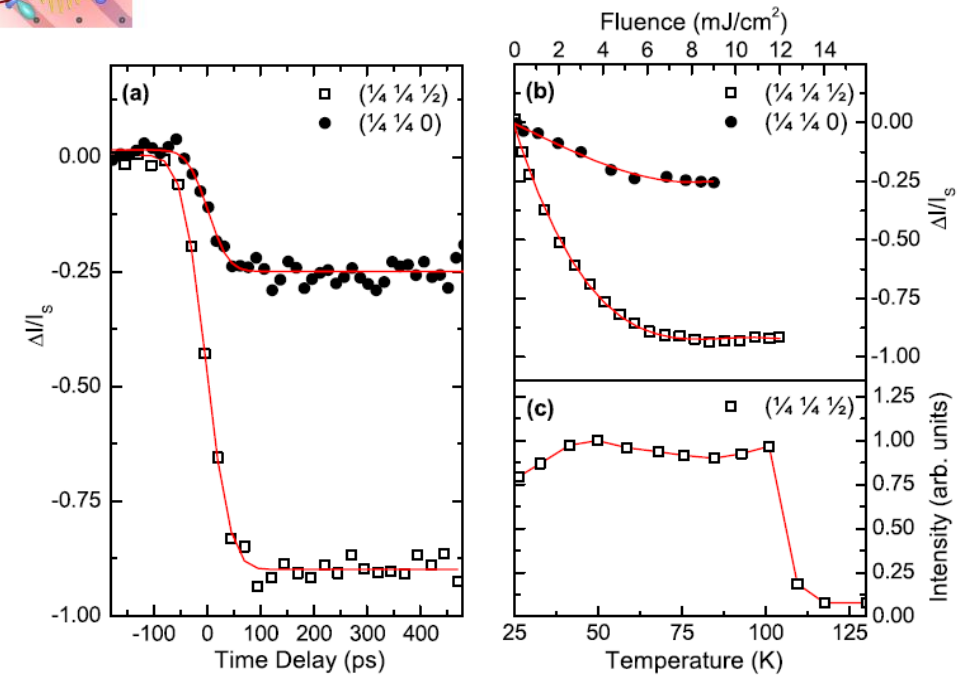

PRL **106**, 217401 (2011)

Summary

Synchrotron X-rays provide powerful, element-specific probes of magnetism.

XAS, XMCD and XMLD reveal electronic structure, spin/orbital moments and magnetic anisotropy.

Multiplet and charge-transfer effects are essential for understanding transition-metal X-ray spectra.

X-ray imaging and time-resolved techniques allow magnetic structures and ultrafast magnetisation dynamics to be visualised.

Resonant X-ray diffraction reveals complex magnetic order, including non-collinear structures, propagation vectors and multiferroic behaviour

For further reading on magnetism studied by diffraction techniques see